1985

Turbulent flow in a curved streamwise corner

Ping-Ho Tsai
University of Iowa

TURBULENT FLOW IN A CURVED STREAMWISE CORNER

by

Ping-Ho Tsai

A thesis submitted in partial fulfillment
of the requirements for the degree of
Master of Science in Mechanical
Engineering in the Graduate College
of The University of Iowa

August 1985

Thesis supervisor: Professor Virendra C. Patel

Graduate College
The University of Iowa
Iowa City, Iowa

CERTIFICATE OF APPROVAL

MASTER'S THESIS

This is to certify that the Master's thesis of

Ping-Ho Tsai

has been approved by the Examining Committee for the thesis requirement for the Master of Science degree in Mechanical Engineering at the August 1985 graduation.

Thesis committee: _____
Thesis supervisor

_____
Member

_____
Member

ACKNOWLEDGMENTS

The author wishes to express her sincere appreciation to Professor V. C. Patel for his suggestions and guidance. Financial support for this project was provided by the Graduate College of the University of Iowa and the Office of Naval Research through the Special Focus Research Program in Ship Hydrodynamics under Contract N00014-83-K-0136. The author owes a debt of gratitude to her grandfather and parents for their patience and constant encouragement during the course of this work.

ABSTRACT

This thesis is concerned with a study of the turbulent boundary layer in the corner region of a curved duct. The pressure-driven secondary flow is investigated by experiments and calculations. Measurements of pressure distribution and mean-velocity components are made at three streamwise stations in the convex corner of a curved duct and the results are compared with calculations using a finite-difference numerical method.

TABLE OF CONTENTS

LIST OF FIGURES

CHAPTER I

INTRODUCTION

The flow in a streamwise corner is considered. It is a three-dimensional turbulent flow bounded by two walls, which may be straight or curved. This type of flow can be external as well as internal and occurs in many practical applications. The flow around blade-hub junctions and wing-body junctions are examples of external streamwise corner flow. The flow in long ducts and channels fall under the category of internal streamwise corner flows. All of these flows are characterised by the development or decay of streamwise vorticity which alters the primary flow field. Alternatively, there exists a secondary flow which is superimposed on the primary streamwise flow.

Secondary motion in internal flows is important in a variety of engineering applications. For example, the pressure drop in developing or fully-developed flow in duct bends affects the pumping power needed. The heat transfer is enhanced by the secondary motions in the cooling coils of heat exchangers. The flow in aircraft-engine intakes and heat transfer in turbomachinery components are also affected by secondary motion. River meanders and variations in bend

topology are induced by secondary motion. In blood flow, the length required for fully-developed flow after a bifurcation and the site of extrema in the wall shear stress are important in the understanding of the buildup of cholesterol on the vessel walls.

In external flows, secondary motion arises in three-dimensional boundary layers and in boundary regions such as wing tips and wing-body junctions. While conventional boundary-layer theory accounts for the former, it excludes boundary regions where the surface curvature is either discontinuous, as in corners between two walls, or not small compared with boundary-layer thickness, as in the flow around wing tips and in corners with fillets. The flow in a corner is of special interest since it provides the boundary conditions for the boundary-layer flow in regions remote from the corner. Practical applications arise in wing-fuselage junctions in aerodynamics, hull-appendage junctions in ship hydrodynamics, and blade-hub junctions in turbomachinery. The formation and decay of the longitudinal vortices in corners, and the possibilities of corner-flow separation, are phenomena of particular interest in these applications.

Prandtl (1952) classified secondary flows according to the mechanism which generates them. Pressure-driven secondary flow, or secondary flow of the first kind, is that

which results from the radial pressure gradients which balance the centrifugal acceleration due to the curvature of the streamlines. Such secondary flows arise in curved ducts and channels, wing-body junctions as well as in turbomachinery. The secondary flow in three-dimensional laminar and turbulent boundary layers is primarily of this type. The magnitude of the secondary flow thus depends on the curvature of the mean streamlines. Another type of secondary flow, called secondary flow of the second kind, occurs only in turbulent flow and is generated by the gradients of the Reynolds stresses. This is also called shear-driven or turbulence-driven secondary flow. In straight noncircular ducts and channels, the secondary-flow velocities due to this mechanism are usually small, of the order of 2 to 3 percent of the average velocity. In turbulent flow in curved ducts and channels, both types of secondary motion is present but, if the curvature is large, secondary motion of the first kind becomes predominant.

This thesis is concerned with the turbulent boundary layer developing in the corner region of a curved duct. This flow, therefore, possesses features which are found in both internal and external flows mentioned above. Also, if the curvature is large, the secondary motion is primarily pressure-driven.

1.1 Literature review

A comprehensive review of the rather extensive literature on secondary flows is well beyond the scope of the present thesis. Hawthorne (1951) has discussed the use of invicid-flow approximations in the vorticity-transport equation for the calculation of weak secondary motion in a variety of complex internal and external flows, and many approximate methods of solution have been derived for applications in turbomachinery. The recent review of flow in curved pipes by Berger, Talbot and Yao (1983) contains some 168 references although it is primarily concerned with laminar incompressible flow in circular pipes! We shall not be concerned with laminar flow here although it is recognized that the mechanism responsible for secondary motion of the first kind operates in both laminar and turbulent flows. However, reference will be made to some recent experimental work in laminar flow to the extent that it facilitates the interpretation of results in turbulent flow.

The existence of secondary motion of the second kind in turbulent flows has been recognized since the early experiments of Nikuradse (1926) in straight prismatic ducts. Considerable effort has been devoted in recent years to the development of turbulence models which can properly account for this stress-driven secondary motion. Reference may be

made to the papers by Gessner (1973), Launder and Ying (1973), Tatchell (1975), Reece (1977), Naot and Rodi (1982) and Demuren and Rodi (1982), for progress in this area.

Experiments and calculations involving turbulent flow in curved corners are relatively few and recent. These investigations can be classified in two categories, namely internal and external flows. The former category includes fully-developed flow in curved rectangular ducts in which the curved section is preceded by a long straight upstream segment. Developing boundary-layer flow in the entrance region of curved ducts, and unbounded flow in the corner formed by two intersecting surfaces, at least one of which is curved (e.g. wing-fuselage junction), are examples of external flow. Although stress-driven secondary motion is present in both cases, pressure-driven secondary motion may dominate if the streamwise curvature is large. In the following, we shall first review the available experimental information on the flow in curved corners. These problems have also been addressed in recent years by numerical calculation methods. These will be reviewed in a subsequent section.

1.1.1 Experiments on turbulent flow in curved corners

Detailed experiments in fully-developed flow in a 90-degree bend of a 40 mm square duct have been performed by

Humphrey, Taylor and Whitelaw (1977) and Humphrey, Whitelaw and Yee (1981) using LDV instrumentation and water as the working fluid. The former were restricted to laminar flow. The latter considered turbulent flow at a duct Reynolds number of $4x10^4$. Mean-velocity distributions and four components of the Reynolds-stress tensor were measured at four sections in the bend. Later on, these experiments were repeated by Taylor, Whitelaw and Yianneskis (1982) in developing flow with thin boundary layers at the duct inlet. More recently, Humphrey, Chang and Modavi (1982) have performed measurements in fully-developed flow in a 180-degree duct, while Taylor, Whitelaw and Yianneskis (1982) have performed experiments in S-shaped ducts to study the influence of curvature reversal. As expected from momentum considerations, the secondary motion in turbulent flow is weaker than that in laminar flow, and the secondary motion in developing turbulent flow is smaller than that in fully-developed turbulent flow. On the flat walls, the mean flow is driven toward the center of curvature of the duct, so that the flow on the outer concave wall is divergent and that on the inner convex wall is convergent. Thus, in fully-developed flow, a strong secondary motion from the inner to the outer wall is generated at the duct center. In a developing boundary-layer flow, however, the secondary motion in the inviscid core is weak and the boundary layers

on the inner and outer walls develop a strong three-dimensional character. Together, the measurements reveal that the secondary flow velocities reach maxima of 15 to 20 percent of the bulk velocity in the duct and are therefore much larger than the stress-driven secondary flows observed in straight ducts.

Experiments in a 5x10 inches rectangular (WxH) 120-degree duct bend with a straight downstream section, and in a 18x27 inches 120-degree duct bend have been conducted by Bruun (1979). The latter arrangement was also used by Wang (1982). These authors made measurements of the mean-velocity components and turbulence quantities by hotwire anemometers. McMillan (1982) and Rojas, Whitelaw and Yianneskis (1983) have made measurements in rectangular diffusing bends. The general features of the mean flow and turbulent stresses in all these flows are similar to those observed in ducts of uniform cross section. It should be noted that, in the experiments of Rojas et al., the diffusion was sufficiently mild to avoid separation.

Early experiments in external corner flows involved flow visualization in the region of the horseshoe vortex that forms at the leading edge of a body intersecting a plane wall. The most recent exploration of the flow in the juncture were performed by Kubendran, McMahon and Hubbartt (1985). To date, no detailed data are available on the very

complex three-dimensional flow due to the occurrence of flow reversal. However, the decay of the vortex within the corner boundary layer has attracted much attention in view of the practical importance of the flow. The vortex transports fluid from the boundary layer on the body into the boundary layer on the plane and therefore influences the boundary layer development on both surfaces.

Turbulent boundary layers in straight external corners have been investigated by Mojola and Young (1972), Shabaka (1979), McMahon, Hubbartt and Kubendran (1983) and Dickinson (1984). In all cases, attention has been focused on the decay of the leading-edge vortex, and only the recent experiments provide some information on the Reynolds stresses. We note that this flow is somewhat similar to the developing flow in curved ducts insofar as the secondary motion is concerned, but with two important differences: (a) the vortical motion decays in the external flow while it is enhanced in the case of the duct, and (b) the viscous-invicid interaction in the external flow may be weak whereas that in the duct flow cannot be neglected.

In summary, we note that data pertaining to boundary-layer development in a curved streamwise corner are rather limited. Most earlier measurements have emphasized duct flows in which there is no separation. There is therefore a need to explore corner flows from a boundary-layer

perspective and consider situations leading towards corner-flow separation.

1.1.2 Calculations of turbulent flows involving curved corners

Different numerical techniques and turbulence models have been employed to calculate fully-developed and developing flows in ducts and external corner flows. Examples of such solutions are contained in Kline, Cantwell and Lilly (1982), where the curved-duct experiments of Humphrey (1977) and the corner-flow experiment of Shabaka (1979) were selected as test cases for the 1980-1981 Stanford Conferences on the calculation of complex turbulent flows. From the solutions presented there and elsewhere (for example, Humphrey, Whitelaw and Yee, 1981; Kreskovsky, Briley and McDonald, 1981; Humphrey, Chang and Modavi, 1982; Chang, 1983) it appears that the distribution of the streamwise (primary) velocity can be predicted with reasonable accuracy but neither the secondary velocity components nor the turbulence parameters are predicted well. At the present time it is not clear whether the poor performance of the calculation methods is due to the deficiencies of the numerical techniques used or the turbulence models. A difficulty that is encountered in the application of turbulence models in corner flows is concerned with the treatment of the wall boundary conditions

since almost all models employ some variant of the law of the wall whose validity near a corner has not been established. Thus, calculation methods suffer from uncertainties which can be resolved only by recourse to more detailed experiments in the corner region.

In the development of practical calculation methods for laminar and turbulent flow in geometries involving corners, most investigators have followed Patankar and Spalding (1972) and Caretto, Curr and Spalding (1973), who proposed the so-called partially-parabolic approximations to the Navier-Stokes or the Reynolds-averaged Navier-Stokes equations. For flows involving a predominant (primary) flow direction, they suggested that streamwise diffusion due to viscosity and turbulence may be neglected in the complete equations. In Cartesian coordinates (ξ_1, ξ_2, ξ_3), the partially-parabolic equations for an imcompressible fluid are:

$$\frac{\partial}{\partial \xi_1}(\rho u_1) + \frac{\partial}{\partial \xi_2}(\rho u_2) + \frac{\partial}{\partial \xi_3}(\rho u_3) = 0$$

$$\frac{\partial}{\partial \xi_1}(\rho u_i u_1) + \frac{\partial}{\partial \xi_2}(\rho u_i u_2) + \frac{\partial}{\partial \xi_3}(\rho u_i u_3) = -\frac{\partial p}{\partial \xi_i} + \frac{\partial \tau_{i2}}{\partial \xi_2} + \frac{\partial \tau_{i3}}{\partial \xi_3}$$

where ξ_1 is the predominant flow direction, u_i are the velocity components, τ is the laminar and/or turbulent

shear stress, p is pressure, ρ is density of the fluid and the subscript i designates the coordinates.

The above equations, together with a turbulence model, have been used for the calculation of a variety of complex flows. In general, the momentum equations are solved, after assuming some pressure field, by marching in the direction of the primary flow, and the pressure field is then determined so as to satisfy the equation of continuity. A number of such iterations is required to obtain a converged solution. We note that, in such calculations only the pressure needs to be stored in the entire three-dimensional domain and therefore computer-storage requirements are considerably smaller than those for the complete elliptic equations.

1.2 Outline of the present study

It is evident from the foregoing brief review that experimental investigations of turbulent boundary layers in curved streamwise corners are quite limited and there is practically no data on boundary layers developing toward separation. The recent experiments in developing flows in curved ducts and the corresponding calculations have clearly indicated the complexities of such flows. Additional experiments, with emphasis on the boundary layer in the corner, are obviously required to provide data which can be

utilized in guiding the development and verification of calculation procedures.

This thesis describes the first phase of a comprehensive experimental study whose major long-term objectives are to obtain detailed mean-flow and turbulence data in boundary layers in convex and concave streamwise corners, with a variety of imposed pressure gradients, and to study the nature of corner-flow separation. The design and construction of the flow facility, and preliminary measurements of the surface pressure distributions and mean-velocity components are described in Chapter 2. In order to guide the interpretation of the data and future experiments, an existing calculation method has been adopted to perform calculations for the present experimental geometry. The method is outlined and the calculations are compared with the experimental data in Chapter 3. Finally, Chapter 4 summarizes the major conclusions and recommendations for future directions of the research project.

CHAPTER II

EXPERIMENTAL STUDY OF THE FLOW IN A CURVED CORNER

2.1 Introduction

A small blower-type wind tunnel was constructed at the Institute of Hydraulic Research in 1982 to study corner boundary layers. This is shown schematically in figure 2.1. The cross section of the tunnel is rectangular. An initially straight section is followed by a section that is curved in the horizontal plane so that the top and bottom walls remain flat while the inner and outer walls are curved with constant radii of curvature. In the design of the curved test section, provision was made to independently vary the radii of curvature of the inner and outer walls so that a wide variety of convex and concave corner boundary layers with different imposed pressure gradients could be studied.

The present investigation is the first to be made in this tunnel. In view of this, an important preliminary task was to ascertain the flow quality in the tunnel. Measurements with simple pitot probes at several streamwise stations revealed nonuniformities in the pressure and

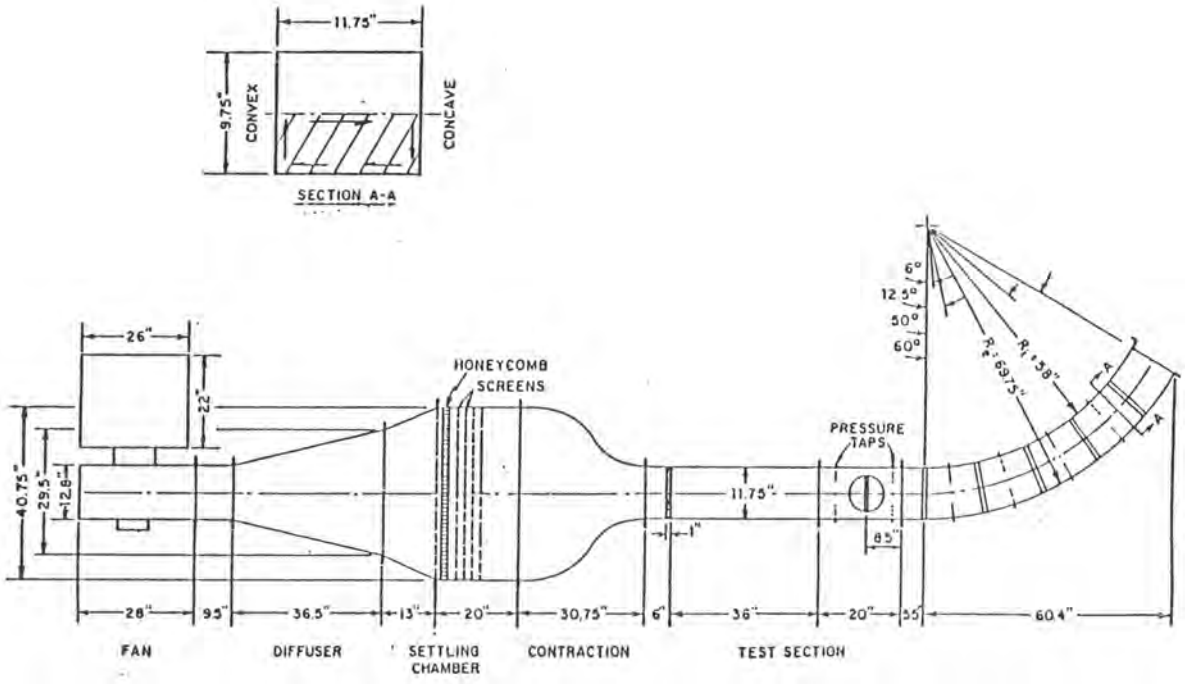

Figure 2.1. Layout of the wind tunnel.

velocity distributions. These also indicated geometric distortions in the curved portion of the test section due to the use of rather thin plexiglass side walls and the several ports which were provided in these walls for probe traverse. Major modifications were therefore made to the original design. These included the replacement of the honeycomb, installation of additional screens in the settling chamber, and a reconstruction of the entire test section using thicker, 3/16-inch, plexiglass for the side walls, replacing the original plywood top wall with a 1/2-inch thick plexiglass wall, smoothing and painting the bottom plywood wall, adding suitable stiffeners to the curved walls to maintain geometrical integrity, and carefully aligning and securing all sections such that the walls intersected at the corners at right angles. The reconstruction also provided an opportunity to install closely-spaced pressure taps on the new top- and side-walls of the test section. The reconstruction was carried out while retaining the original flexibility of varying the geometry of the test section. Due to the extensive effort devoted to this phase, and the subsequent tests for flow quality, the experiments could not be conducted in as great a detail as had been planned originally.

2.2 The wind tunnel

The tunnel configuration used for the present experiments is shown in figure 2.1. The centrifugal blower is followed by a flexible coupling to remove vibrations and a short transition piece that matches the blower outlet to the inlet of a wide-angle diffuser constructed in two sections. Three 14-mesh screens are fitted at the diffuser junctions to prevent separation. The settling chamber is 40.75 x 33.75 inches (WxH) and is fitted with a honeycomb (0.145 inch cell diameter, 2 inches long) and four 16-mesh screens. The 12:1 contraction then leads to the rectangular test section of width W = 11.75 inches (29.85 cms) and height H = 9.75 inches (24.76 cms). The initial straight portion of the test section is constructed in two segments, 42 and 20 inches long. These are followed by a 5.5-inches straight portion and the curved section with inner and outer wall radii of 58 and 69.75 inches, respectively. The total turning angle of the curved portion is 60 degrees. The short straight inlet portion was designed to precede the duct bend with any turning angle, regardless of the subsequent curvatures of the inner and outer walls. The air exits to the atmosphere at the end of the curved section. The tunnel velocity is controlled by varying the area of the inlet to the blower.

A one-inch wide sand-paper strip is installed around the test section, 6 inches downstream of the contraction exit, to promote transition. The second straight segment is fitted with a circular port to facilitate mounting of probes for calibration purposes. The top wall of the curved section is provided with radial slots through which probes can be installed. Those slots are closed by appropriate plugs when they are not in use. Pressure taps (.042 inch diameter) are installed on the walls of the contraction and the test section, except on the bottom surface of the curved bend, at several longitudinal stations. The longitudinal positions of the pressure and velocity measuring stations are shown in figure 2.2, and a typical distribution of the taps around the test section is shown in figure 2.3. The close spacing in the corner region is desirable for accurate determination of the transverse pressure gradients.

2.3 Instrumentation

A visual study of the flow using a wool tuft indicated no separation in the corners. This also showed that yaw angles near the duct exit were of the order of 10 degrees from the tangent line of the bend. A slight asymmetry of the flow about the duct centerline ($x_2/H = .5$) was observed near the exit.

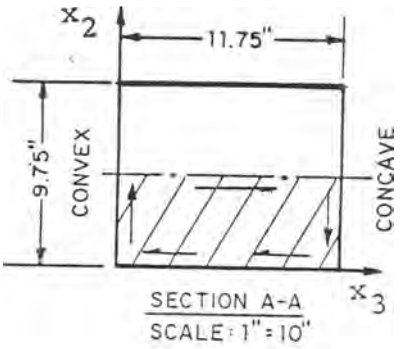

Press Station	Velocity Station	X (cm;degree) 1
P01		-55.8
	A	-35.5
P02		-20.3
	B	0.0; 0.0°
P1		17.0; 6.0°
	C	35.4;12.5°
P2		52.4;18.5°
	D	70.8;25.0°
P3		87.8;31.0°
	E	106.2;37.5°
P4		123.2;43.5°
	F	141.6;50.0°

where W=29.845cm, H=24.765cm

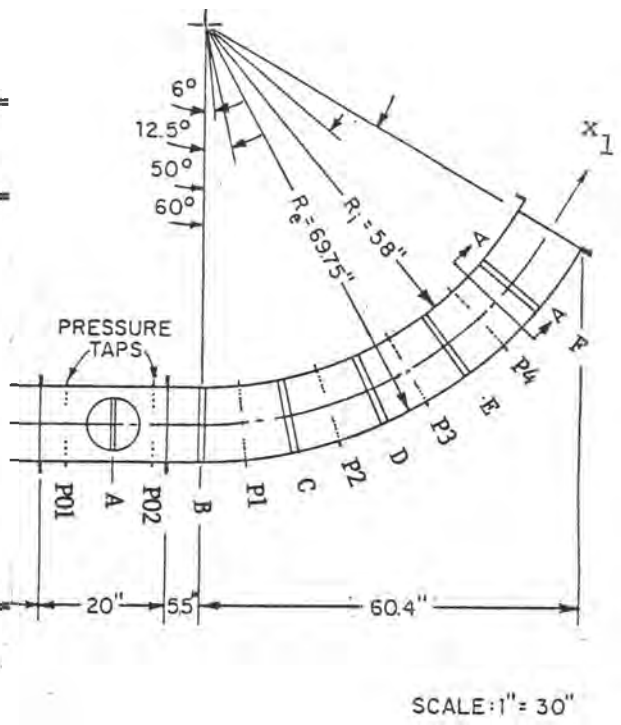

Figure 2.2. Pressure and velocity measuring stations and coordinates.

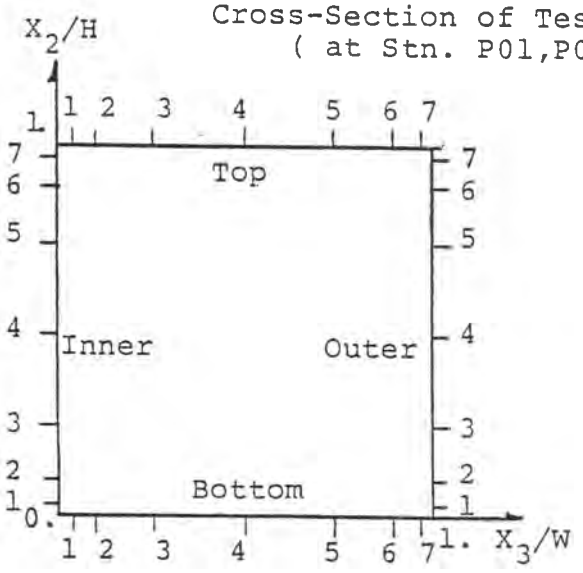

Hole No.	X_2 Cms	X_3 Cms
1	0.64	0.64
2	2.54	3.02
3	6.35	7.78
4	12.39	14.92
5	18.42	22.07
6	22.23	26.83
7	24.13	29.12

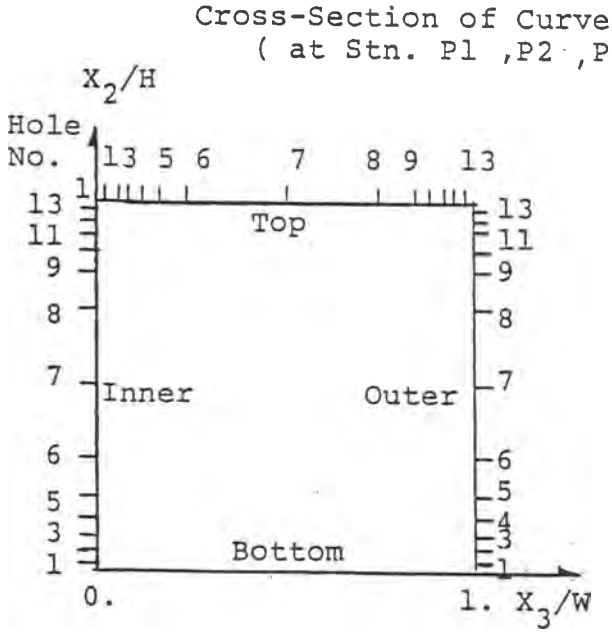

Hole No.	X_3 Cms	X_2 Cms
1	0.32	0.32
2	1.27	1.27
3	2.22	2.22
4	3.49	3.49
5	4.76	4.76
6	7.30	7.30
7	14.92	12.38
8	22.54	17.46
9	25.08	20.00
10	26.35	21.27
11	27.62	22.54
12	28.58	23.50
13	29.53	24.45

Figure 2.3. Locations of pressure taps.

2.3.1 Pressure measurements

For the measurement of pressure, a differential alcohol manometer and a differential pressure transducer were used. The former was used to monitor the tunnel reference pressure and the latter was used to measure wall pressures and pitot pressures.

The pressure information from the wall taps and from the pitot probes was processed with the aid of the HP-1000 mini-computer. The computerized data-acquisition system consisted of a 48-hole scanivalve, the IIHR-designed Scanivalve position circuit, a Scanco Solenoid Controller, a Statham PMSTC+0.3-350 pressure transduser, a transducer balancing circuit, a DANA amplifier and signal conditioner, a multimeter, and the PRESTON Analog-to-Digital Converter Subsystem(Cramer,1984). The fast triggering of the scanivalve position circuit and solenoid controller reduces the operation time and the need for a great number of transducer and signal-conditioner systems. The pressure transducer has a standard range of $\pm$0.3 psid, and a full-scale output of $\pm$4 mV/V nominal, zero balance of $\pm$0.2% of full scale,and a combined nonlinearity and hysteresis of less than 0.01%/degree F from -65 to +250 degrees F. Ideally, therefore, the accuracy of this transducer can be up to 0.002 V. Figure 2.4 shows the calibration curve for the pressure transducer against the manometer reading.

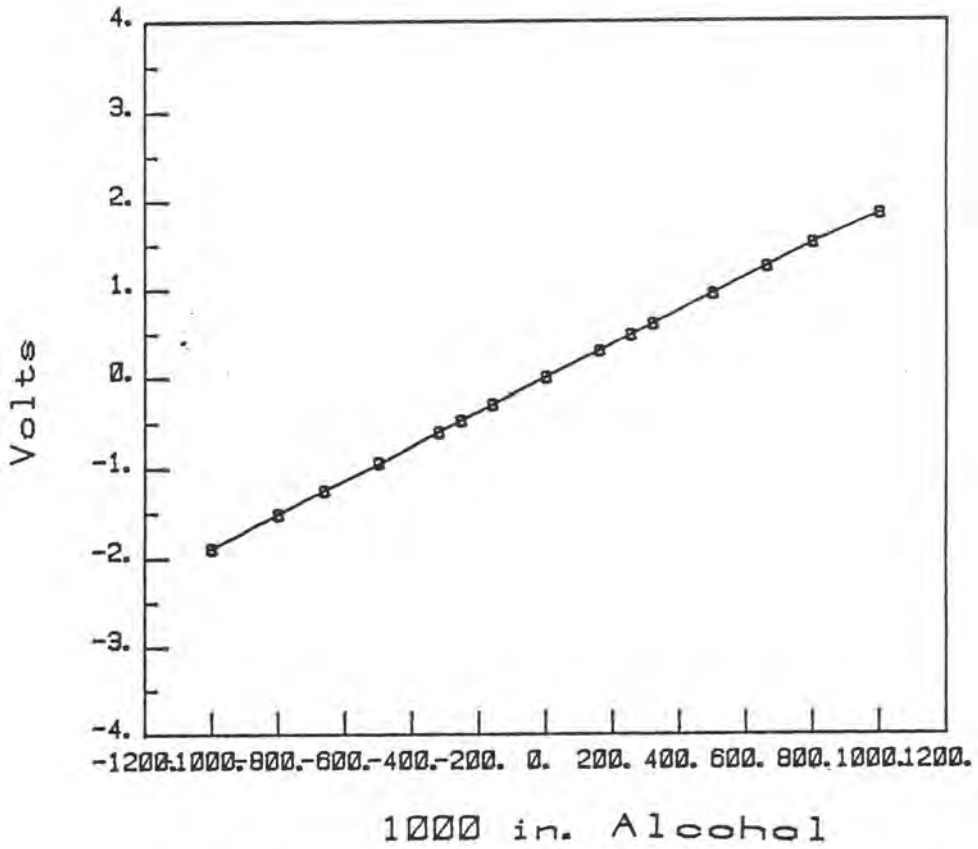

Figure 2.4. Calibration curve for pressure transducer.

The data aquisition and processing programs were made to first record the information about the experimental conditions such as date, time, location of the probe, temperature, zeros, tolerance of errors, reference pressure, number of measurment points, etc. With the help of the system subroutines, the programs can position the scanivalve, amplify the transducer signal, and digitize as well as store the data on the computer. To ensure that the mean data were stationary, the inputs to the analog-to-digital converter were low-pass filtered. A frequency of 50 Hz and two 8-second averaging periods, in between which there is a 8-second recess, were used. The procedures were repeated if the difference between the two averaged pressure readings was not within the tolerance of 0.02 volt or 2% error. The processing of the velocity data was made only after allowing an adequate recess for stablizing the pressure from the probe when the probe was moved to a new position.

2.3.2 Probe traverse

The probe traversing mechanism was designed such that it can be used for any probe with a straight stem. As shown in figure 2.5, it consists of two rack-and-pinion arrangements that enable the probe to be moved in the vertical and transverse directions in the duct. The probe

can be locked into position by the use of setscrews on the probe holder, which is designed so that three-dimensional rotation can be achieved. The mechanism is mounted on the upper wall of the tunnel by means of clamps. Centimeter scales are provided for the vertical and transverse directions. These allow positioning of the probe at the desired location within ±0.025cm. Initial positioning of the probe in the vertical direction was made by means of levels, using the bottom surface and the sidewall of the duct as guides. A setsquare lying on the top surface of the duct was used to align the probe tip along the line perpendicular to the transverse direction.

2.3.3 Five-hole probe

A five-hole pitot tube provides a simple and reliable means for measuring the magnitude and direction of the mean velocity. For the present experiment, the probe was mounted at known positions. It is not rotated at each point to obtain a null reading of two outer tubes, although Christianson and Bradshaw (1981) suggest the use of null-reading probes to reduce the influence of turbulence.

a) Probe geometry

A goose-necked five-hole pitot probe was made as shown in figure 2.6. Initially, the probe tip was located on the axis of the stem. However, preliminary measurements

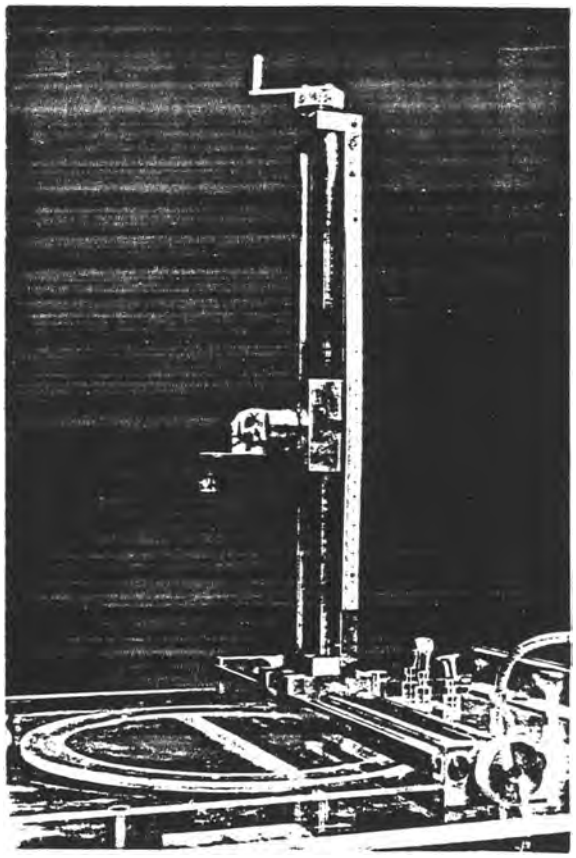

Figure 2.5. Configuration of probe traverse.

indicated interference from the stem when the probe tip was located close to the walls of the tunnel. Since this precluded accurate measurements in the important corner region, the probe was modified by cutting it at the stem and providing a 45 degree bend on the main stem. The two parts were then attached by means of screws. With the new arrangement the probe can be used to make measurements in the lower convex corner or the lower concave corner by simply turning the stem relative to the probe. The probe assembly used for the present measurements in the convex corner is shown in the figures 2.7 and 2.8.

The outside diameter of the probe tip is 3/16 inch (0.48cm). There is one hole at the center and four holes on each of the 45-degree-inclined planes. The holes are 1/64-inch diameter, and are identified as C (center), N (north), S (south), W (west) and E (east) when viewed from the front, as shown in figures 2.6 and 2.9. Inside the probe body, these holes are connected to five brass tubes which then lead to flexible plastic tubes in the stem.

b) Calibration of the probe

The five-hole probe was calibrated in the small, open-jet wind tunnel of the IIHR. The calibration was performed prior to cutting the probe stem as described above. Since the probe tip and the main body of the probe remained

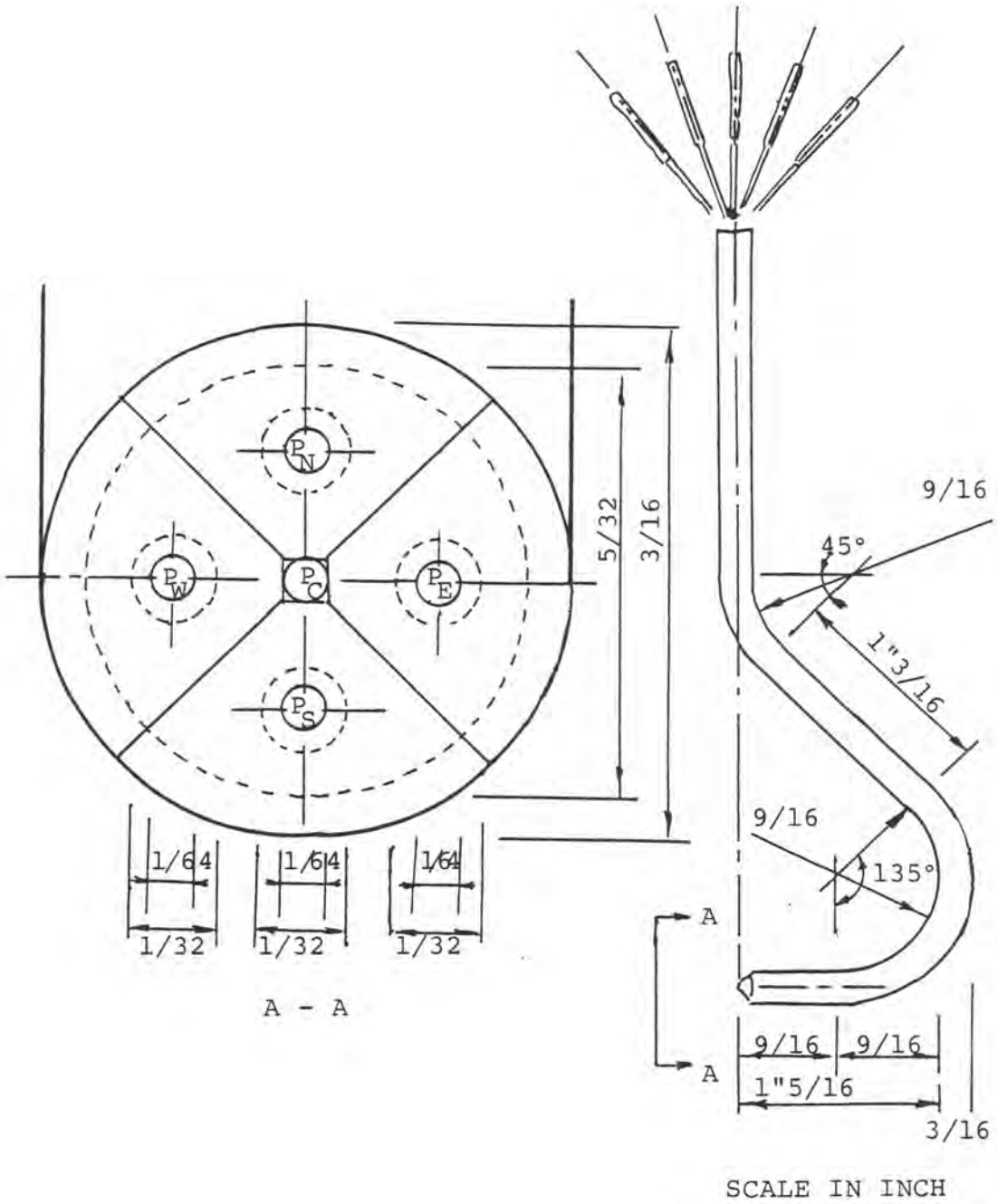

Figure 2.6. Geometry and notation of goose-necked five-hole probe.

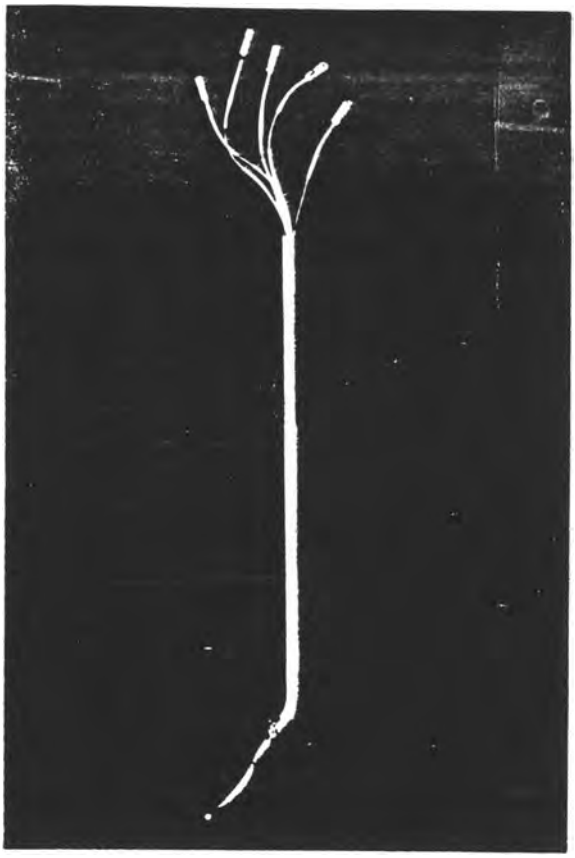

Figure 2.7. Front-view of the probe.

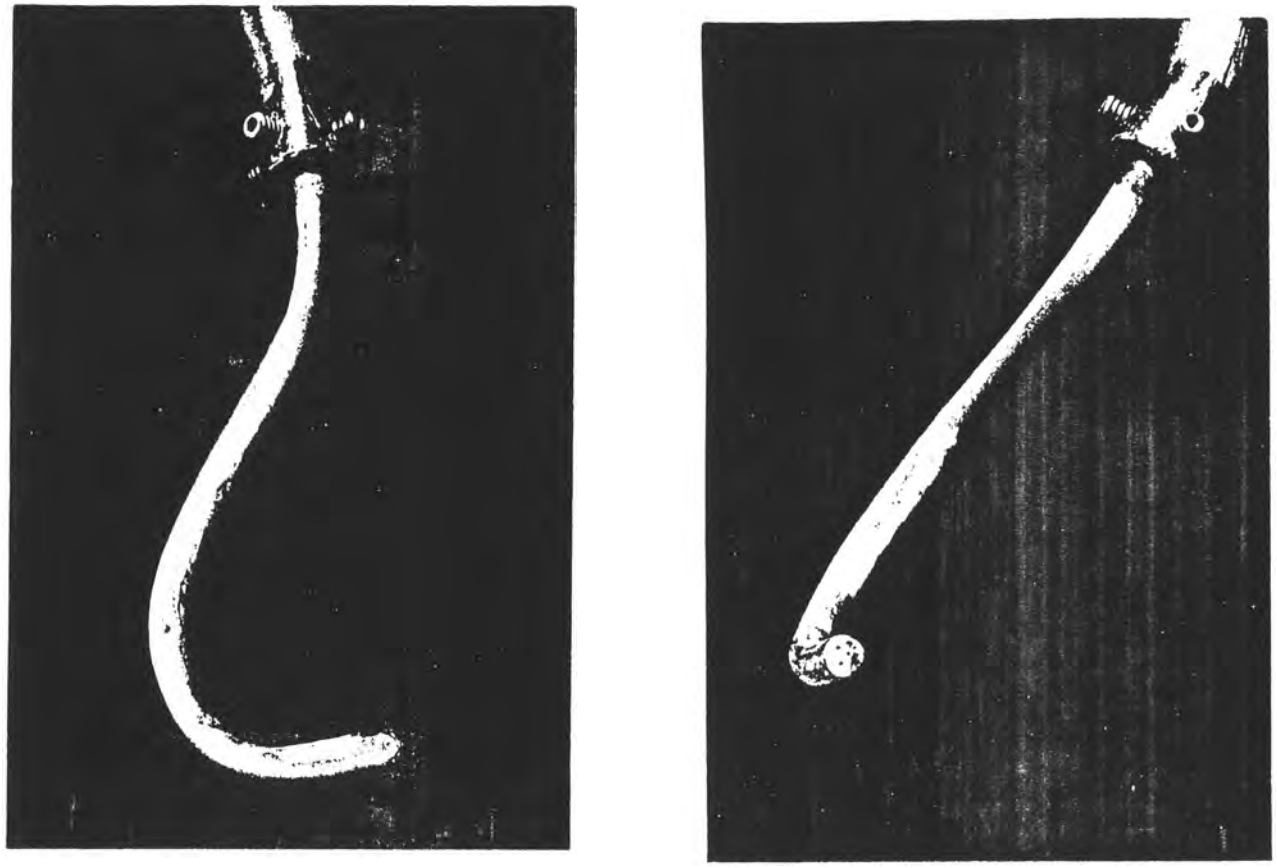

Figure 2.8. Configuration of the probe tip and junction.

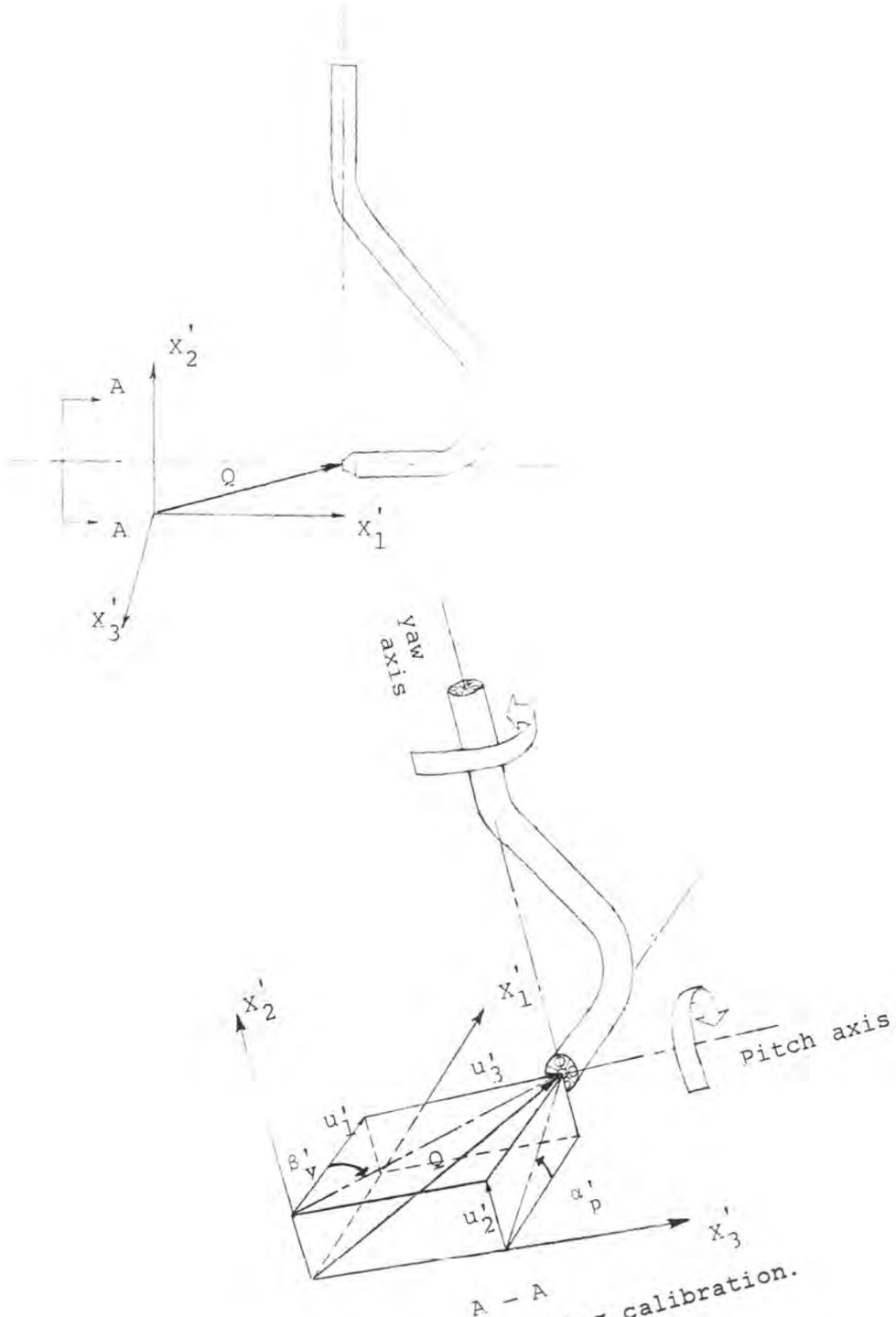

Figure 2.9. Coordinates during calibration.

unchanged, and the alignments were carefully checked, it was assumed that the calibration also remains unchanged. Spot checks of the calibration were later made in the straight portion of the test section to confirm this assumption. The computer-based data acquisition system was not used during the calibration. Instead, mean voltages from the transducer were obtained by using an integrating and averaging digital voltmeter. Usually it took about 10 to 60 seconds to reach steady readings due to the damping effect of the long thin tubes.

During calibration, the reference dynamic pressure was obtained from a standard Prandtl probe and was kept constant at 0.986 inch alcohol, and the reference total pressure was measured by a total pressure probe. Both probes were located at the rear of the five-hole probe such that there was no mutual interference. Two protractors, one mounted on the probe stem to record the yaw angle (β_y' in figure 2.9), and another mounted on the probe support to record the pitch angle (α_p' in figure 2.9), were used. With the reference dynamic pressure kept constant, the probe was set at several positions with known pitch and yaw angles. The pressure differences between each hole and the total pressure probe were measured. The calibration was carried out in the range of -30 to +30 degrees in yaw and pitch, with an increment of 2.5 degrees.

The following yaw and pitch calibration coefficients are then defined (see figures 2.6 and 2.9)

$$FM = 4\ P_C - (P_N + P_S + P_W + P_E)$$

$$R = FM / FM0$$

$$FK = (P_W - P_E) / FM$$

$$FL = (P_S - P_N) / FM$$

where P_C, P_N, P_S, P_W and P_E are the pressure readings of the C, N, S, W and E holes, and FM0 is the value of FM at the null position. Figure 2.9 shows the angles of yaw and pitch when the probe was calibrated. The yaw and pitch angles are defined such that a positive angle corresponds to a positive component of resultant velocity in the probe coordinates (x_1', x_2', x_3') shown in figure 2.9. The coefficient FK primarily indicates the yaw angle while FL indicates the pitch angle. The ratio R represents the joint influence of yaw and pitch on the coefficient FM, which is sensitive to the dynamic pressure.

Figure 2.10 shows a contour plot of the ratio R over the entire range of yaw and pitch calibration angles. The values of R>1 at some points with small positive yaw angles indicate a velocity greater than that at the null position, assuming ideal construction and alignment of the probe. Figure 2.11 shows the variation of FK versus FL for different yaw and pitch angles. It is seen that the relation between FK and FL can be approximated by suitable polynomials. For some large angles of pitch and yaw (typically, greater than 25 degrees), these coefficients show considerable scatter. This may be due to separation from the probe tip. For the present experiments in the corner flow, however, the coefficients were less than 3.0 and therefore the results are not subject to this scatter. It was also found that the coefficient FM0 is a linear function of the reference dynamic pressure, $1/2\ \rho\ Q^2$, where Q is the resultant velocity, as shown in figure 2.12.

The effects of turbulence, wall-proximity and mean shear on the probe readings have not been taken into account in the subsequent use of the above calibrations in the corner flow experiments because correction procedures for five-hole probes, in general, and for the geometry used here, in particular, are not available. These effects should, however, be borne in mind in any detailed evaluations of the data.

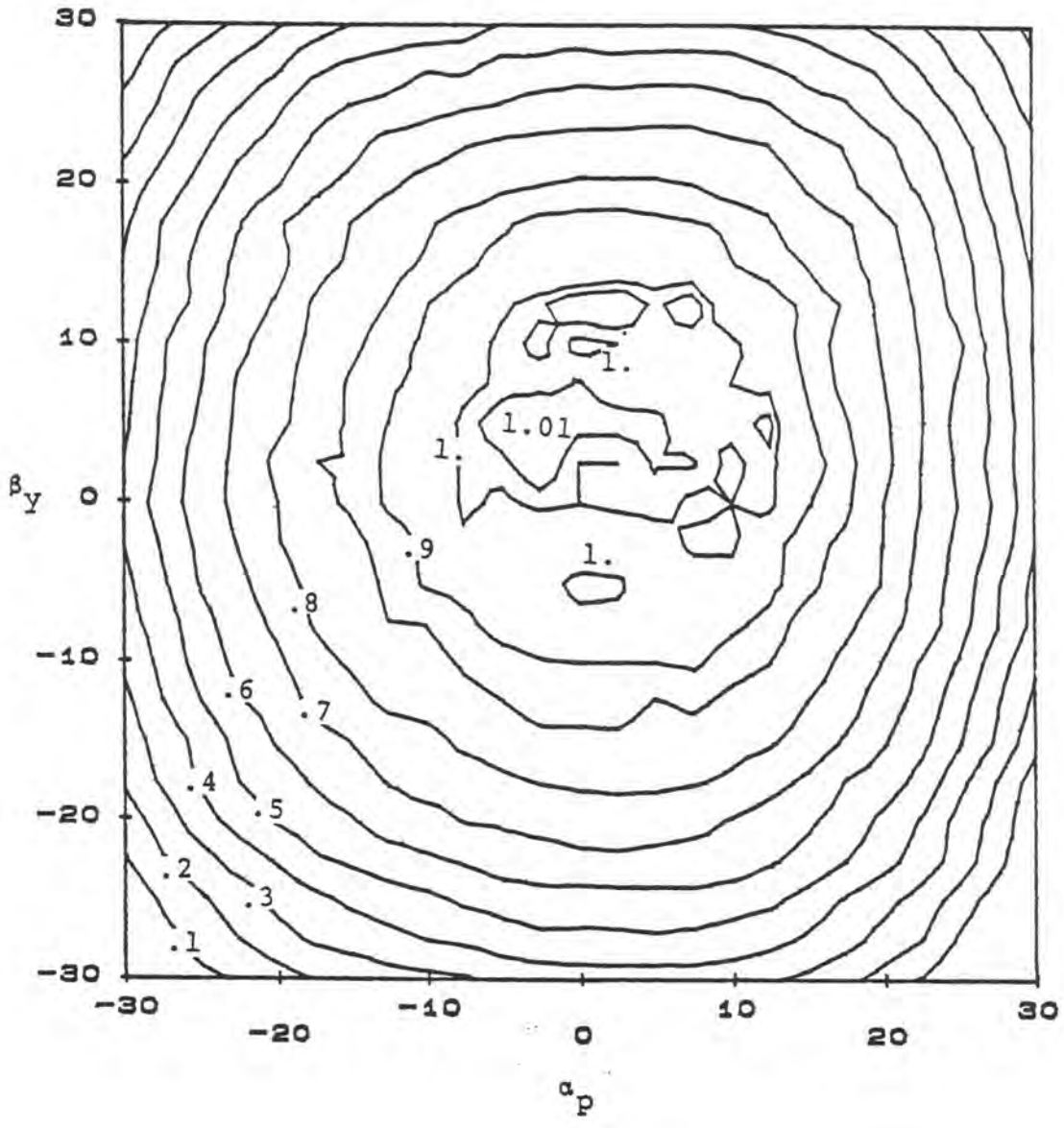

Figure 2.10. Contour plot of ratio R.

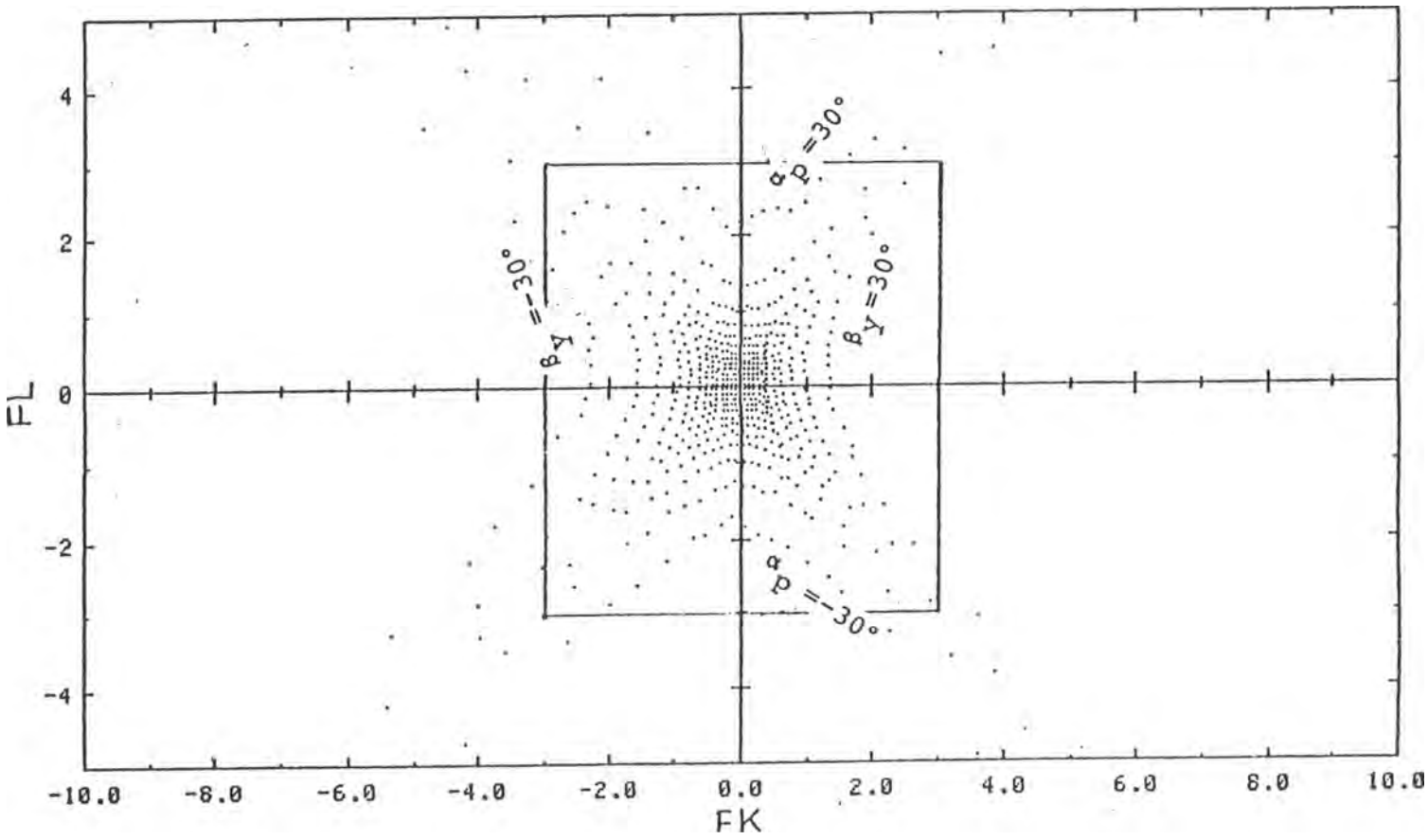

Figure 2.11. Plot of probe calibration coefficients FK versus FL.

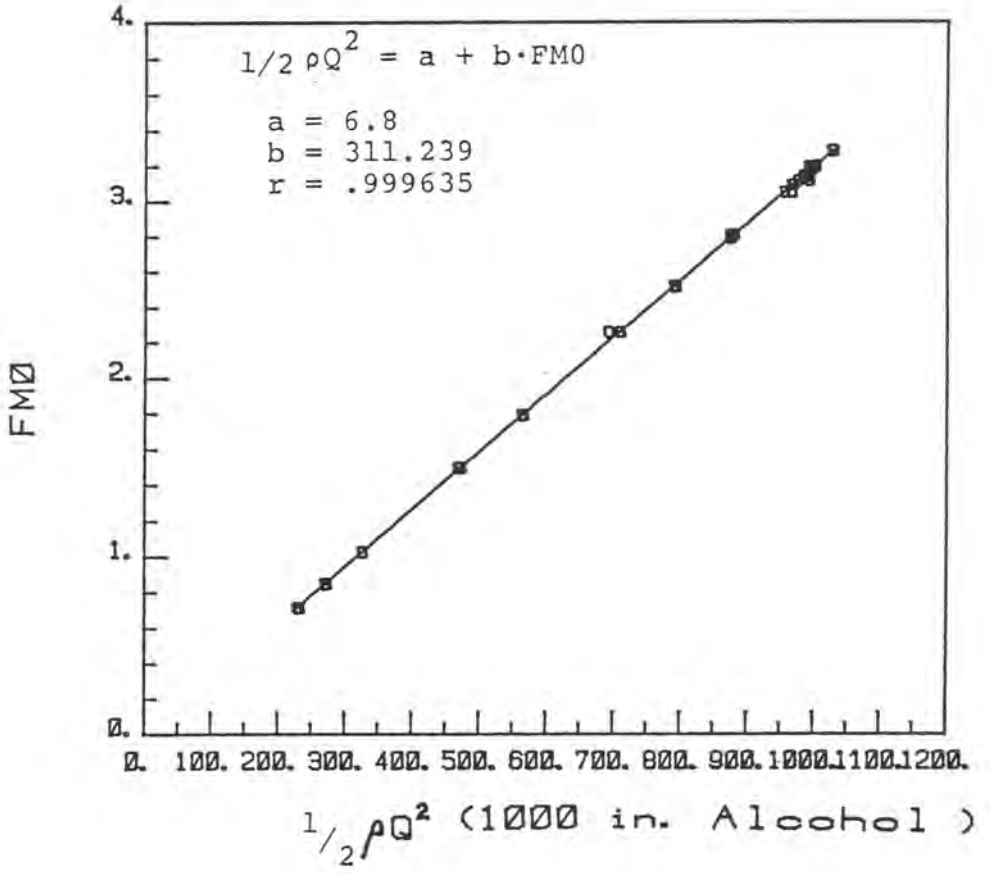

Figure 2.12. Probe calibration curve.

2.4 Experimental procedures

2.4.1 Tunnel reference conditions

In the experiments in the curved-duct tunnel, the first measurement section P01 (figure 2.2) is used as the reference station. Since the pressure and velocity are essentially constant at this section, the pressure measured by the top center tap (hole no. 4 on the top surface in figure 2.3) is used as the reference pressure, Pref, and the velocity at the center of this cross section is used as the reference velocity, Uref.

A relationship between the pressure difference ($P-P_{ref}$), where P is the pressure at the beginning of the contraction, and the reference dynamic pressure, $1/2\,\rho U_{ref}^2$, (i.e. the "tunnel calibration") was established by measuring the latter by a standard Prandtl probe. This is shown in figure 2.13. The probe was then removed to avoid disturbances propagating downstream, but the pressure difference ($P-P_{ref}$) was monitored by a manometer and kept constant at 0.986 (±0.03) in alcohol in all experiments. With the variations in temperature (and density) taken into account, the reference velocity was 18.0 (±0.25) m/s.

In the presentation of the data, all quantities are made dimensionless with the reference conditions noted above. Thus, the pressure p at any point is quoted in terms of a pressure coefficient

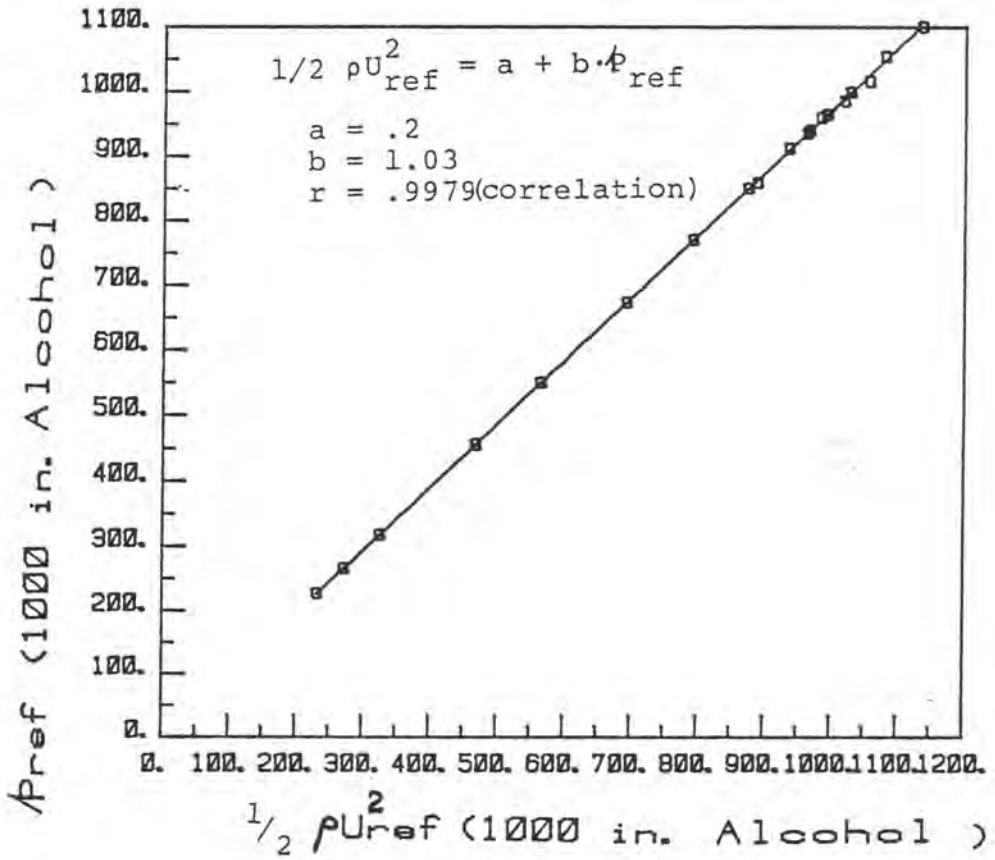

Figure 2.13. Tunnel calibration curve.

$$C_p = \frac{P - P_{ref}}{\frac{1}{2} \rho U_{ref}^2}$$

and the velocity components are nondimensionalised by U_{ref}.

2.4.2 Velocities from five-hole probe

A noniterative calibration method was utilized to obtain the yaw and pitch angles, and the velocity components, from the five-hole probe calibrations described in the previous section. The pitch and yaw coefficients, FL and FK, respectively, were approximated by fourth-order least-square polynomials. Let α_p' and β_y' be the pitch and yaw angles of the resultant velocity corresponding to the probe axes. Thus, for constant pitch and yaw angles, the approximated coefficients FL' and FK' from the values of FK and FL of the calibration data (discrete points in figure 2.14) can be expressed by

$$FL'(m) = \sum_{k=0}^{4} A(m,k) \; FK^k(m)$$

$$FK'(n) = \sum_{k=0}^{4} B(n,k) \; FL^k(n)$$

where m,n are related to $\alpha_p'(m)$ and $\beta_y'(n)$ (i.e. calibration angles). The resulting polynomials are shown as

the solid and dashed lines in figure 2.14. Each of these is associated with a constant angle and the increment is 2.5 degrees.

With the probe located at any point, the experimental values of FL and FK are first determined from the measured values of P_C, P_N, P_S, P_W and P_E. These are then used, together with the known polynomials, to determine the location of the operation point in the calibration chart (see figure 2.15). Then, the unknown pitch and yaw angles are found by interpolation, i.e.

$$\alpha_p' = \frac{a}{a+b}\,\alpha(m) + \frac{b}{a+b}\,\alpha(m-1)$$

$$\beta_y' = \frac{a}{a'+b'}\,\beta(n) + \frac{b}{a'+b'}\,\beta(n-1)$$

where $a = FL - FL'(m-1)$, $b = FL'(m) - FL$

and $a' = FK - FK'(n-1)$, $b' = FK'(n) - FK$.

The magnitude of the velocity is obtained by first determining the ratio R from the contour plot of figure 2.10, again by linear interpolation as shown in figure 2.16, i.e.

$$R = \Delta\alpha\cdot\Delta\beta\cdot\left(a\cdot b\cdot R(m,n) + a\cdot(1-b)\cdot R(n,m-1) + (1-a)\cdot b\cdot R(n-1,m) + (1-a)\cdot(1-b)\cdot R(n-1,m-1) \right)$$

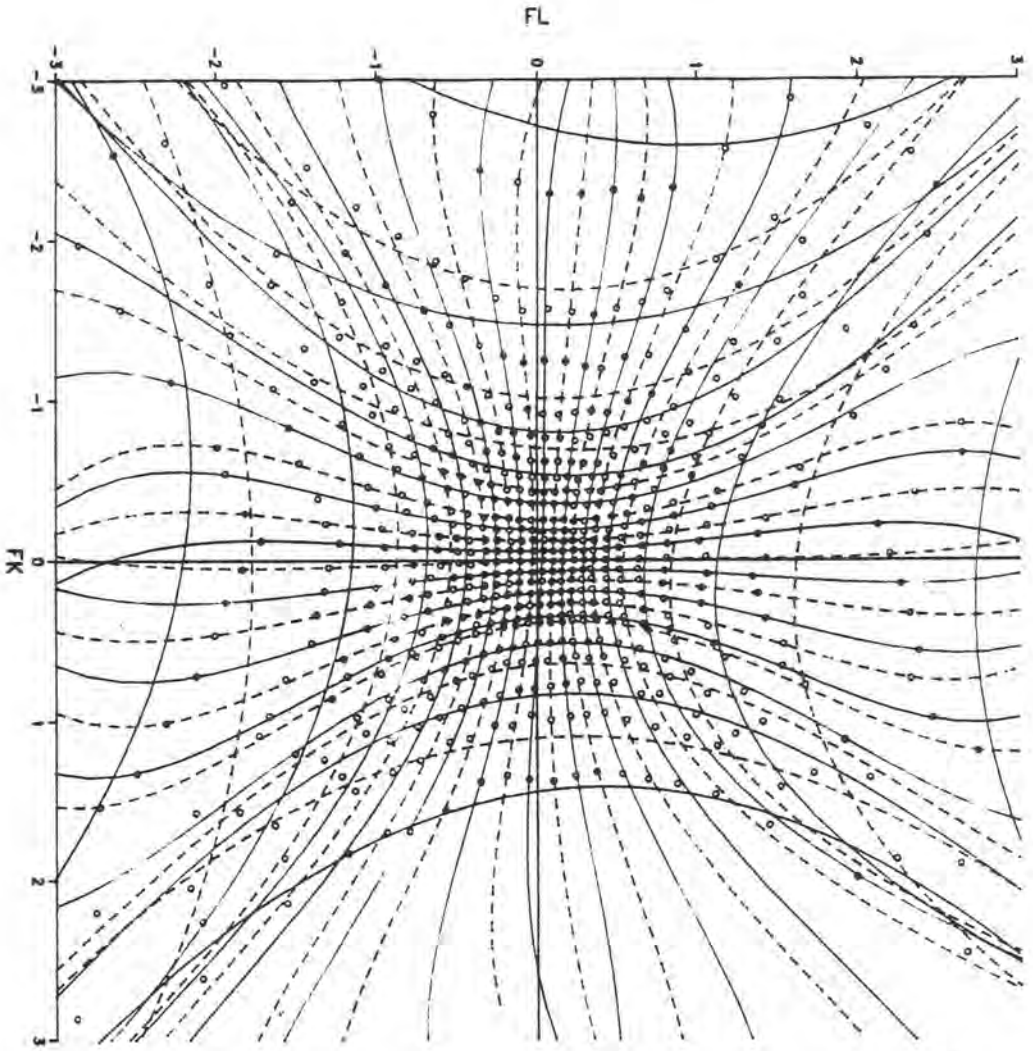

Figure 2.14. Approximated calibration coefficients FK versus FL. (discrete points for data and continuous lines for approximated polynomials with an increment of 2.5 degree).

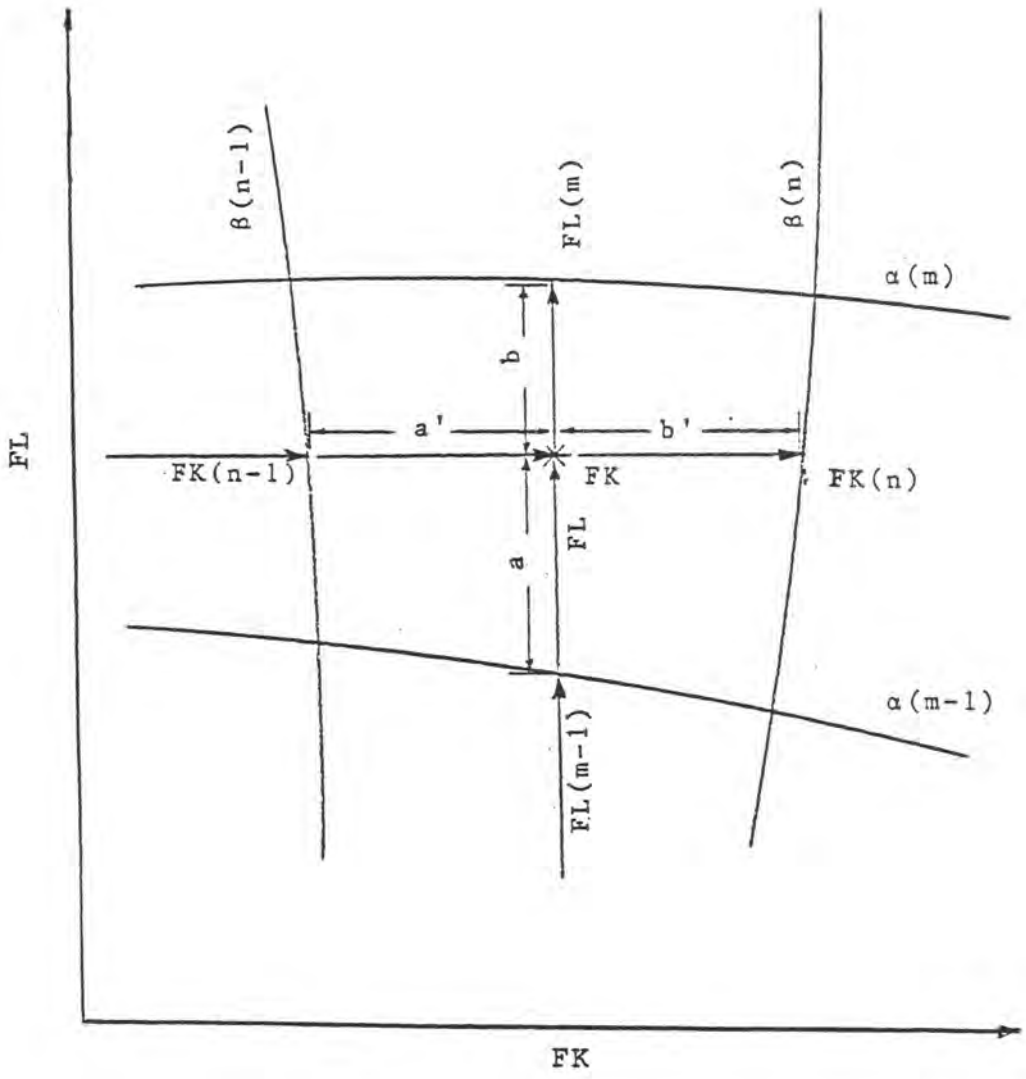

Figure 2.15. Interpolation of coefficients to find the unknown angles.

where $a = [\ ^{\alpha}p' - \alpha(m-1)\ ] / \Delta\alpha$, $b = [\ \beta y' - \beta(n-1)\ ] / \Delta\beta$

and $\Delta\alpha = \alpha(m) - \alpha(m-1)$, $\Delta\beta = \beta(n) - \beta(n-1)$

Since FMO=FM/R, the magnitude of the velocity Q can be interpolated from the calibration curve of figure 2.12.

The resultant velocity components u_1', u_2', u_3' corresponding to the probe axis (x_1', x_2', x_3') can be obtained from (see figure 2.17)

$$u_1' = \left(\frac{Q^2}{1 + \tan^2 \alpha_p' + \tan^2 \beta_y'} \right)^{1/2}$$

$$u_2' = u_1' \cdot \tan \alpha_p'$$

$$u_3' = u_1' \cdot \tan \beta_y'$$

For the measurements near the inner wall, reported here, the angle between the probe axis and the probe stem is as shown in figure 2.17. Therefore, the velocity components (u_1, u_2, u_3) corresponding to the duct coordinates (x_1, x_2, x_3) can be obtained by rotation of the coordinate system, i.e.

$$\begin{aligned} u_1 &= u_1' \\ u_2 &= u_2' \cos\gamma - u_3' \sin\gamma \\ u_3 &= u_3' \cos\gamma + u_2' \sin\gamma \end{aligned}$$

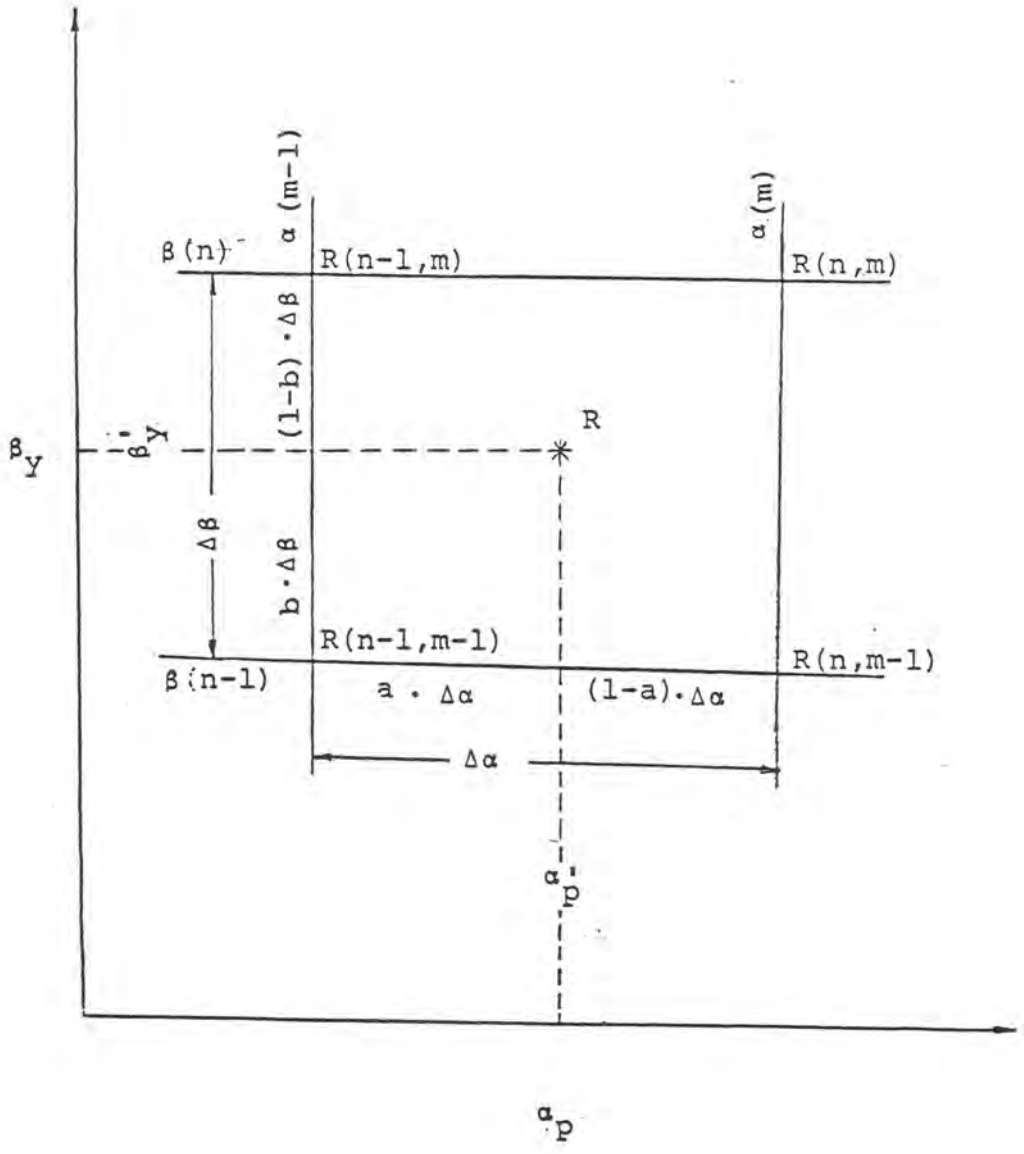

Figure 2.16. Interpolation in ratio R for the velocity.

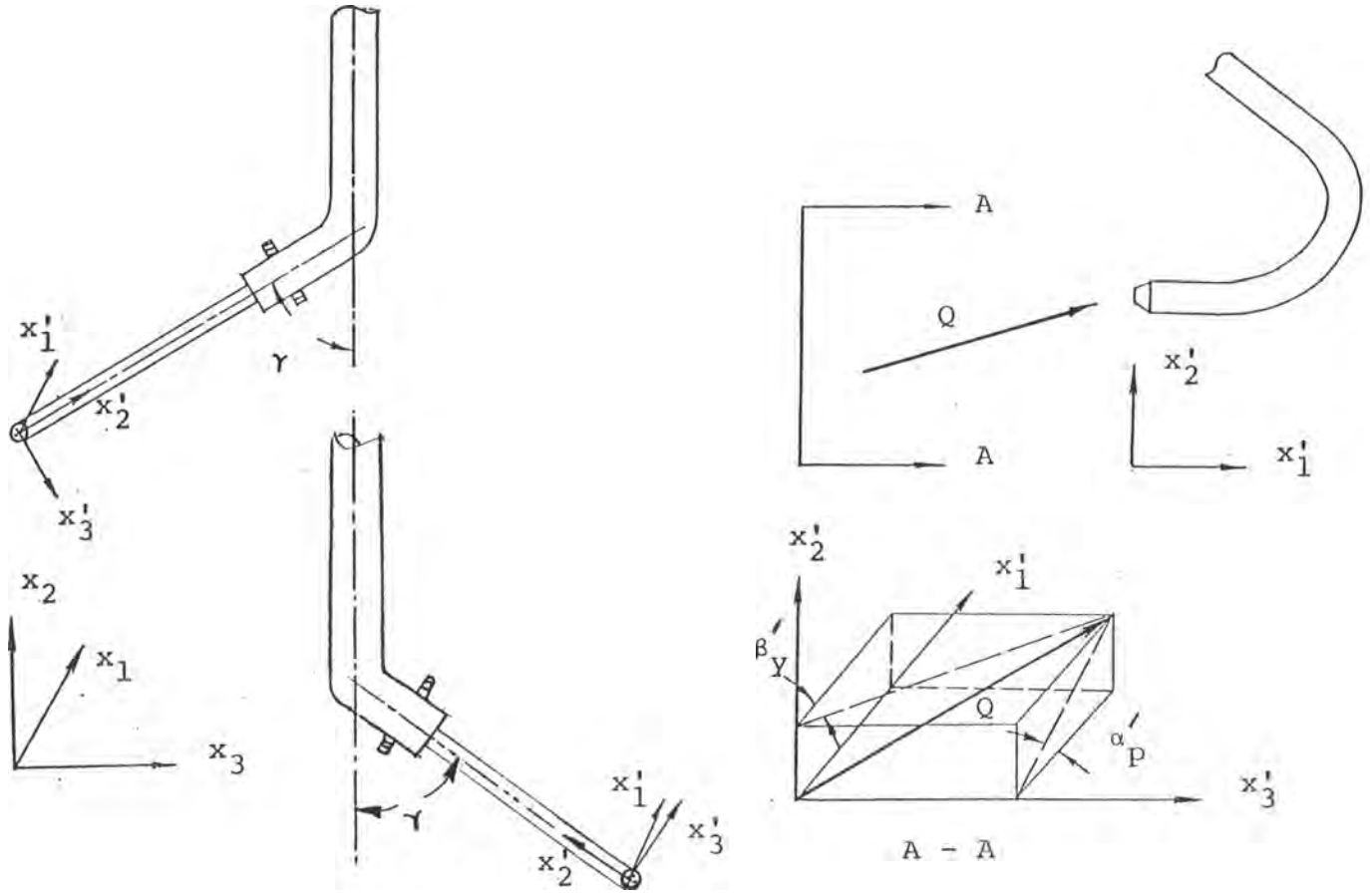

Figure 2.17. Probe and duct coordinates.

For measurements near the outer wall (which may be made later on), the corresponding expressions to be used are

$$u_1 = u_1'$$

$$u_2 = u_3' \sin\gamma + u_2' \cos\gamma$$

$$u_3 = u_3' \cos\gamma - u_2' \sin\gamma$$

As noted earlier, the velocity components are nondimensionalized by the reference velocity, i.e.

$$U_1 = u_1 / U_{ref}$$

$$U_2 = u_2 / Uref$$

$$U_3 = u_3 / Uref$$

and the nondimensional resultant velocity is

$$Q^* = Q / U_{ref} = \left(\frac{\frac{1}{2}\rho Q^2}{\frac{1}{2}\rho U_{ref}^2} \right)^{1/2}$$

Also, the yaw and pitch angles in duct coordinates are

$$\alpha_\rho = \tan^{-1}(u_2/u_1), \qquad \beta_y = \tan^{-1}(u_3/u_1).$$

2.5 Results and discussion

2.5.1 Initial conditions

Since the conditions at the initial station in the straight duct (station P01 for pressure, and station A for the velocity field) are used as the reference conditions for the subsequent data, and also as the initial conditions for the calculations presented in the next chapter, it is useful to first review the measurements at these sections. Figure 2.18 shows the wall pressure distribution around the duct at station P01. It is seen that the pressure is constant (Cp = 0) all around and consequently there should be no pressure-driven secondary motion. This is confirmed by the velocity field measured by the five-hole probe at station A.

Figure 2.20 shows the distribution of the longitudinal velocity component U1 along 15 normals (A1 through A15 in figure 2.19) to the bottom wall in the range of $x_3/W < 0.7$. The thickness of the boundary layer on the walls is of the order of 0.1 H (3 cm) and outside the boundary layer the velocity is essentially constant. Thus, we have a developing flow further downstream. The components U2 and U3 of the secondary motion are shown in figures 2.21 and 2.22, respectively. It is seen that these are at most of the order of 0.03 U_{ref} close to the wall, and much smaller

elsewhere. The somewhat larger values near the walls may be attributed to possible wall-interference or shear effects on the probe rather than to any secondary motion. In any case, the cross-flow angle implied by the largest value of 0.03 U_{ref} is of the order of 1.7 degrees, which is close to the accuracy with which the probe can be located geometrically in the duct. The results at the inlet station are therefore indicative of the overall reliability and accuracy of the measurements made with the five-hole probe.

2.5.2 Static pressure measurements

In most recent experiments in curved ducts, emphasis has been placed on the velocity field with little attention to the associated pressure field, although it is the latter that dictates the secondary motion and is of crucial importance in determining the success of the calculation procedures. In view of this, a special effort has been made in the present experiments to measure wall pressure distribution by closely-spaced taps in the corner region.

The pressure distributions measured at five sections (labeled P02, P1, P2, P3, P4) downstream of the inlet section P01 (figure 2.2) are shown in figures 2.23, 2.24, 2.25, 2.26 and 2.27. At station P02, which is in the straight part of the duct some distance downstream of the initial station, the pressure is still constant around the

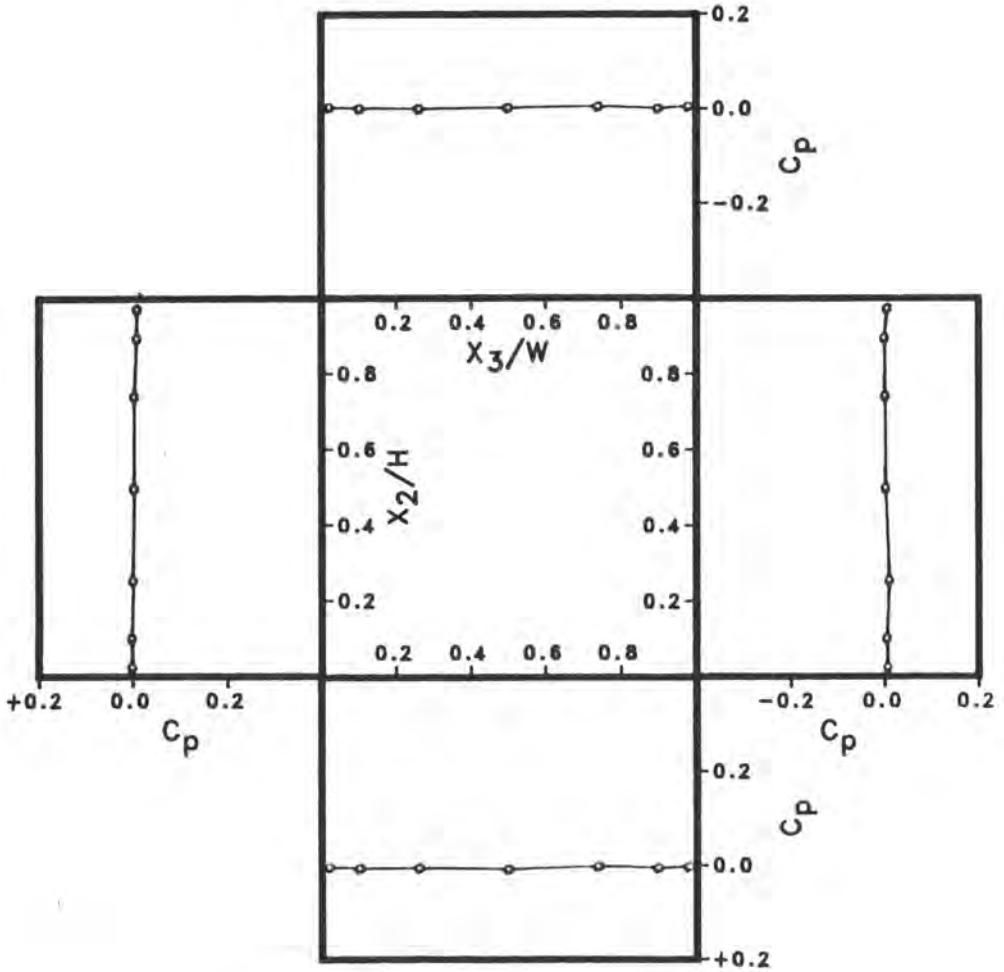

Figure 2.18. Pressure distribution at station P01.

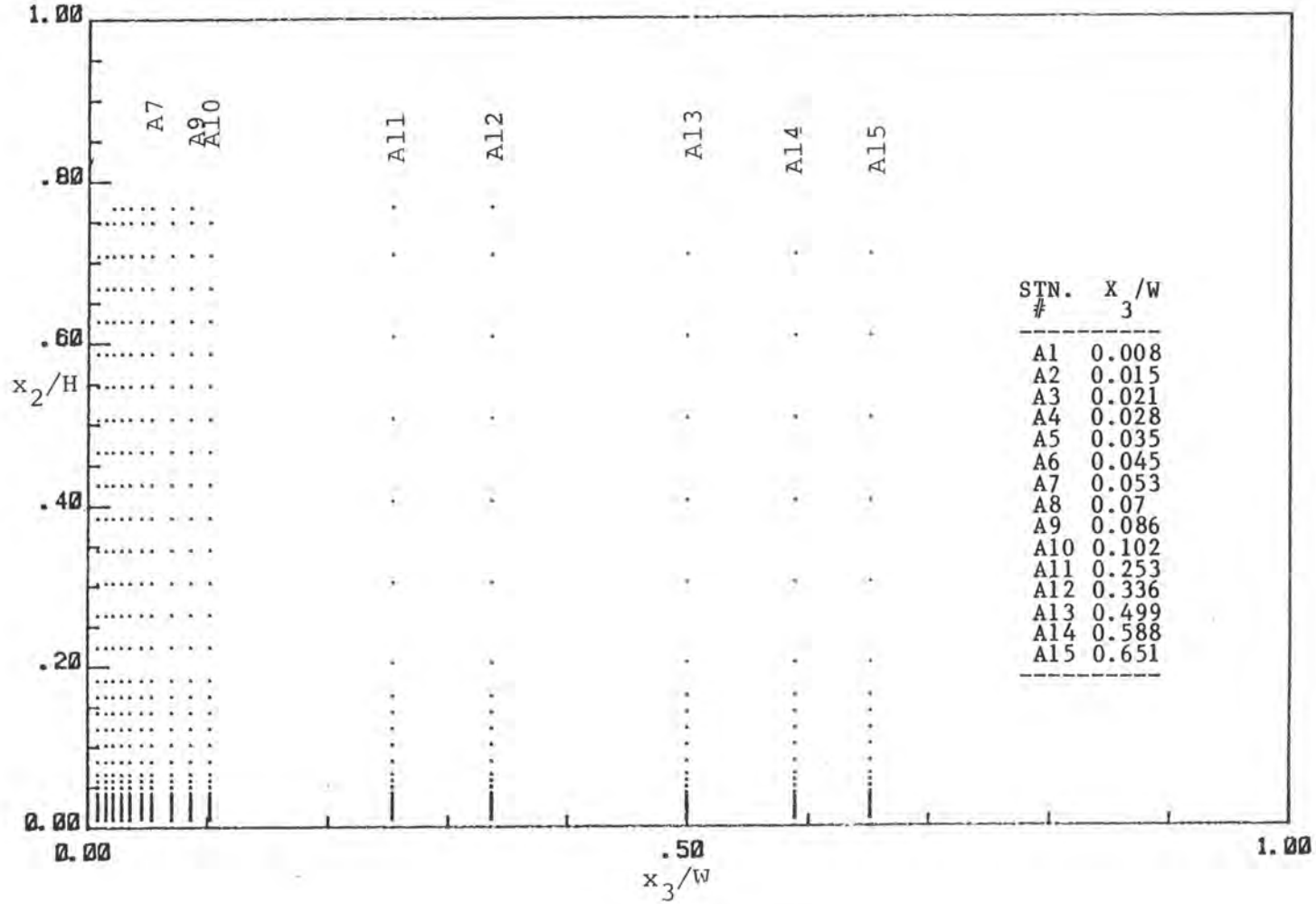

Figure 2.19. Grid distribution at station A.

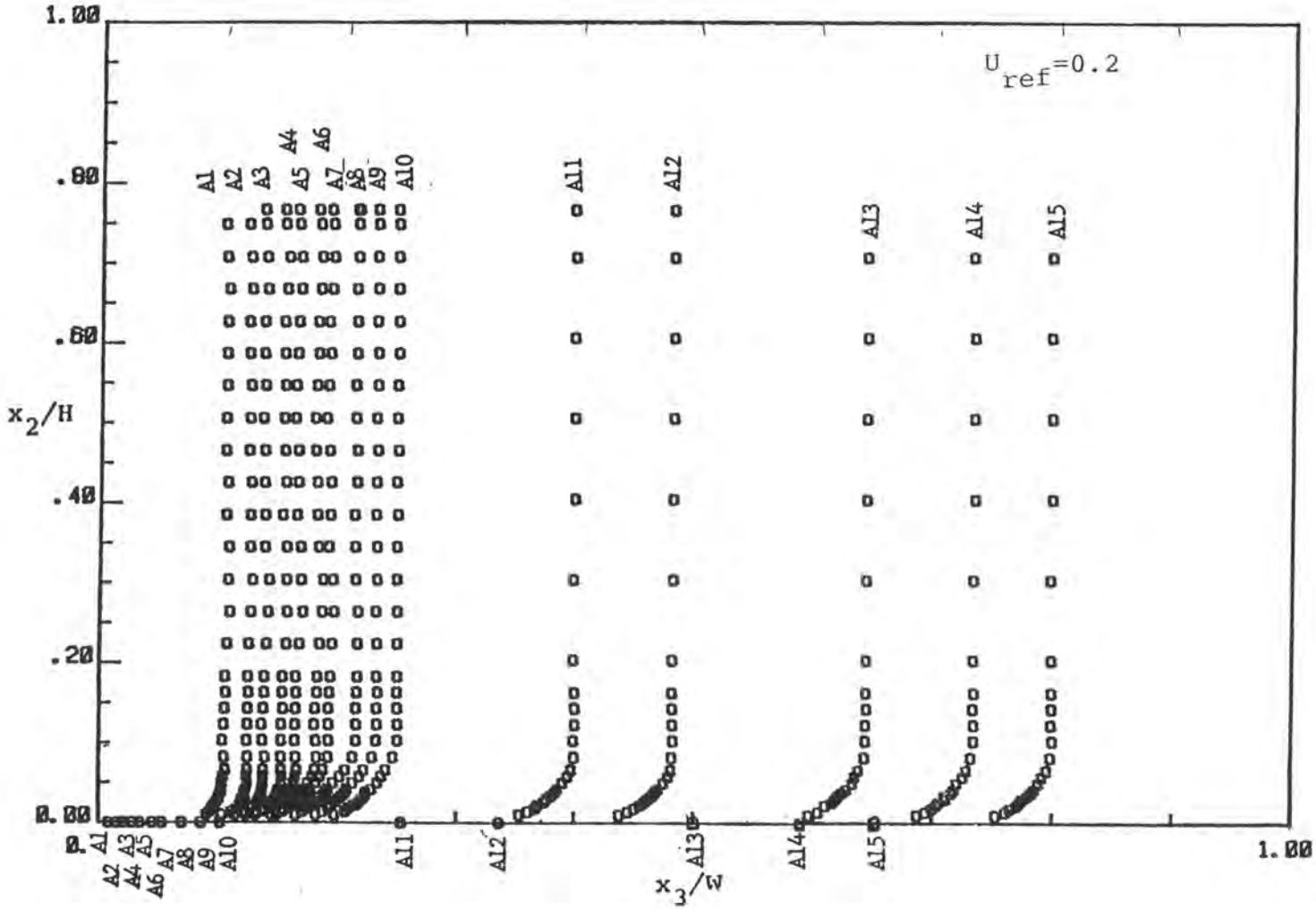

Figure 2.20. U_1 velocity component at station A.

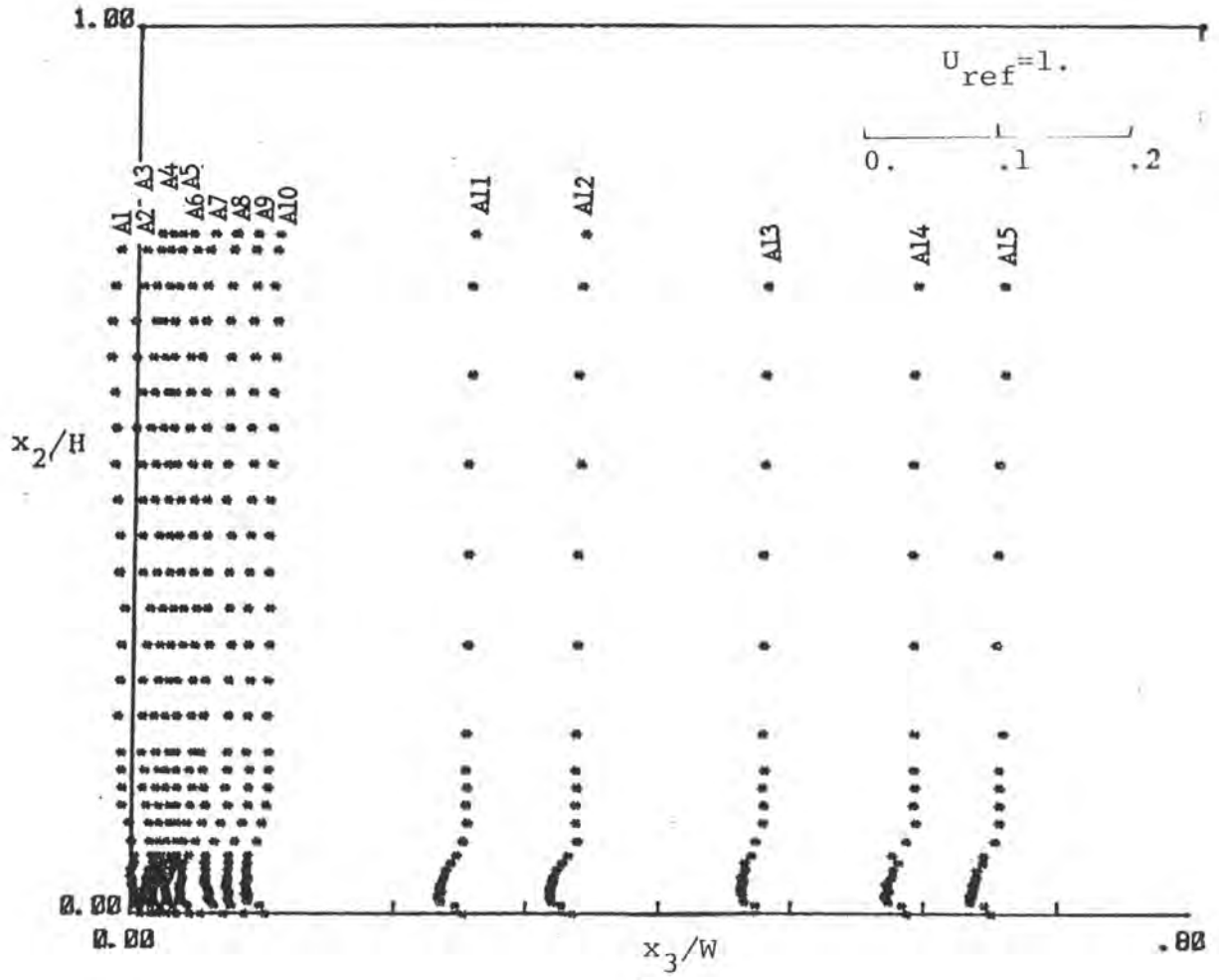

Figure 2.21. U_2 velocity component at station A.

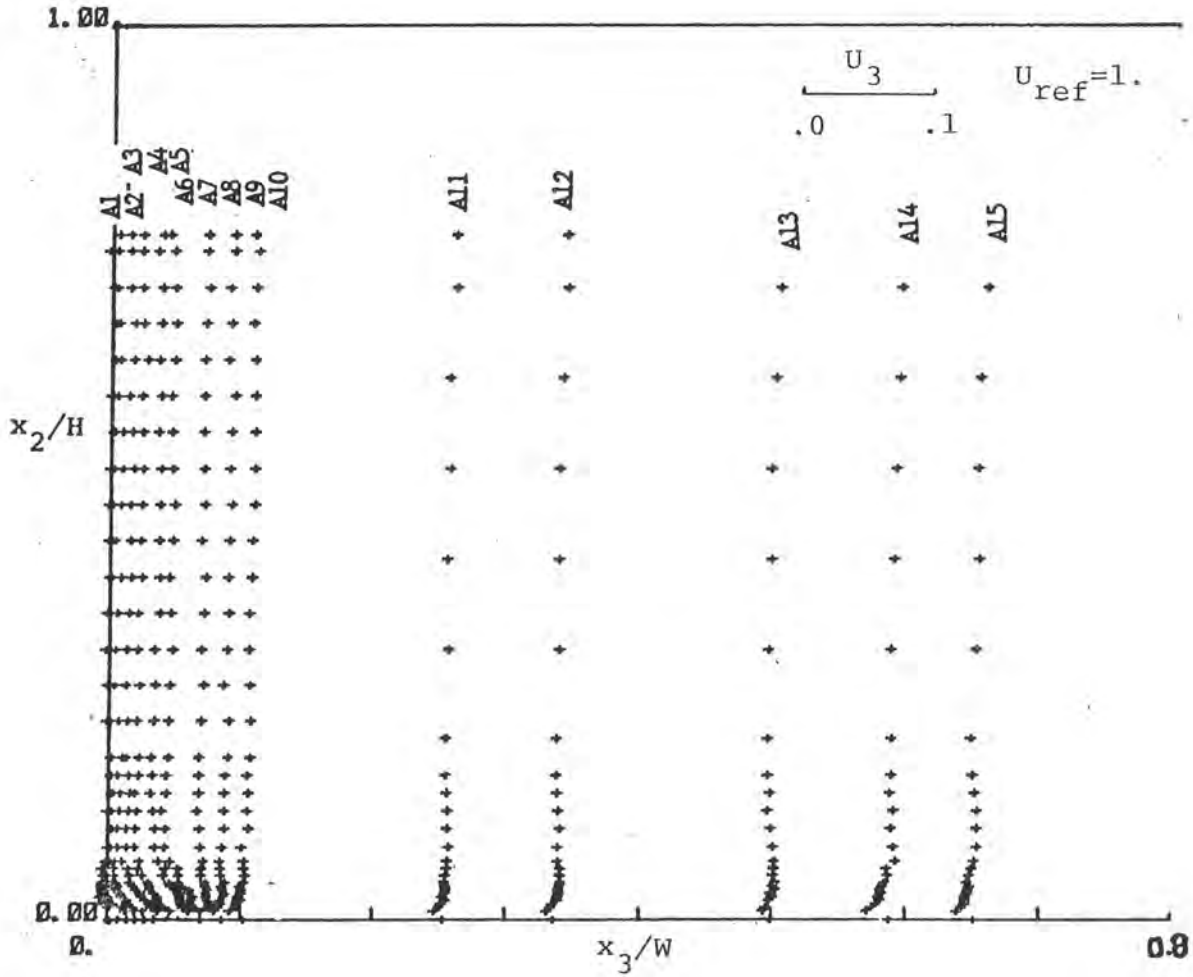

Figure 2.22. U_3 velocity component at station A.

duct but there is a small pressure drop from station P01. Thus, the upstream effect of the curvature is still not felt at this station. In the curved part of the duct, we observe an almost linear drop in pressure from the outer to the inner corner on the top wall. The pressure on the inner convex wall and the outer concave wall remains nearly constant but systematic changes occur in the inner corner on the flat and convex walls as the flow progresses downstream (see figures 2.26 and 2.27). It is seen that there is an initial decrease in pressure with distance from the corner before the pressure rises along the top flat wall and remains constant on the convex wall. This may indicate the presence of a corner vortex. All figures show that the pressure distributions on the convex and concave walls are symmetric about the horizontal centerplane and therefore the lack of pressure data on the bottom wall is not a major deficiency.

The pressure distributions on the top wall at all six measuring stations are shown again in figure 2.28 to observe the evolution of the pressure field. We note two special features. First, we see a slow evolution of the radial pressure gradient (dCp/dx_3) as the flow enters the bend. The gradient over the central part of the outer wall increases from station P1 to reach a nearly constant value at stations P3 and P4. Thus, the pressure field responds

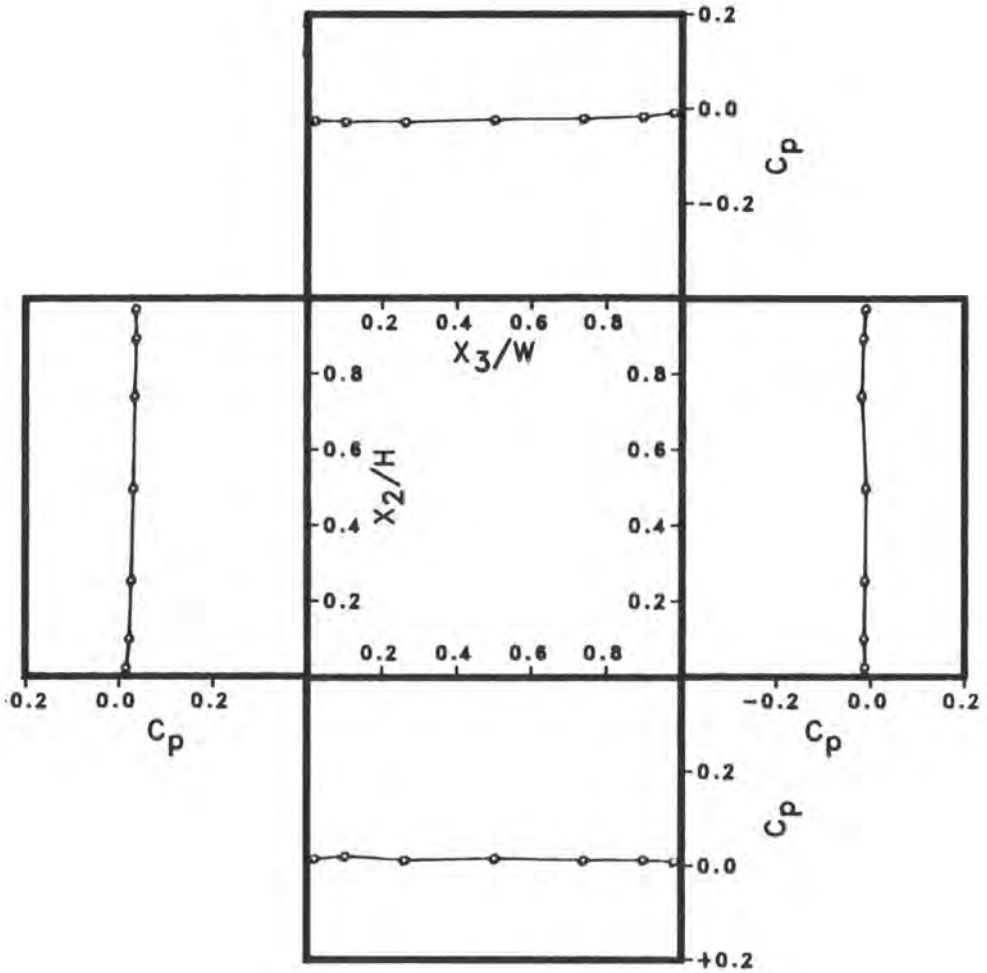

Figure 2.23. Pressure distribution at station P02.

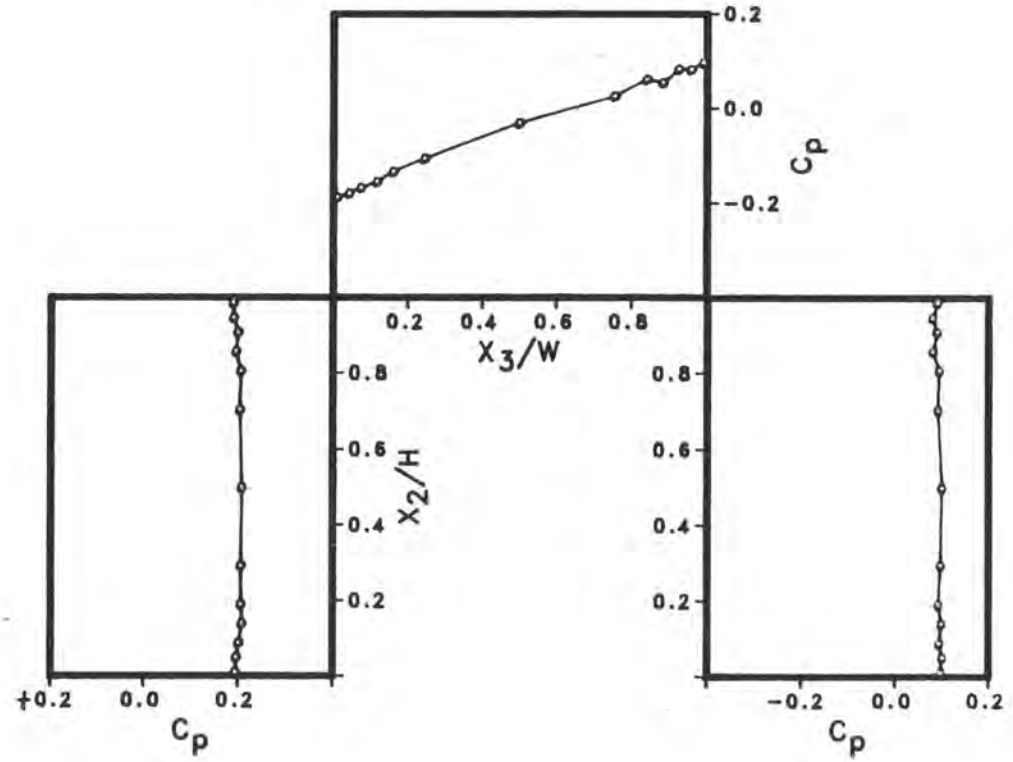

Legend

• P1

Figure 2.24. Pressure distribution at station P1.

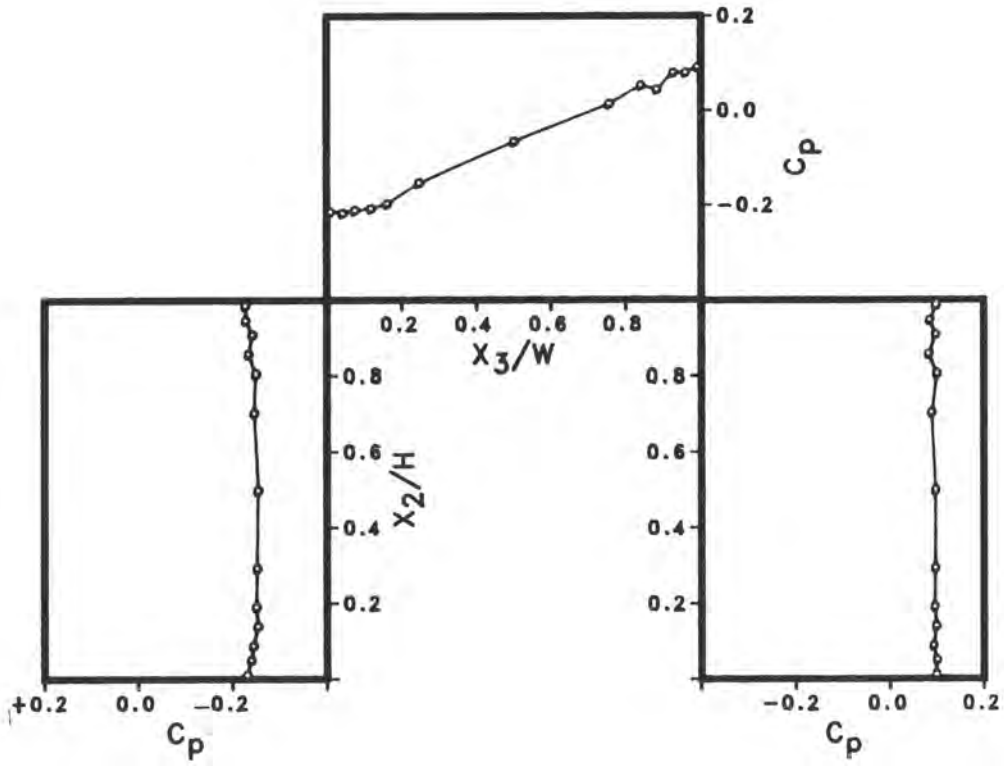

Legend

P2

Figure 2.25. Pressure distribution at station P2.

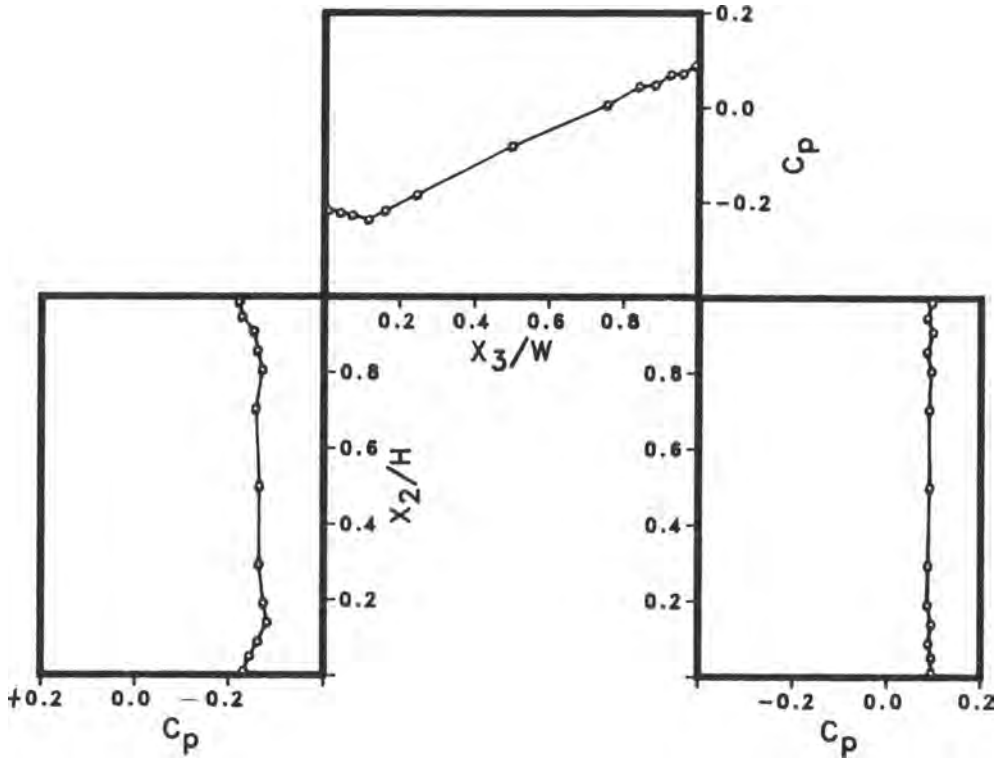

Legend

P3

Figure 2.26. Pressure distribution at station P3.

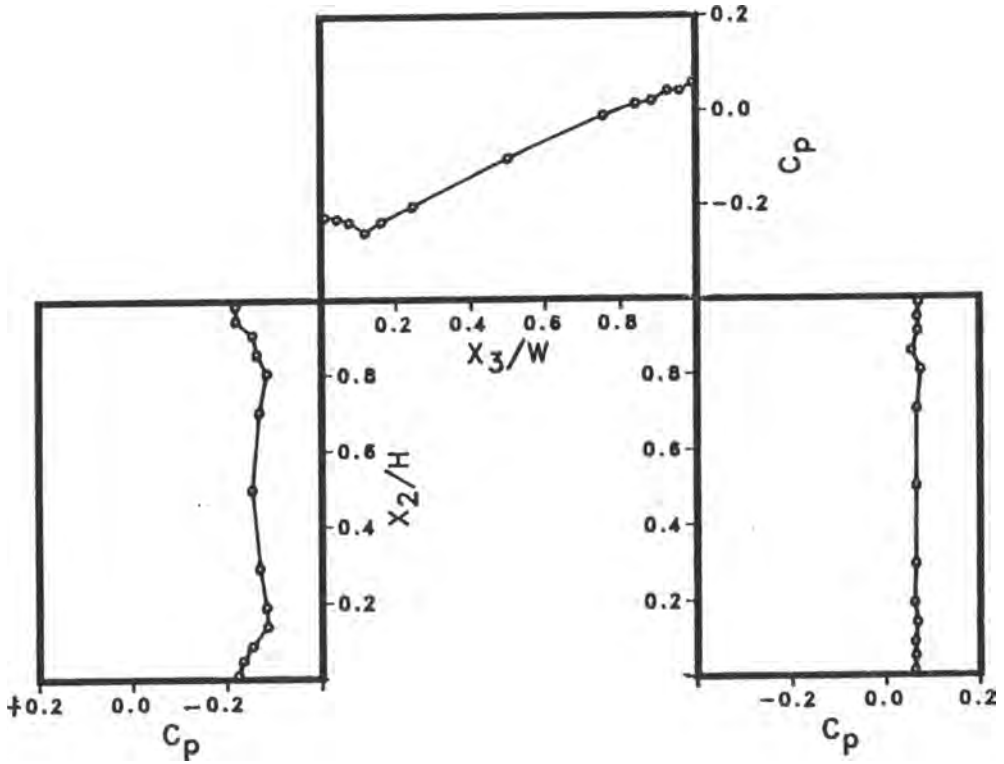

Legend

• P4

Figure 2.27. Pressure distribution at station P4.

rather slowly to the imposed change in duct curvature. Second, the changes in the pressure distribution near the inner corners are now clearly visible. We see the development of a small region ($x_3/W < 0.12$) in which the pressure remains nearly constant at station P2 and decreases in a characteristic fashion at stations P3 and P4. These features are presumably associated with the growth of the corner vortex. It is also interesting to note that similar changes are not found in the concave corner between the outer and top walls.

Finally, the longitudinal variations of pressure along some typical lines on the duct walls are shown in figure 2.29. It is seen that the pressure drops monotonically along the center of the top wall. This, along with the nearly constant pressure observed over the central portions of the inner and outer walls, indicates that the variation of pressure in the vertical direction in the duct is negligible except in the neighborhood of the convex corners. The longitudinal variation of pressure along the centers of the inner and outer walls indicates strong favorable and adverse streamwise pressure gradients associated with the abrupt change in wall curvature between the straight and curved ducts. The spacing of the pressure measuring stations in the streamwise direction is not small enough to define this region precisely but it exists, approximately,

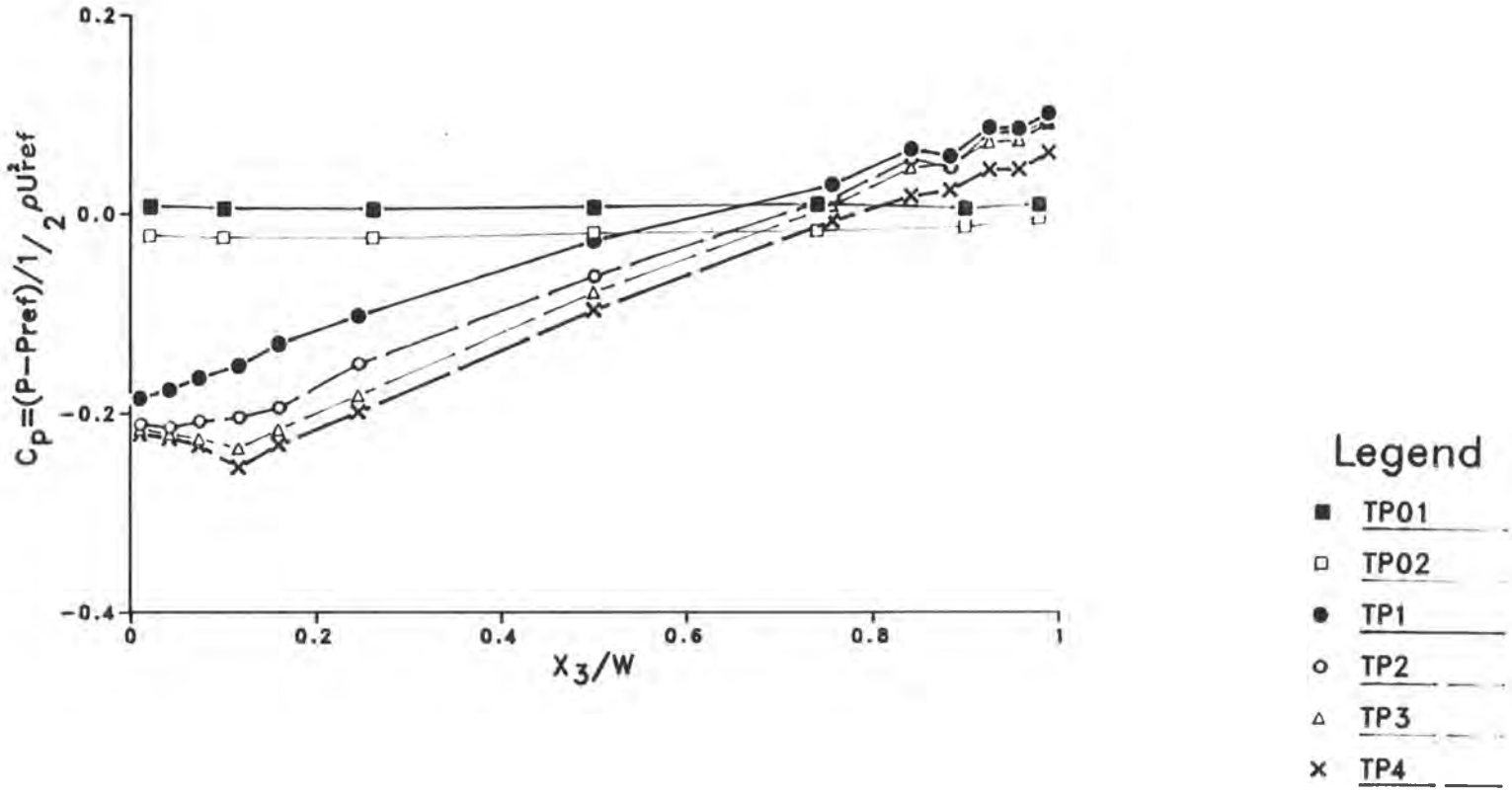

Figure 2.28. Pressure distribution along the top wall.

from somewhat downstream of station P02 in the straight duct to about station P1 in the curved duct. However, earlier investigations with fully-developed flow in a 90-degree duct bend by Ward-Smith (1971) showed that the upstream effect of the bend reached a distance of 1 to 2 duct heights ahead of the bend. The wall-static pressure measurements by McMillan (1982) in a diffuser bend of 40 degrees did not show such a complicated situation in radial pressure distribution in the inner corner region, since the mildly curved divergent channel decreases the effect of the corner vortex. Yet another view of the pressure field in the present case is provided by figure 2.30 in which the pressure variation along several other lines on the top wall are added to those already shown in figure 2.29.

From the foregoing discussion it is clear that the flow in the duct develops under the influence of a rather complex pressure field which is itself dependent on the duct geometry and the flow field within it. The results indicate rather dramatic changes in pressure in the convex corner which need to be explored on the basis of the velocity measurements and supporting calculations.

2.5.3 Velocity distributions

In addition to the velocity measurements at the reference section A described earlier, five-hole pitot

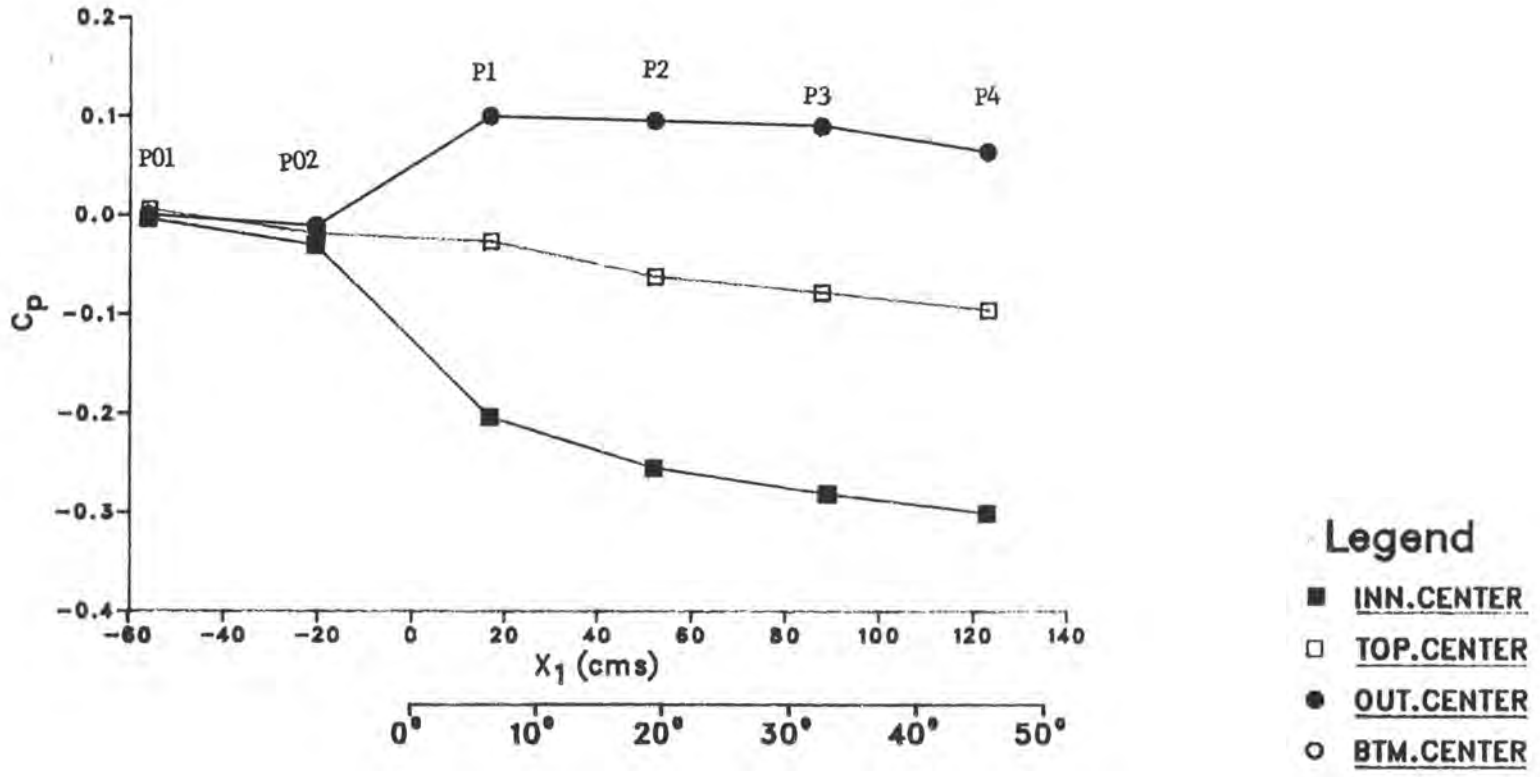

Figure 2.29. Pressure distribuiton along centerline of each wall.

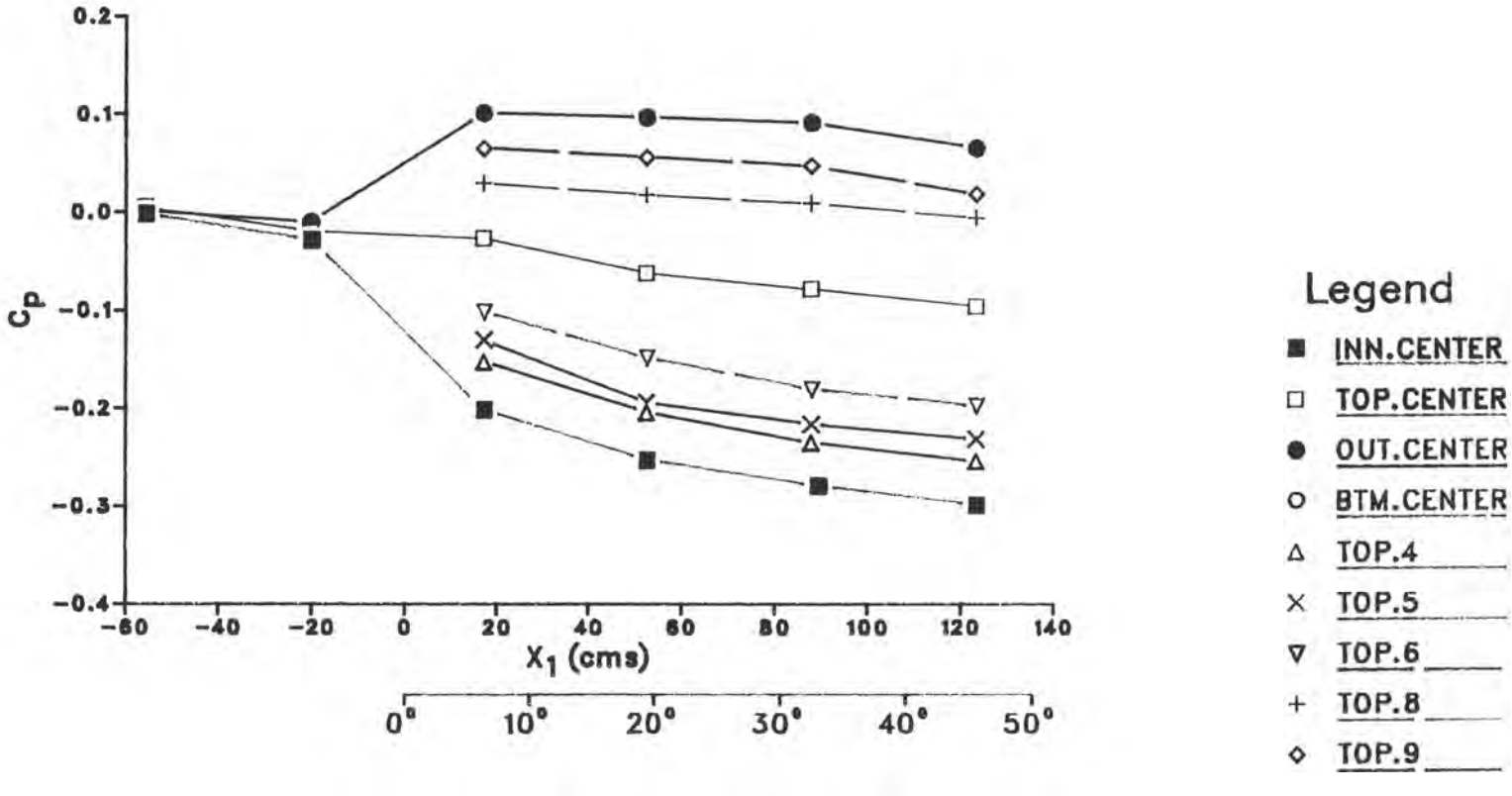

Figure 2.30. Pressure distribuiton along several lines on top wall.

measurements were made at two sections, D and F (see figure 2.2), in the curved duct. These measurement were confined to the region $x_2/H < 0.77$ and $x_3/W < 0.77$, approximately, due to the limitations imposed by the probe geometry adopted for the inner, convex corners. The locations of the measurement points at sections D and F are shown in figures 2.31 and 2.32, respectively. The measurements were made by traversing the probe vertically from the bottom, flat wall at several distances from the convex wall. A dense grid was used near both walls to obtain detailed information on the flow in the corner. At each station, the probe was aligned geometrically with the duct axis. Since the measurements in the central part of section A, where the secondary motion is negligible, indicated small but constant pitch and yaw angles, it was assumed that they were associated with errors in probe calibration or alignment. Therefore, the data at stations D and F were corrected for these constant errors by adding 2.8 degrees to the pitch angles and -0.5 degrees to the yaw angles. In the following presentation and discussion of data, the measurements are identified by a code in which the first letter designates the station and the following number indicates the location of the vertical traverse as shown in figures 2.31 and 2.32.

An overview of the secondary motion generated by the duct curvature at stations D and F is provided by the vector

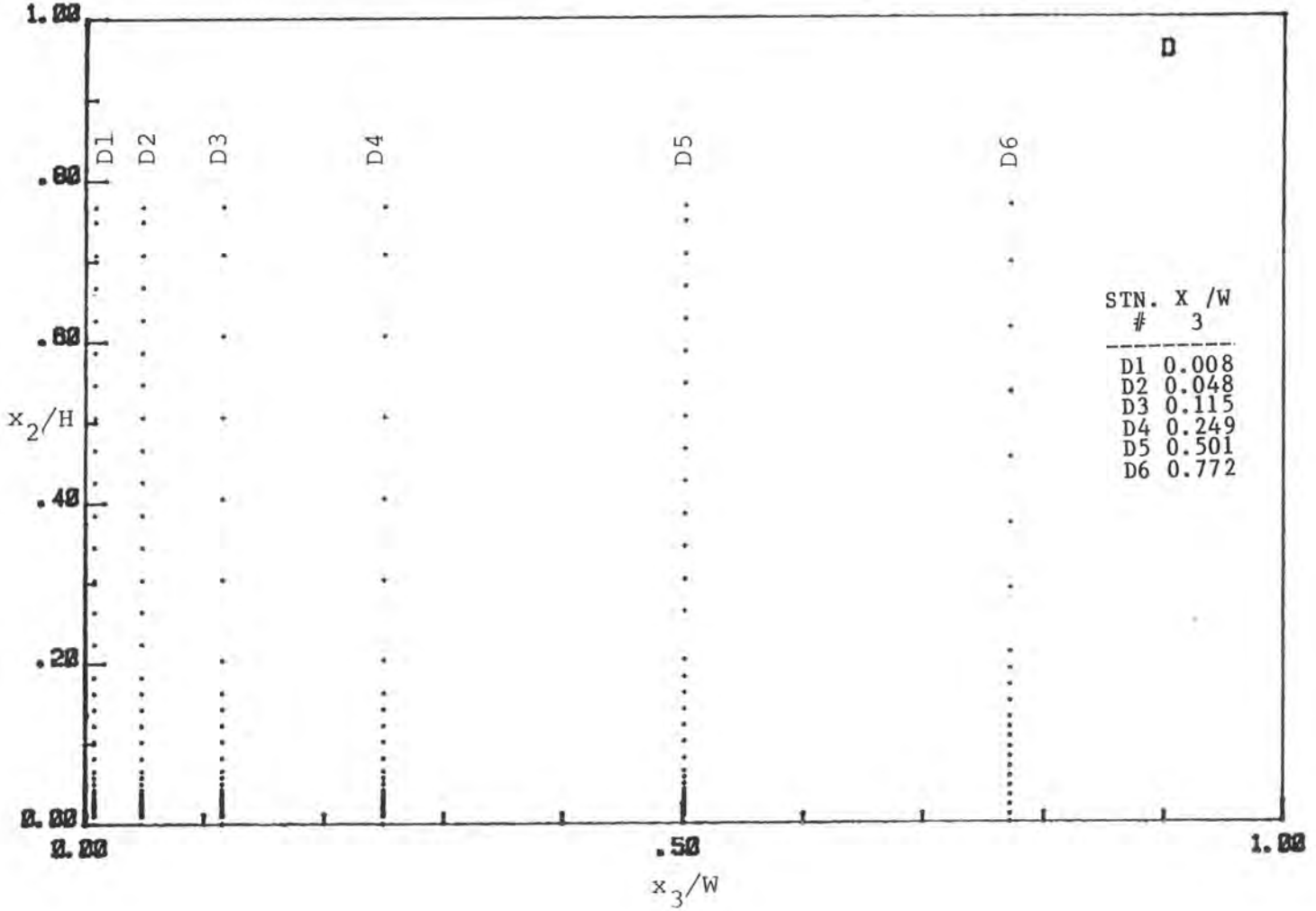

Figure 2.31. Measuring grid at station D.

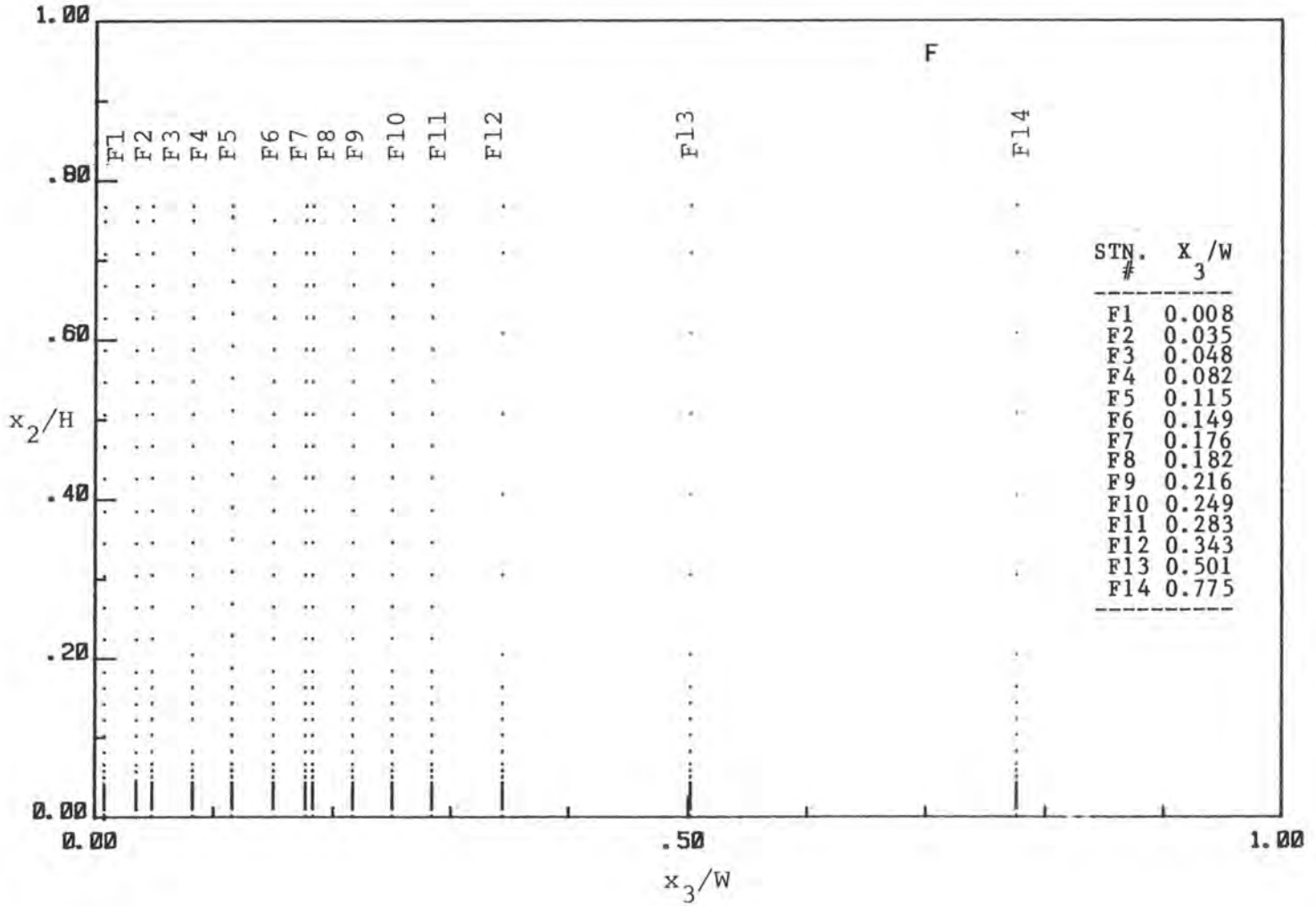

Figure 2.32. Measuring grid at station F.

plots of U2 and U3 components of velocity shown in figure 2.33 through 2.36. In each case, two plots are made : figures 2.33 and 2.35 show the entire domain of measurement, and while 2.34 and 2.36 show the details in a small region near the convex corner. From the former, it is evident that the measured secondary flow is essentially symmetric about the horizontal centerplane, $x_2/H = 0.5$. As expected, we observe a strong secondary motion from the outer concave wall toward the inner convex wall within the boundary layer on the bottom wall. The secondary velocity along the bottom produces a secondary motion along the inner convex wall. On the inner wall, the secondary flow converges towards the center and produces an outflow at the center. The secondary motion in the central core of the duct, outside the wall boundary layers, is quite weak.

There is some evidence of a longitudinal vortex in the inner corner at station D but the data are not spaced closely enough to demonstrate this conclusively. However, the vortex is clearly visible at station F and appears as an elongated structure in the region $x_3/W < 0.2$, $x_2/H < 0.5$, approximately, i.e., it extends all the way to the horizontal centerline of the duct along the inner wall. The present data thus indicate a rather slow development of the corner vortex.

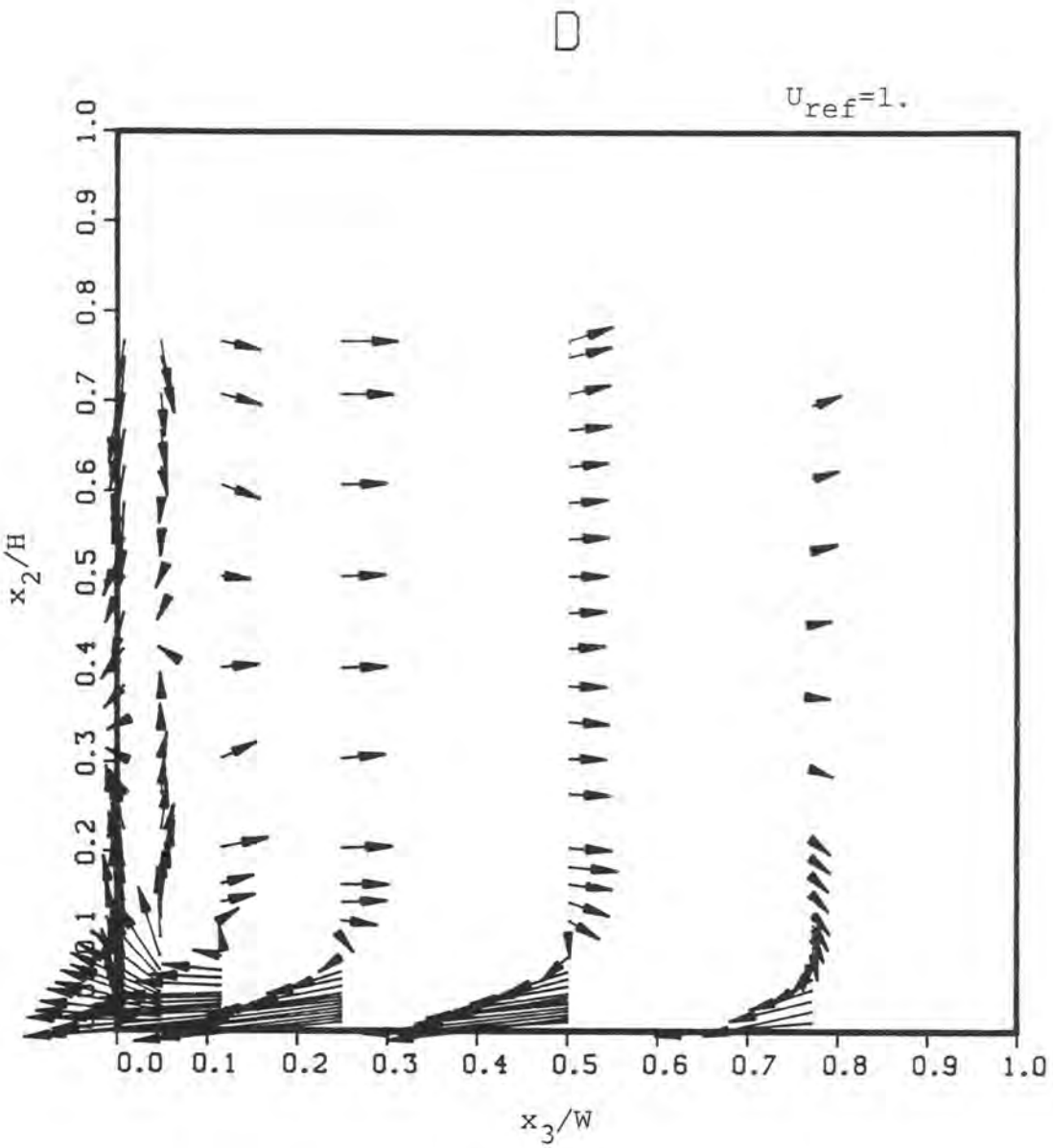

Figure 2.33. Secondary flow at station D.

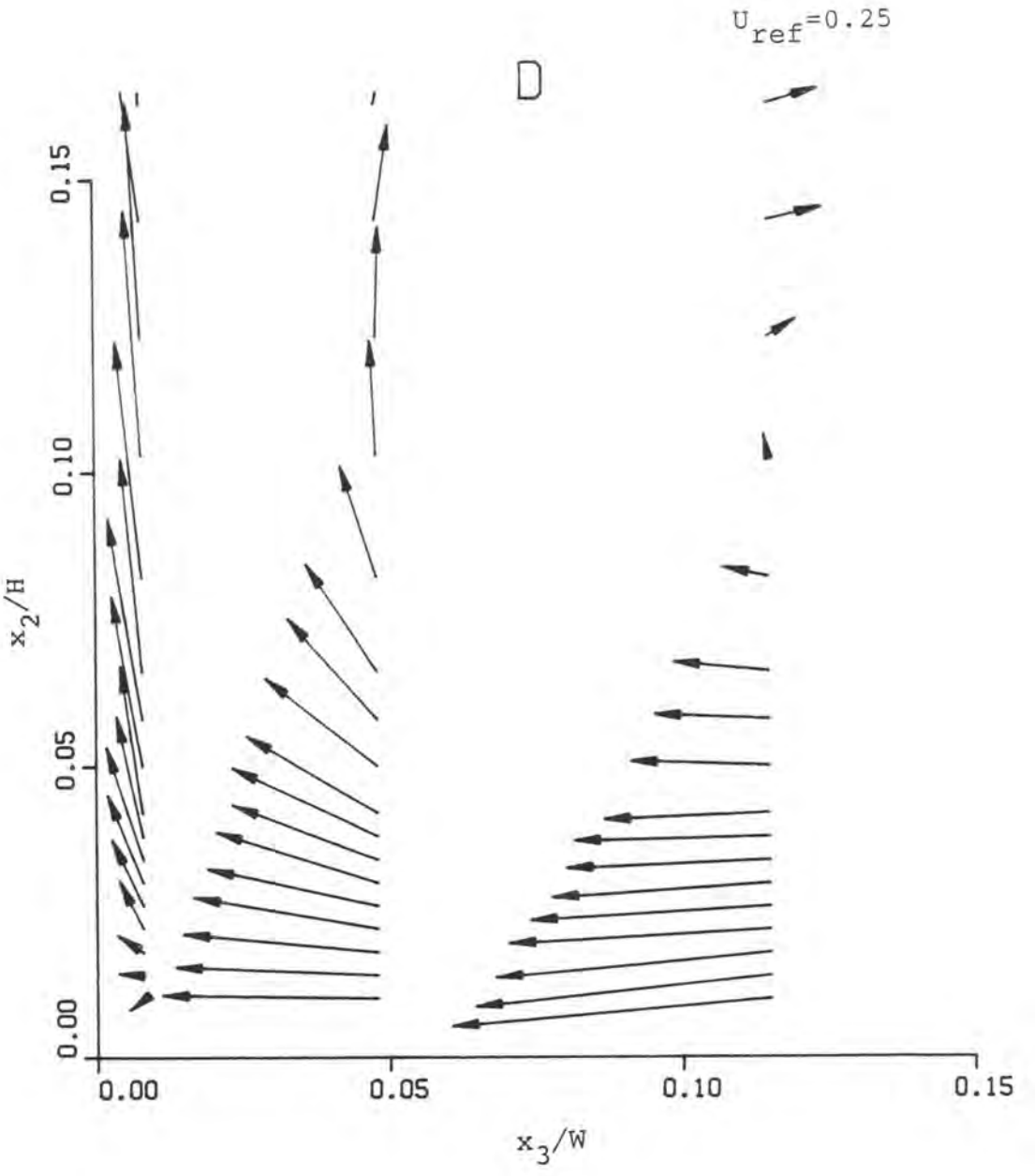

Figure 2.34. Secondary flow at convex corner of station D.

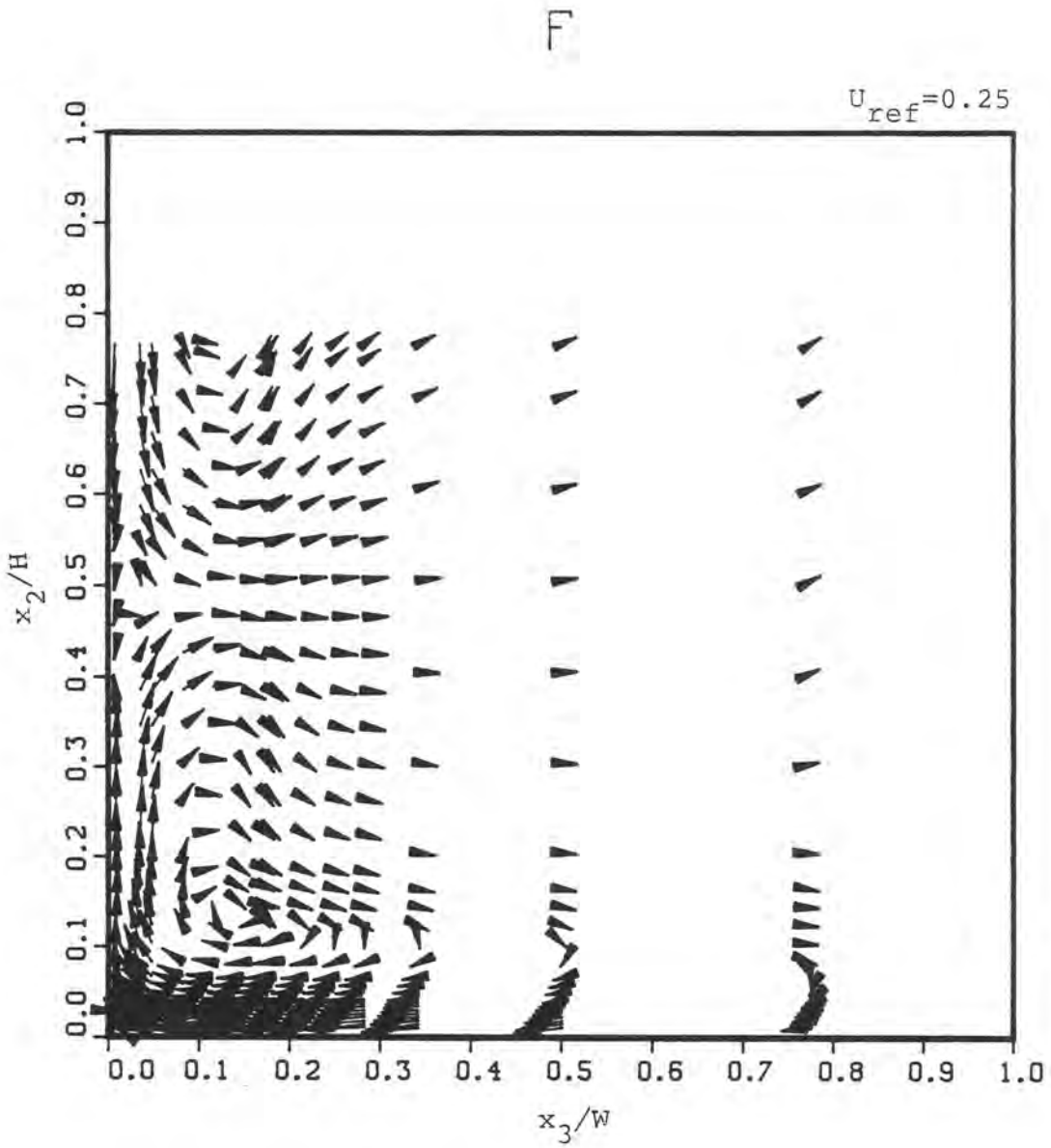

Figure 2.35. Secondary flow at station F.

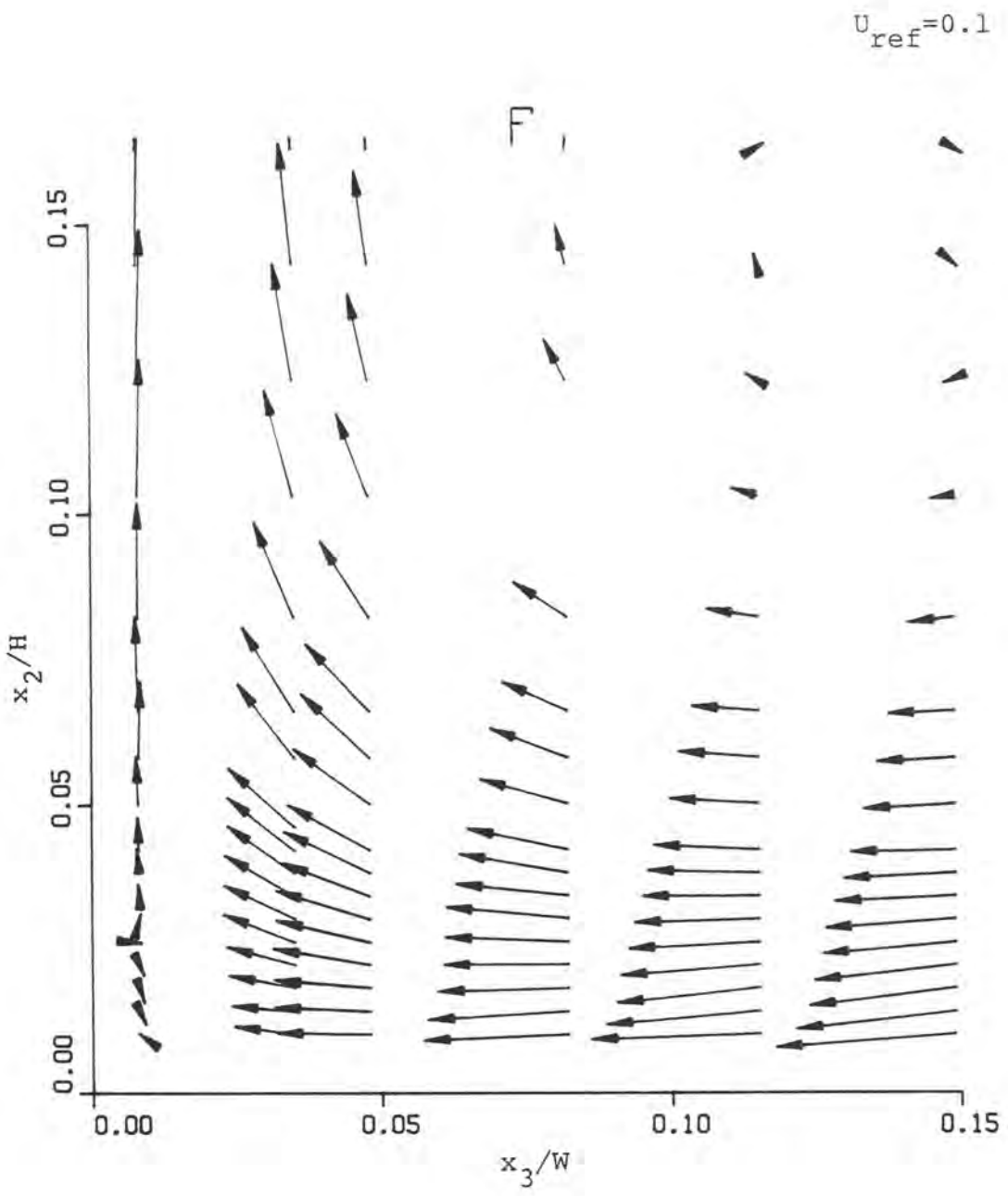

Figure 2.36. Secondary flow at convex corner of station F.

The profiles of the three components of mean velocity, namely U_1, U_2 and U_3, are shown in figures 2.37, 2.38 and 2.39, respectively, for section D, and figures 2.40 to 2.44 for section F. An important observation to be made from all of these is that all components of velocity remain essentially constant in the vertical direction within a large central core of the duct, and large variations occur only in the neighborhood of the walls. In other words, this is a developing duct flow with viscous effects confined to the wall boundary layers and invicid flow outside the boundary layers. With the inlet flow condition chosen here, therefore, the flow in the entire duct is of the boundary-layer type. However, the confinement of the flow within the duct results in a weak secondary motion in the invicid core and a strong interaction between the viscous and invicid regions. The interaction leads to an upstream influence which is evident from the pressure field discussed in the previous section. From figures 2.37 to 2.40, it is apparent that the thickness of the boundary layer at the center of the bottom wall is of the order of 0.2 H at both stations.

The velocity measurements again indicate the essential symmetry of the experimental flow about the horizontal centerplane. For example, the profiles of the longitudinal (U_1), and the transverse (U_3), components are symmetric about $x_2/H = 0.5$, as shown in figures 2.37 and 2.40 for

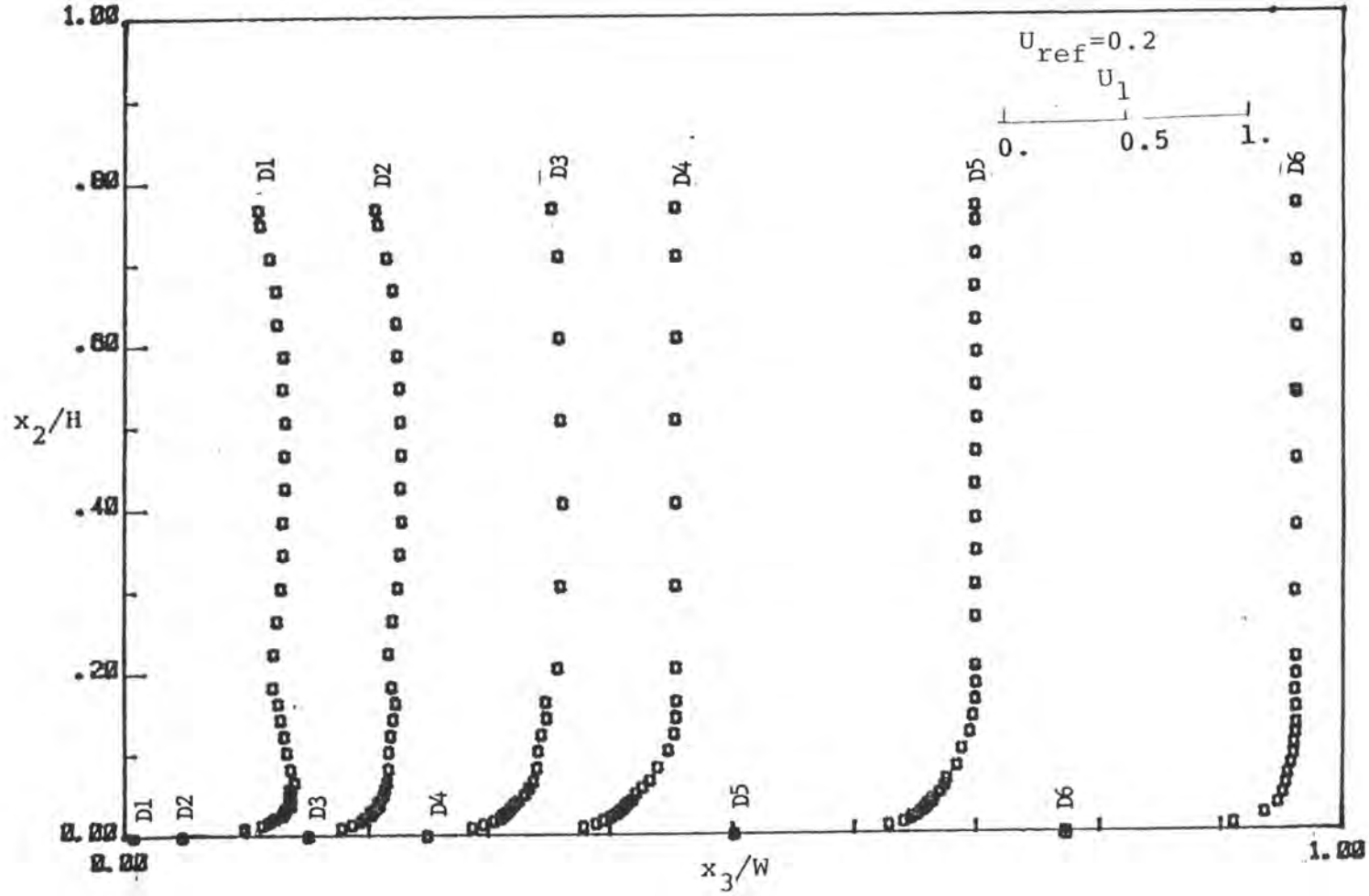

Figure 2.37. U_1 velociy component at station D.

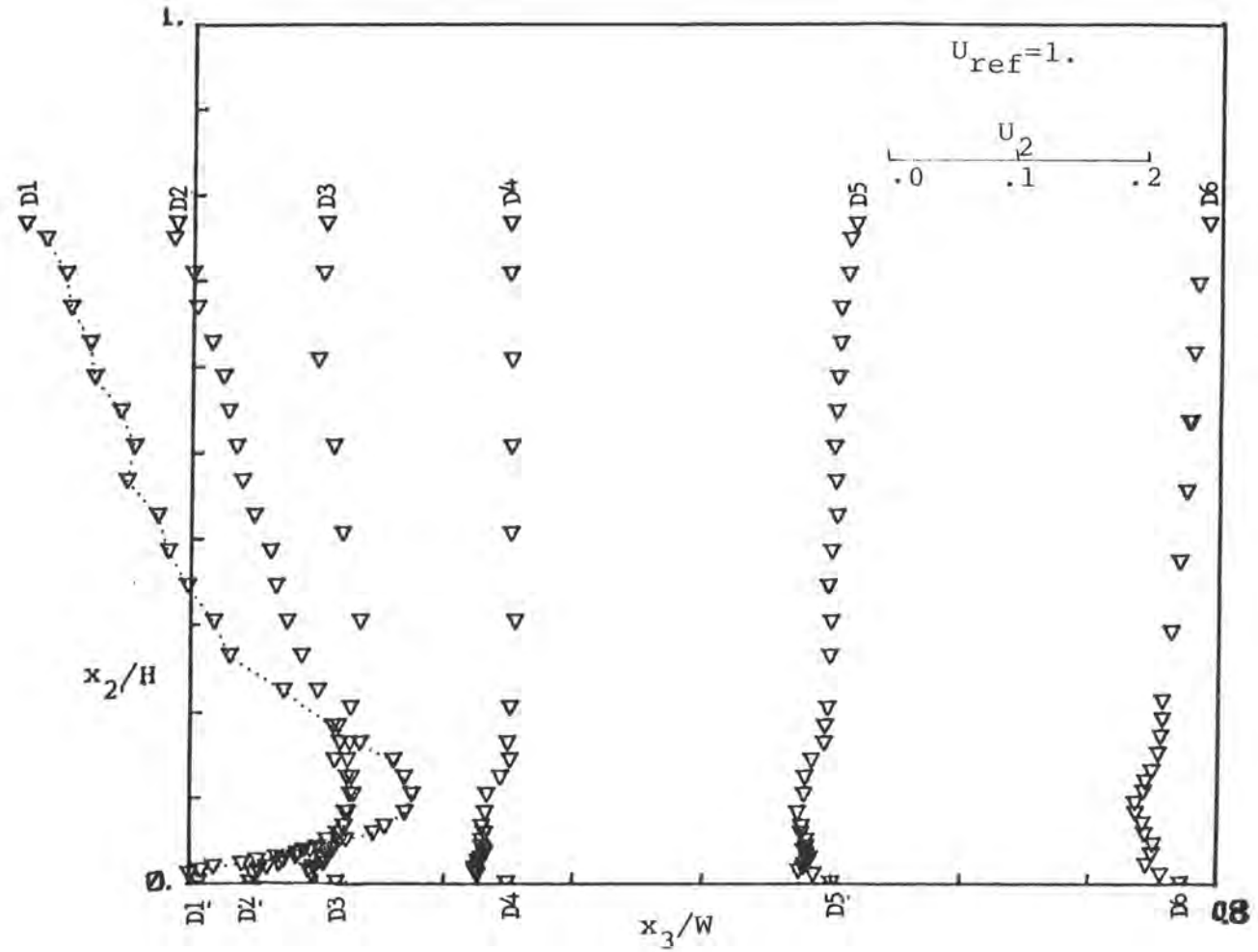

Figure 2.38. U_2 velociy component at station D.

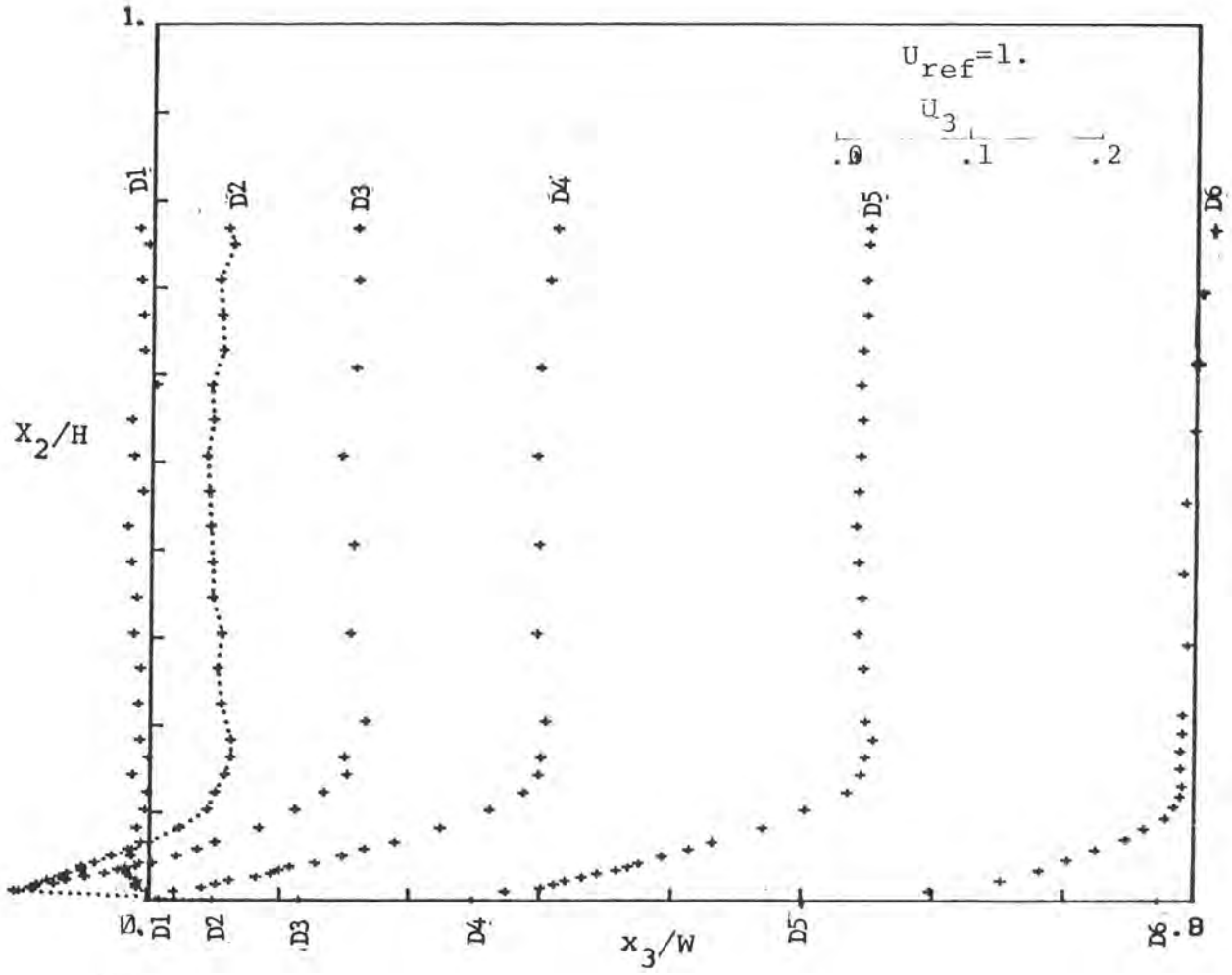

Figure 2.39. U_3 velociy component at station D.

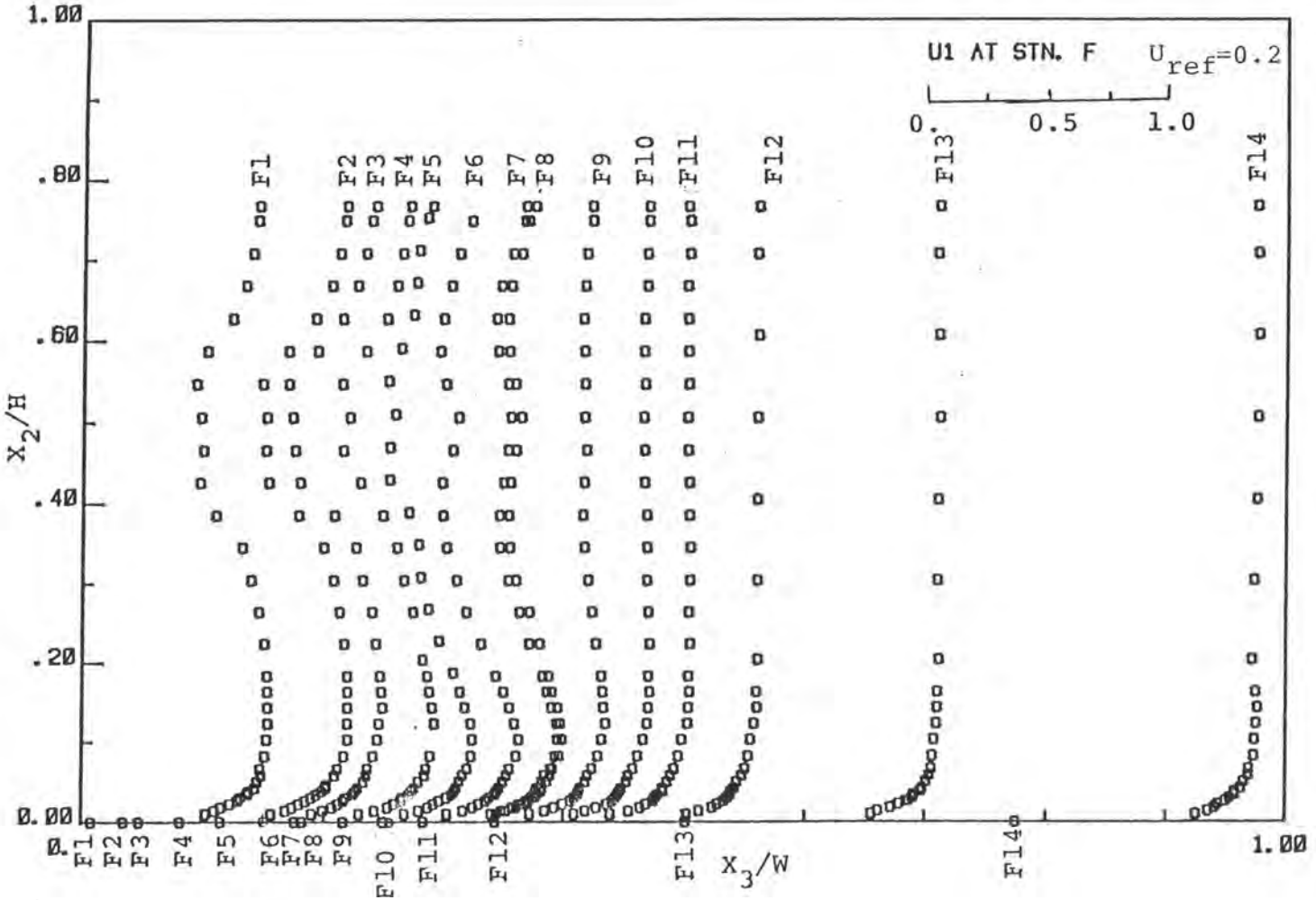

Figure 2.40. U_1 velocity component at station F.

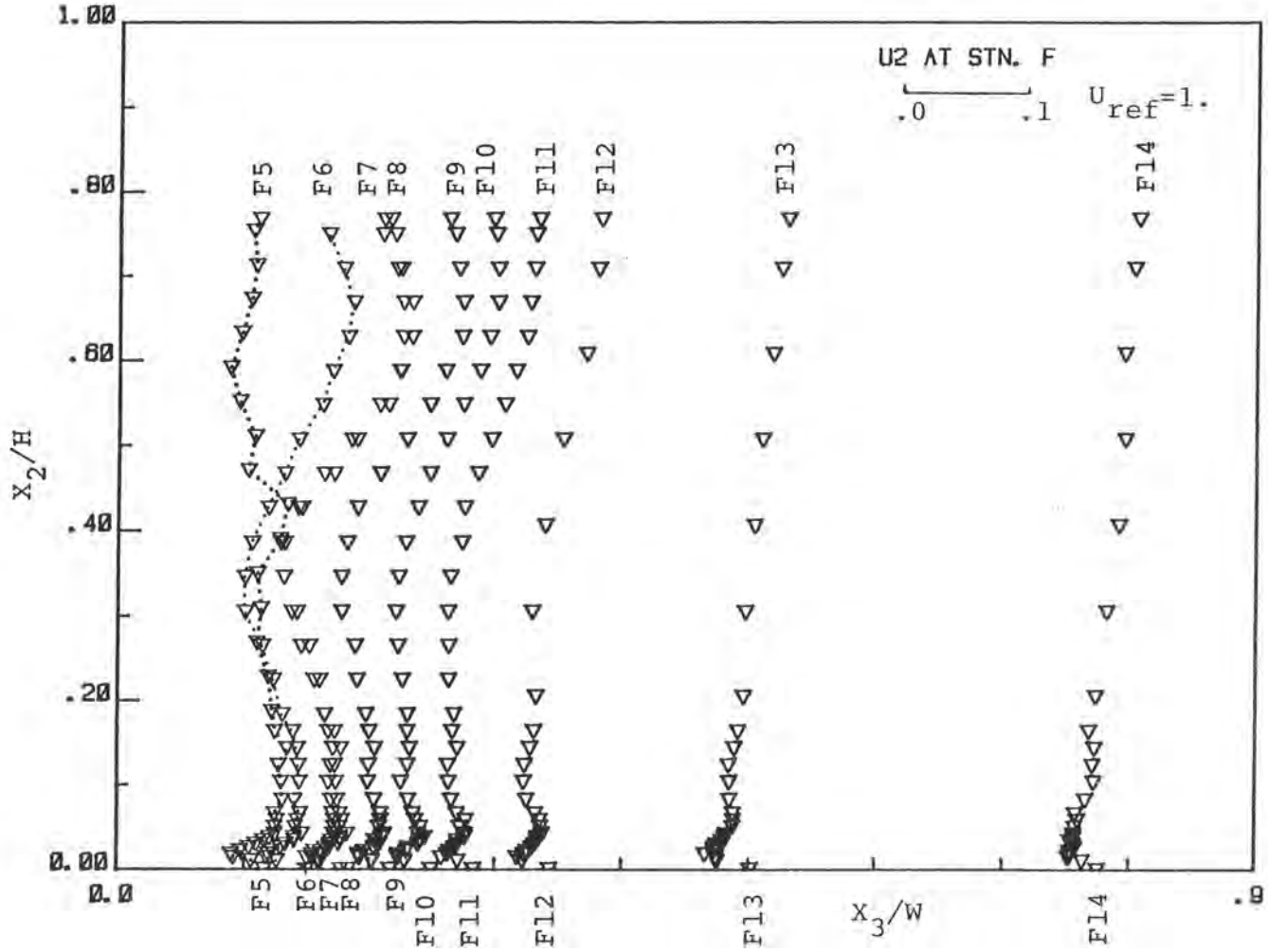

Figure 2.41. U_2 velocity component at station F.

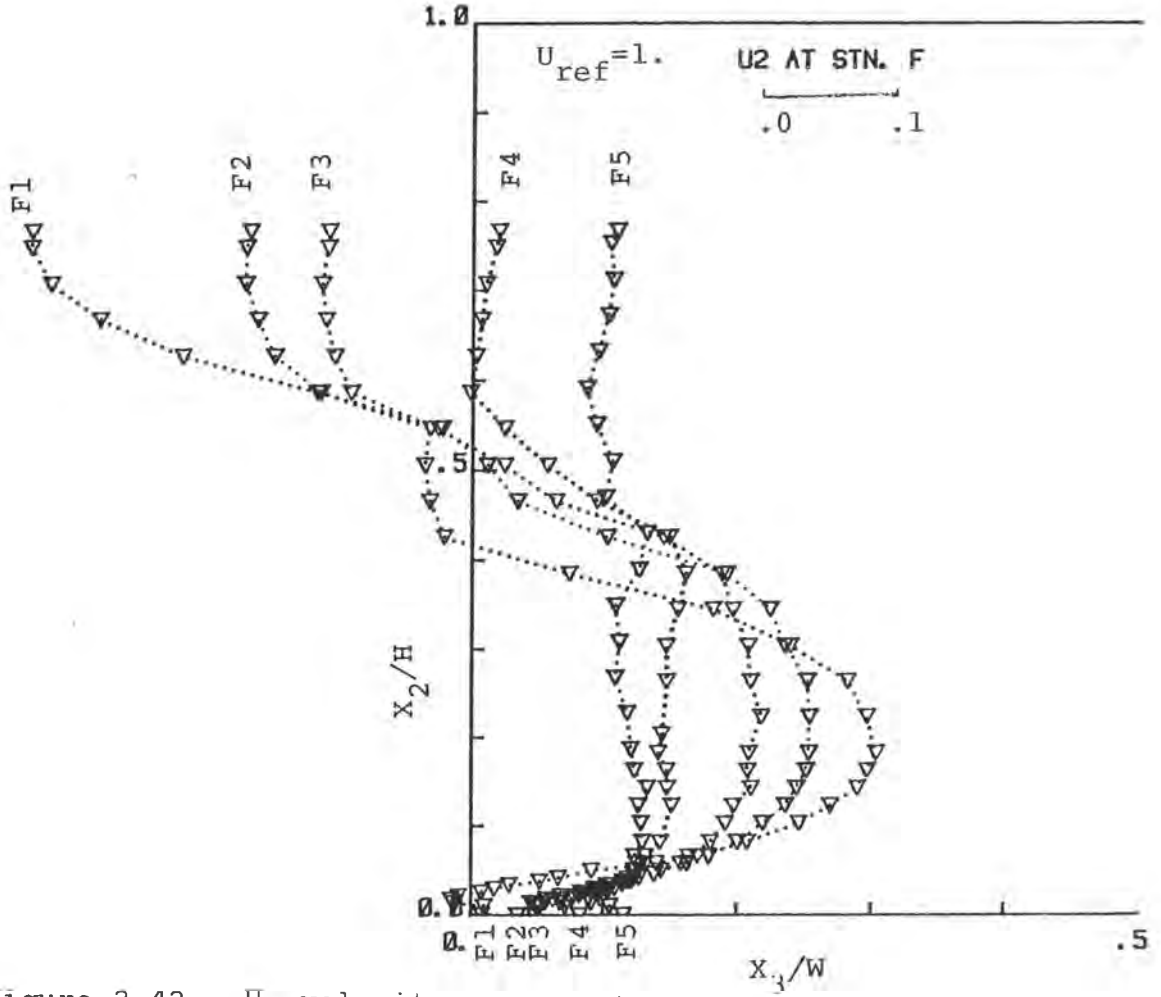

Figure 2.42. U_2 velocity component on convex wall at station F.

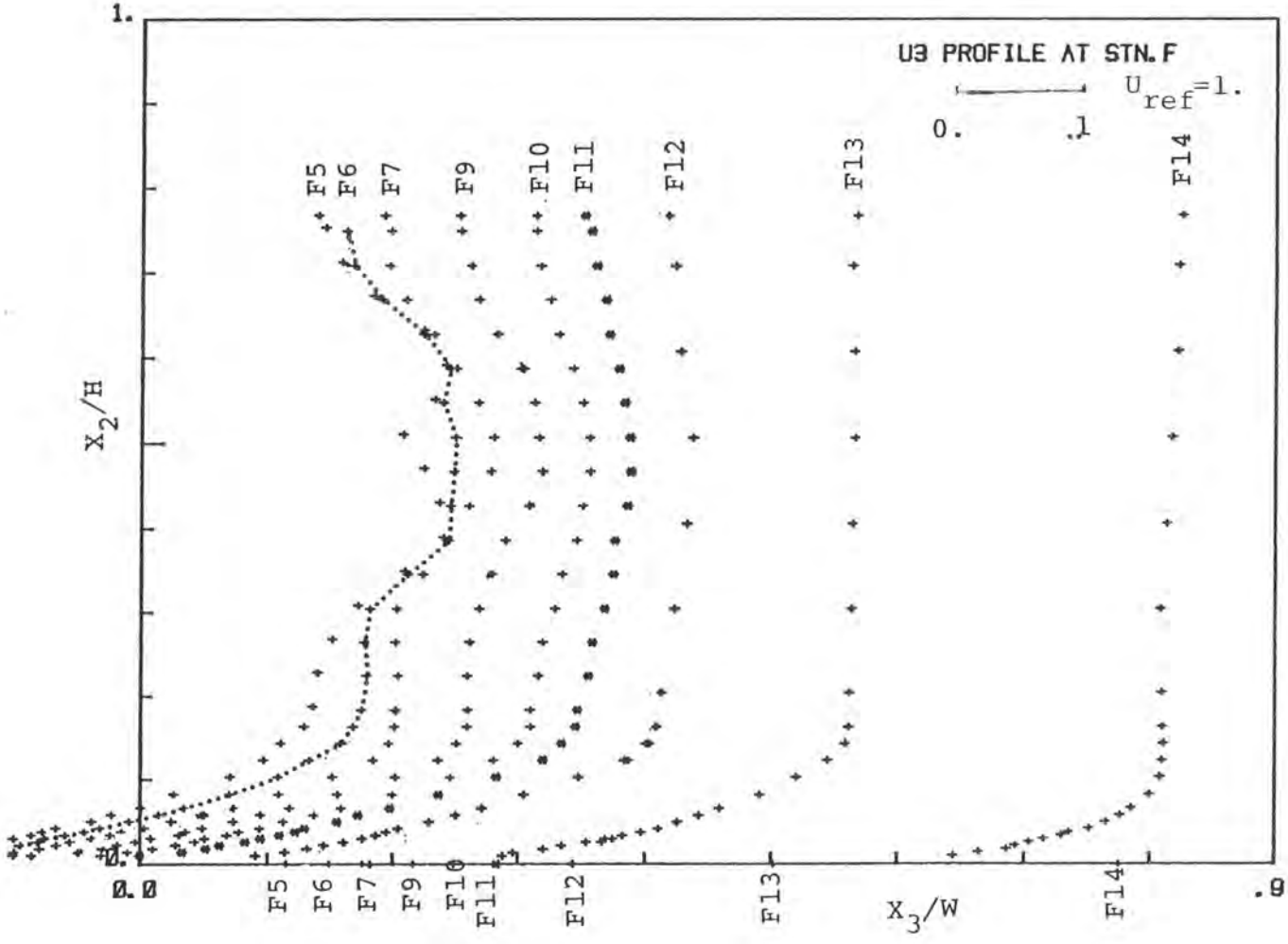

Figure 2.43. U_3 velocity component at station F.

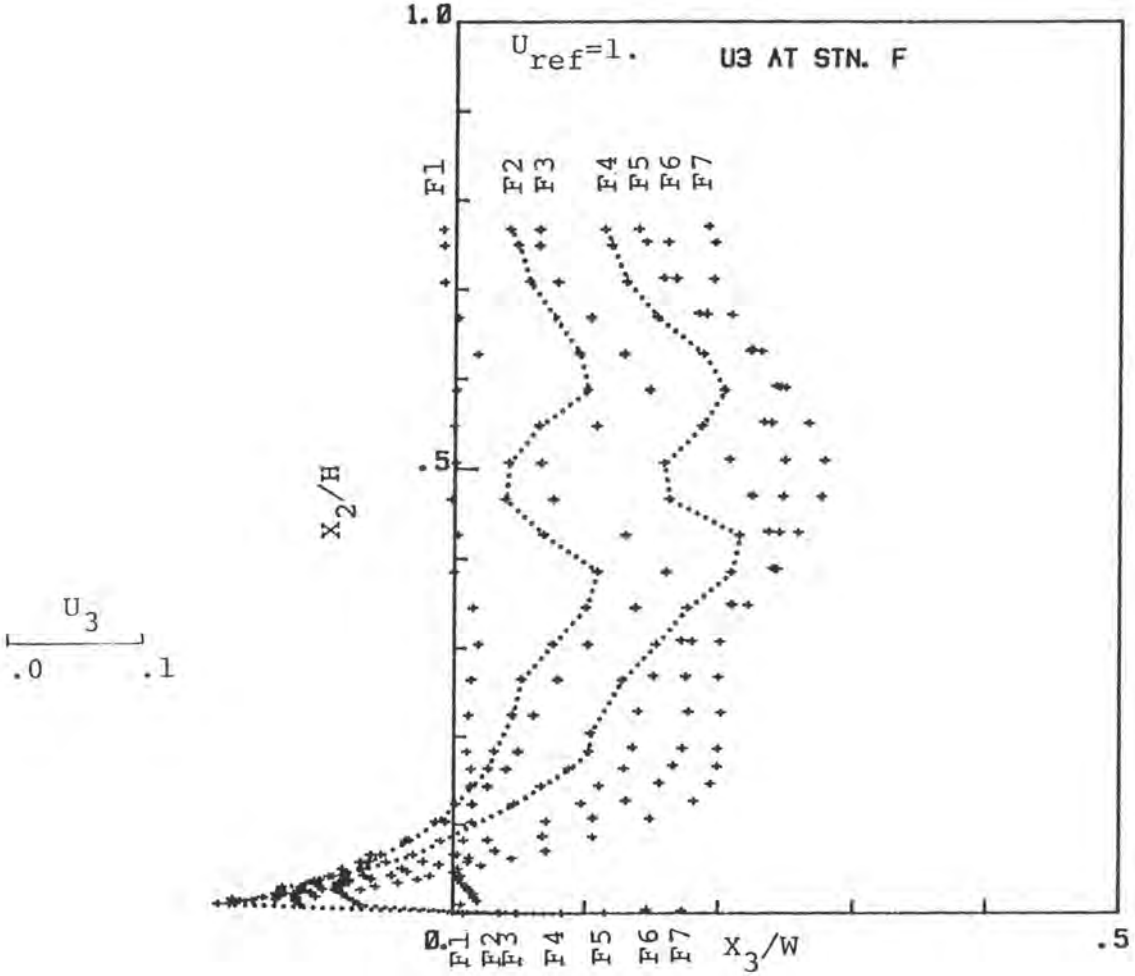

Figure 2.44. U_3 velocity component on convex wall at station F.

station F, even when they show quite characteristic shapes, while the vertical component (U_2) is antisymmetric and changes sign (from upward to downward) around $x_2/H = 0.5$. The detailed velocity profiles shown here are discussed further in the next chapter, together with the results of the calculations.

CHAPTER III

CALCULATION OF DEVELOPING TURBULENT FLOW IN THE CURVED DUCT

As noted in the Introduction, a simultaneous experimental and numerical study is useful in two ways. First, the calculations can be used to guide the conduct of the experiments by identifying the critical areas which need to be explored in detail, and secondly, the experiments can be used to obtain the information that is required in the validation and improvement of calculation methods.

In this chapter, we shall describe the calculations performed for the present experimental configuration using the method of Singhal (1978), and compare the results with the experimental data presented in the previous chapter.

3.1 The calculation method

Since the calculation method and the associated computer program are described in detail by Singhal(1978), it suffices here to highlight the main features of the method. The method solves the partially-parabolic form of the three dimensional, Reynolds-averaged, Navier-Stokes equations in either rectangular or cylindrical coordinates

for internal flows in straight or curved ducts. The k-ε model is used for the turbulent stresses, i.e. the stresses are related to the rates of strain through an isotropic turbulent viscosity, $\nu_t = C_D k^2/\varepsilon$, so that the effective kinematic viscosity ν_{eff} is determined by

$$\nu_{eff} = \nu + \nu_t$$

where k is the kinetic energy of the turbulence, ε is its rate of dissipation, ν is the kinematic viscosity, and C_D = 0.09 is a model constant. Both k and ε are determined from partial differential equations which contain four additional constants. Generally accepted values of these constants are used in the present calculations.

The momentum and the turbulence-model equations are solved by the implicit, staggered-grid, finite-volume numerical scheme of Pratap and Spalding (1975), and the pressure is determined in successive upstream-to-downstream sweeps through the solution domain by solving a pressure-correction equation derived from the continuity equation using the so-called SIMPLE algorithm. The numerical solution excludes the regim between the wall and mesh points closest to the wall. Thus, the boundary conditions at the walls are satisfied indirectly by the use of the so-called

wall-functions which are deduced from the logarithmic law-of-the-wall and the assumption of local equilbrium of turbulence. Consistent with the partially-parabolic approximations, zero pressure gradient at the duct outlet was prescribed.

3.2 Calculations performed

The inputs to the computer program consist of (a) the fluid properties, (b) the duct geometry and the numerical grid in the chosen coordinate system, and (c) a guessed pressure, and distributions of velocity at the initial station and turbulence parameters. For the present calculations, the duct geometry is simple since the cross-section is constant. Therefore, it was necessary to specify only one grid distribution for all cross-sectional planes. In the cross-section, a rectangular nonuniformly spaced grid was used, and 55 nearly uniformly spaced streamwise stations were employed between the inlet section A and the duct exit located after a 60-degree turn (see figure 2.2).

3.2.1 Initial conditions

With the secondary flow neglected at the initial station A, the flow simulation requires only the data for the primary (streamwise) velocity component, U_1. The corresponding turbulence parameters k and ε are established in the program assuming flat plate correlations.

In the present case, the boundary layer thickness at the initial station was assumed constant and equal to about 0.1 H on all four walls. The magnitude of the velocity and the values of k and ε were thus obtained from standard flat-plate correlations within the boundary layer. Outside the boundary layer, U_1 is assumed to be uniform, and k and ε were set to zero. The reference velocity was chosen such that the resultant velocity in the core at the initial station agreed with the experimental value.

3.2.2 Grid dependence and convergence

Calculations were carried out for several cross-sectional grid distributions in order to study the influence of step size on the solutions. A grid of 13 x 13 points for the entire cross-section of the duct and a grid of 9 x 9 in one-half of the duct proved too coarse to resolve the flow in the corners, although convergence of the solutions was achieved in each case. With the finest grids (25 x 25 points) which could be accommodated on the University's Prime 750 computer, numerical oscillations were observed and the solutions failed to converge. The difficulty was traced to the use of the wall functions in the corner region. After much trial, it was concluded that the results with a grid of 15 x 15 points over one-half of the duct gave satisfactory convergence and also adequate resolution of the

flow. The values of the pressure coefficient at several grid points calculated after each sweep are shown in figure 3.1. It is seen that, after some initial oscillation, the solution converges at all points. It appears that about 60 sweeps are required to obtain a converged solution. The solutions obtained with this grid are presented and compared with the experimental data in the next section.

3.3 Results and comparisons with experiments

3.3.1 Pressure distribution

The calculated pressure distributions along several lines on the flat (top) wall and along the centerlines of the outer and inner walls are shown in figure 3.2 in the same format as that used for the experimental data (figure 2.28). It is seen that the results are qualitatively similar to those observed in the experiments. The upstream influence of the bend on the pressure is felt upto station P02 (a distance of 4/5 H or 2/3 W upstream of the bend) and the strong adverse longitudinal pressure gradient on the outer wall and favourable longitudinal pressure gradient on the inner wall due to the change in curvature continue upto station P1 (6 degrees or x_1 = 17cm downstream of the junction between the straight and curved duct). Thereafter, the pressure gradients along all lines become constant all

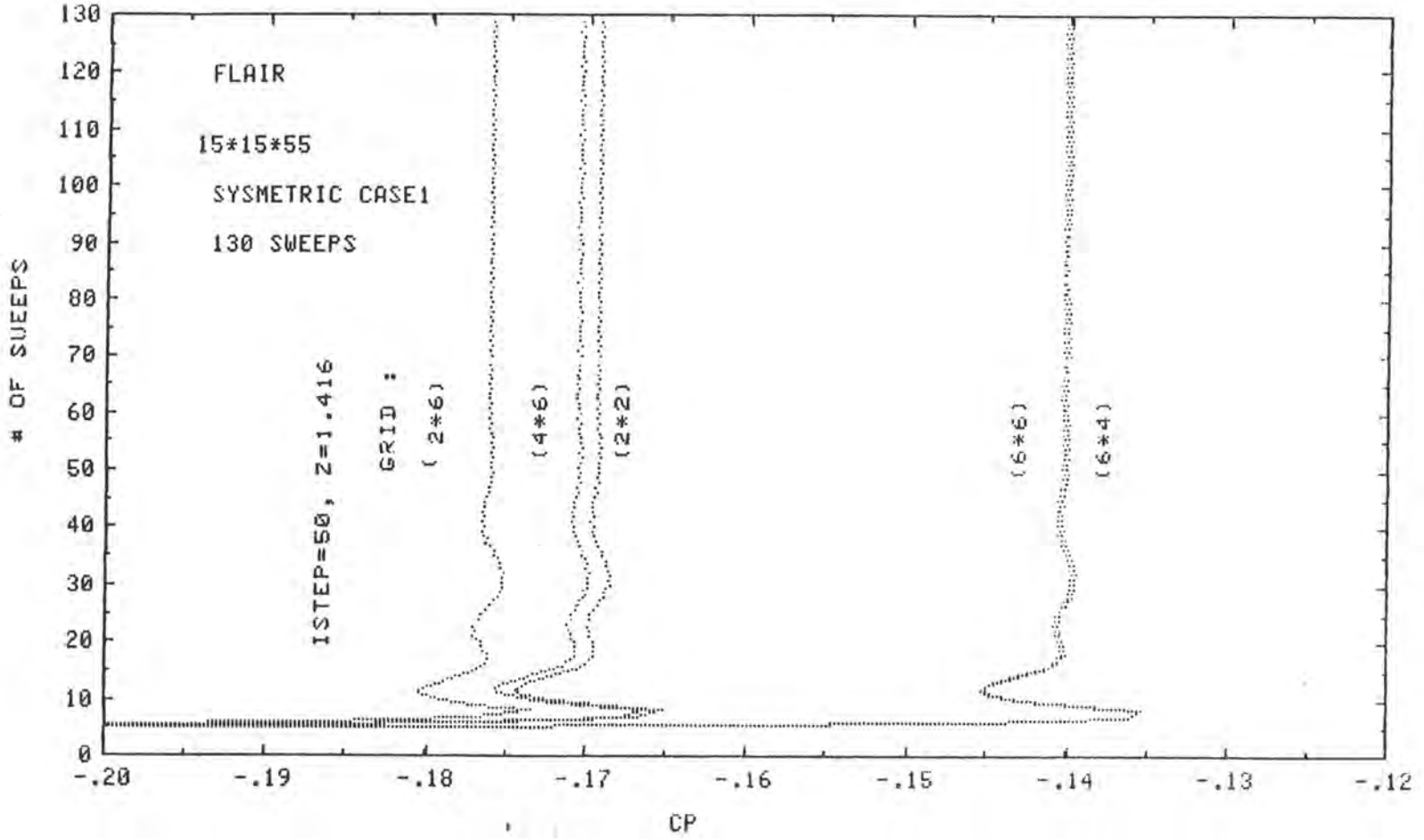

Figure 3.1. Convergence of Cp.

the way upto the station before the duct exit (56 degrees or x_1 = 161 cms).

The peripheral pressure variation at each of the pressure-measurement stations, namely P02, P1, P2, P3 and P4 in the experiment, are presented in figures 3.3, 3.4, 3.5, 3.6 and 3.7. At station P02, which is in the straight portion of the duct, the calculations are in excellent agreement with the experimental data. However, systematic differences are observed in the curved duct, especially in the neighborhood of the inner convex wall. At the first station in the curved duct (P1), the pressure on the outer wall is predicted well but that on the inner convex wall is lower than that measured in the experiments. By the last measurement station (P4, figure 3.7), the calculated pressures are lower on all walls. However, it is interesting to note that the calculations predict the same overall trends as those observed in the experiments and the pressure gradients at all stations depict similar behaviors. In particular, the pressure distributions in the corner region are in qualitative agreement with the data. The details of the radial variation of pressure on the top wall, shown in figure 3.8, indicate the same qualitative features as those of the experiments shown in figure 2.28.

Comparisons with the experimental results along the center of each wall are shown in figure 3.9. The

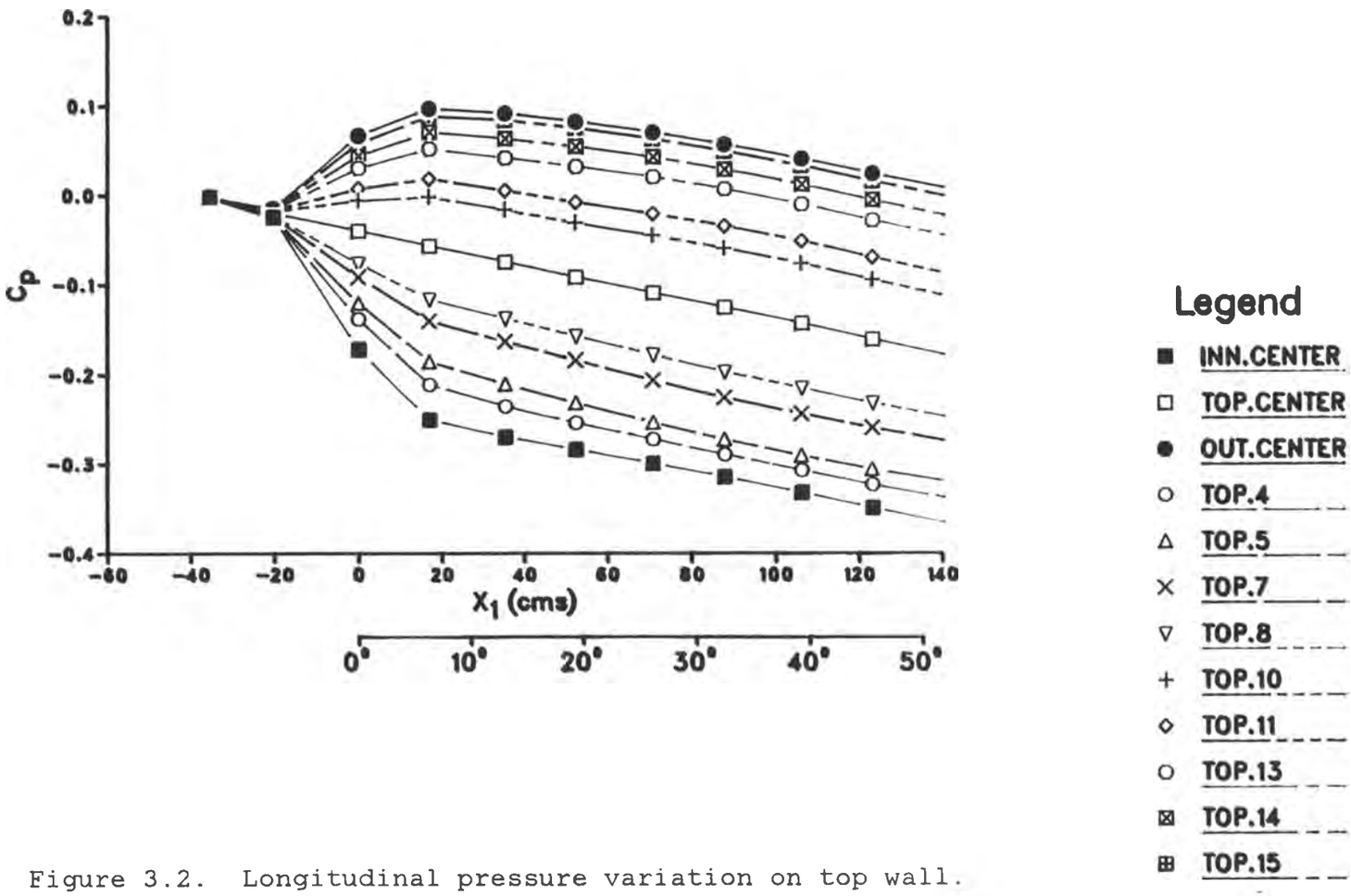

Figure 3.2. Longitudinal pressure variation on top wall.

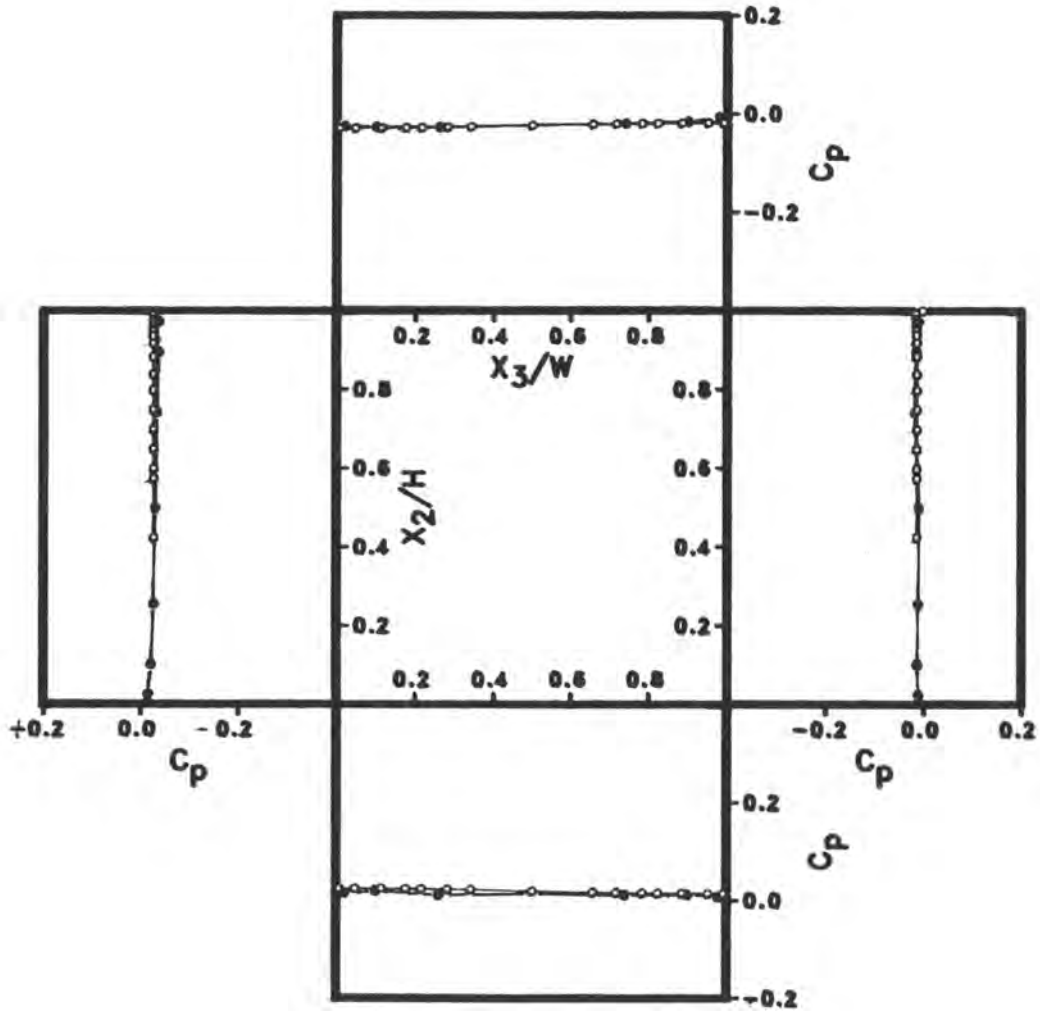

Figure 3.3. Pressure variation at station P02.

Legend

- P02.Calculation
- P02.Measurement

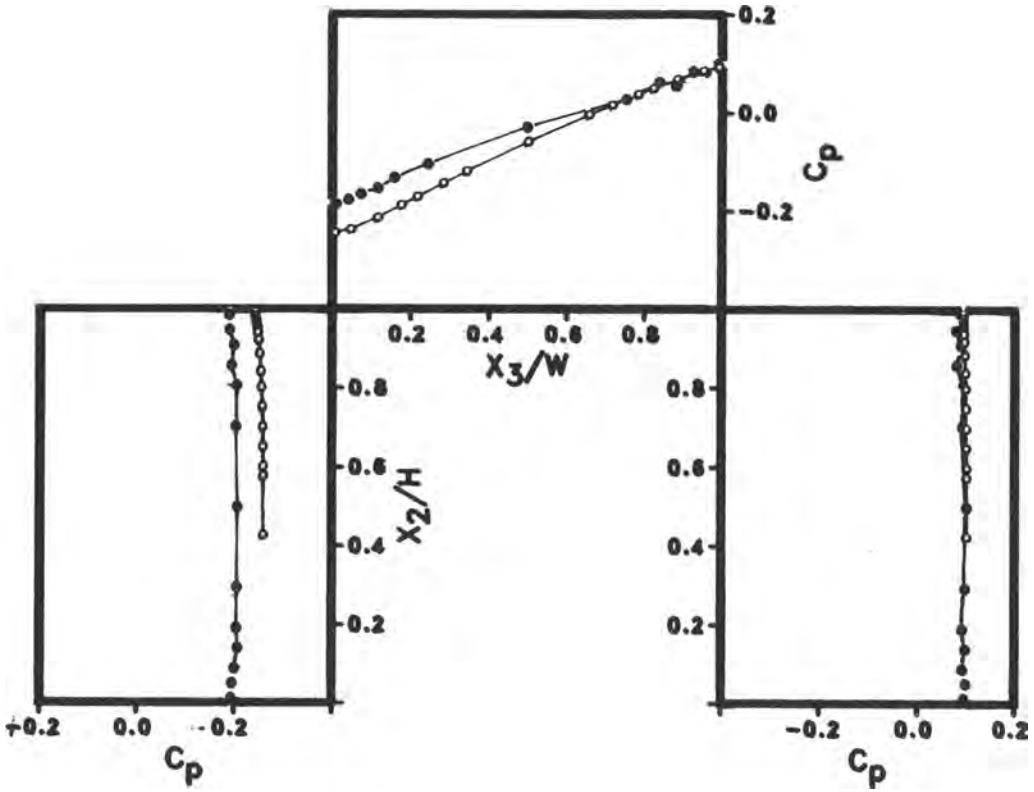

Legend

- P1.Calculation
- P1.Measurement

Figure 3.4. Pressure variation at station P1.

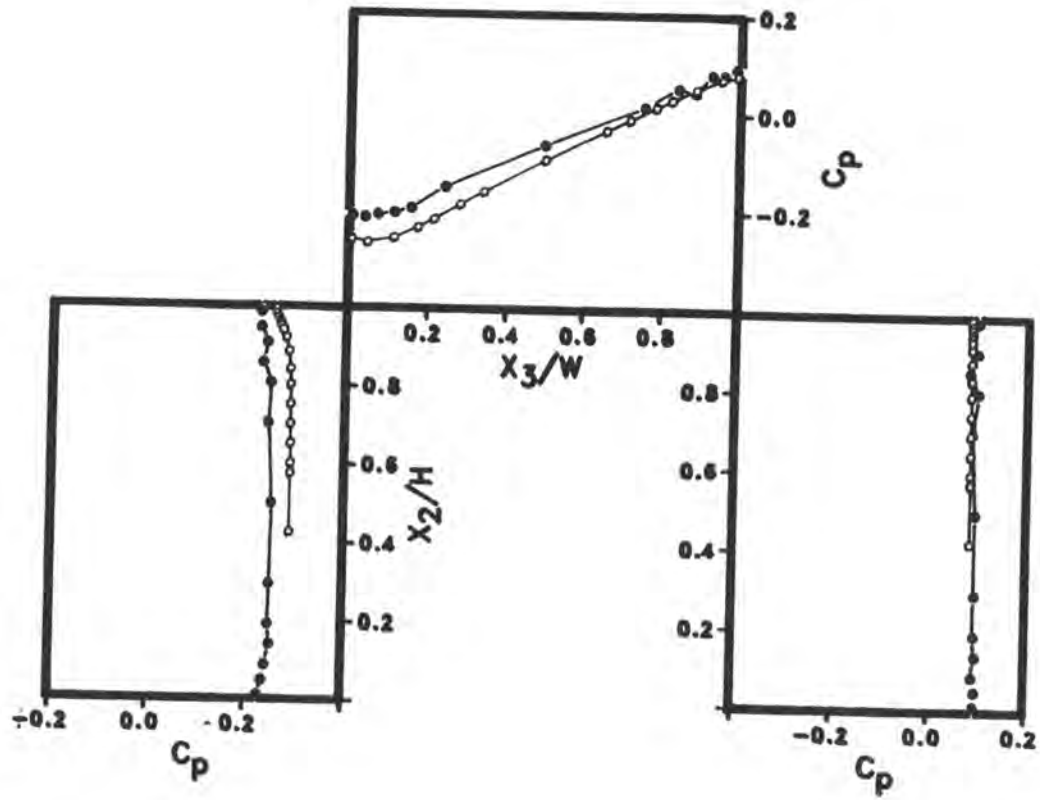

Legend

- P2.Calculation
- P2.Measurement

Figure 3.5. Pressure variation at station P2.

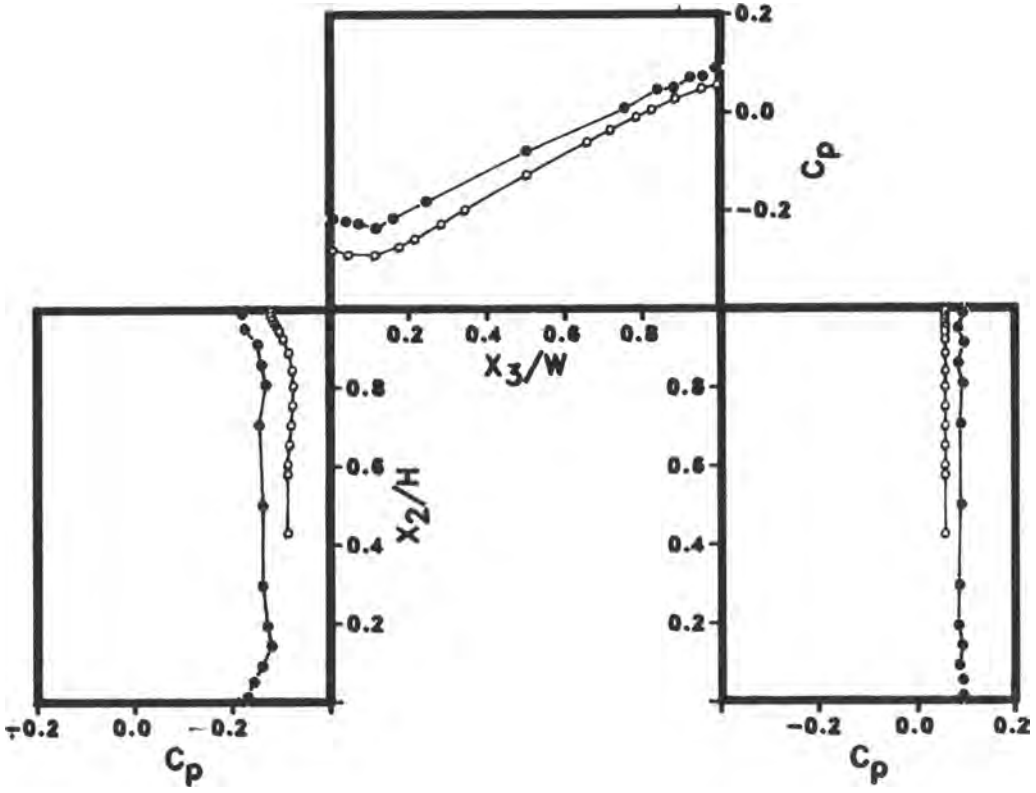

Legend

- ∘ P3.Calculation
- • P3.Measurement

Figure 3.6. Pressure variation at station P3.

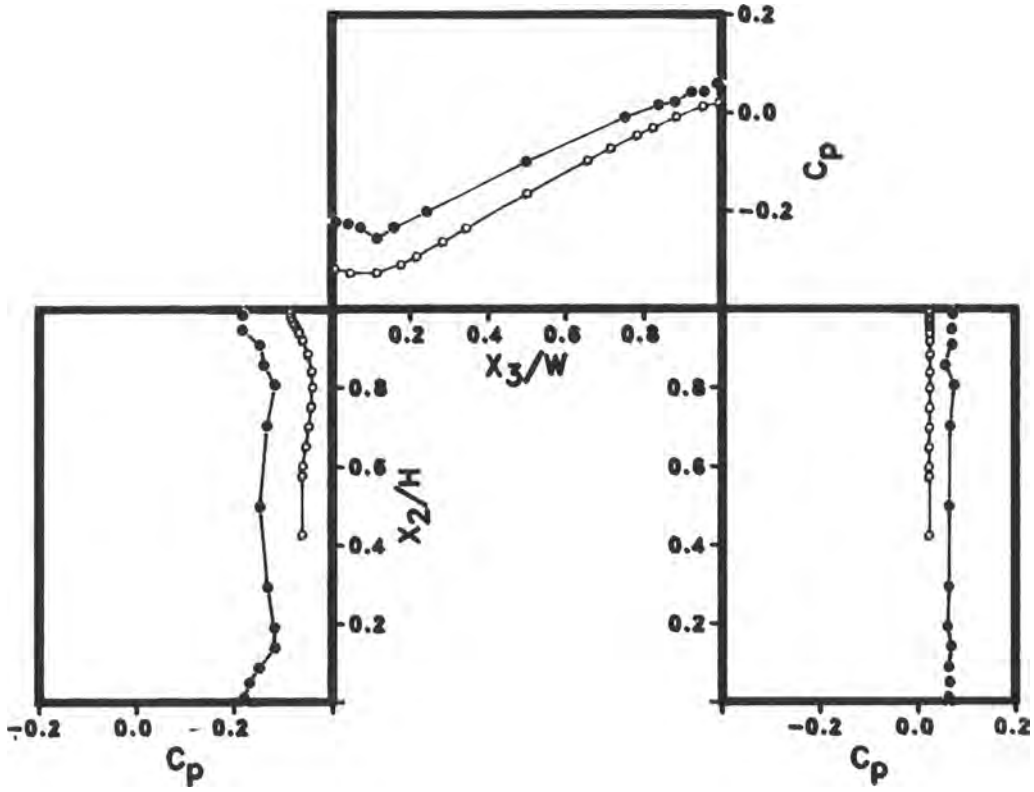

Legend

- P4.Calculation
- P4.Measurement

Figure 3.7. Pressure variation at station P4.

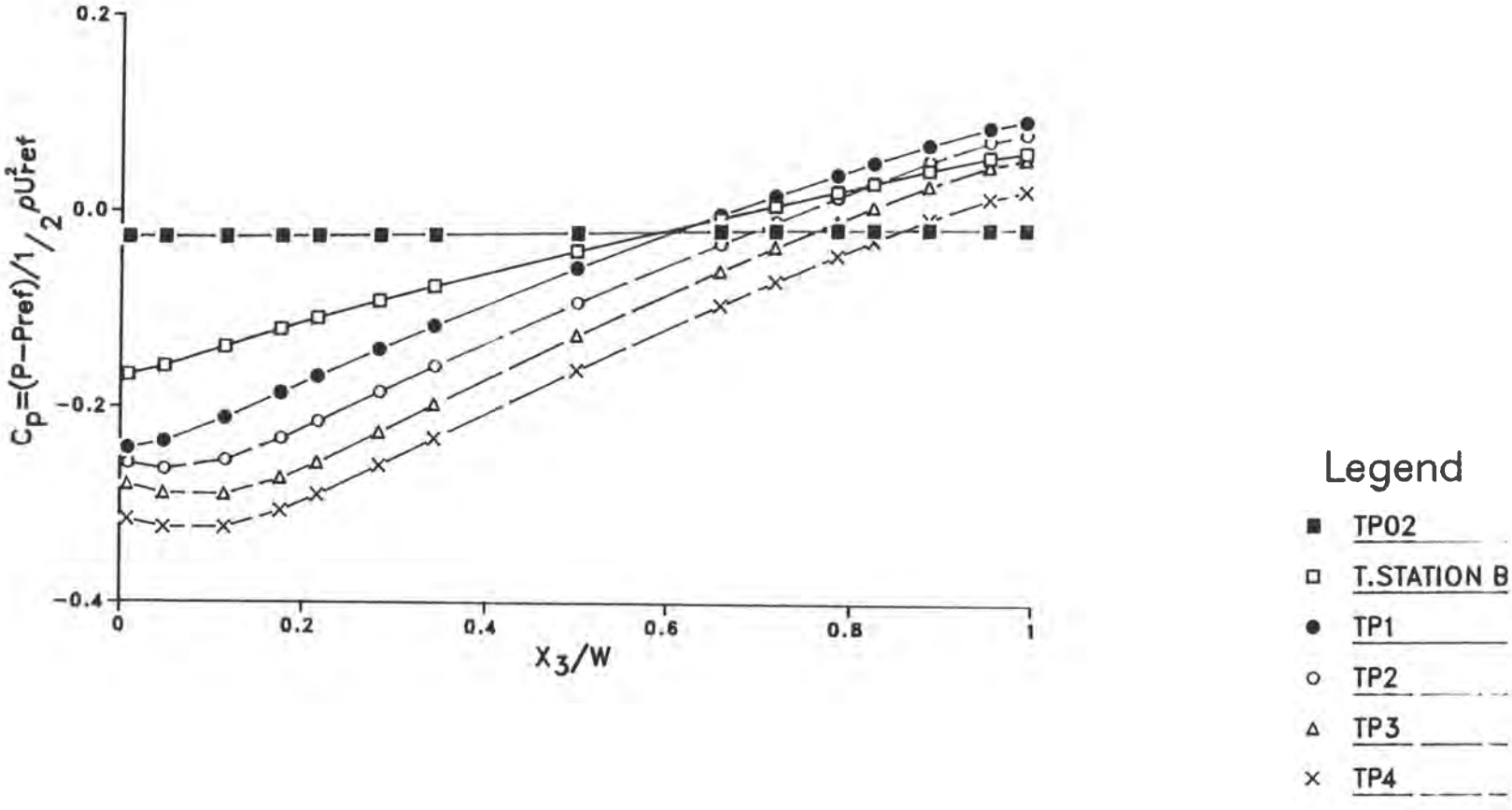

Figure 3.8. Radial pressure variaiton on top wall.

differences between the calculations and experiments are again evident. The disagreement appears to increase in the downstream part of the curved duct. This is probably due to the failure of the downstream boundary condition imposed in the calculations to represent the exit to the atmosphere. The data appear to indicate a faster approach to uniform pressure at exit than the calculations. The problem of the upstream effect of the downstream boundary condition therefore deserves further study.

Detailed investigations of the wall pressure distributions in curved ducts have been carried out by Ward-Smith (1971), who gives extensive comparisons between measurements and potential-flow calculation. However, his results are restricted to fully-developed turbulent flow in bends of 90 and 180 degrees, with and without various downstream tangents, and therefore can not be compared with the present experiments and calculations.

3.3.2 Velocity distribution

An overview of the calculated secondary motion at the two measurement sections in the curved duct, namely D and F in figures 2.2, is provided by the vector plots in figures 3.10 and 3.11, respectively. In each case, the bottom figure shows all the grid points while the top shows only alternate grid points to enhance the clarity. Also, it

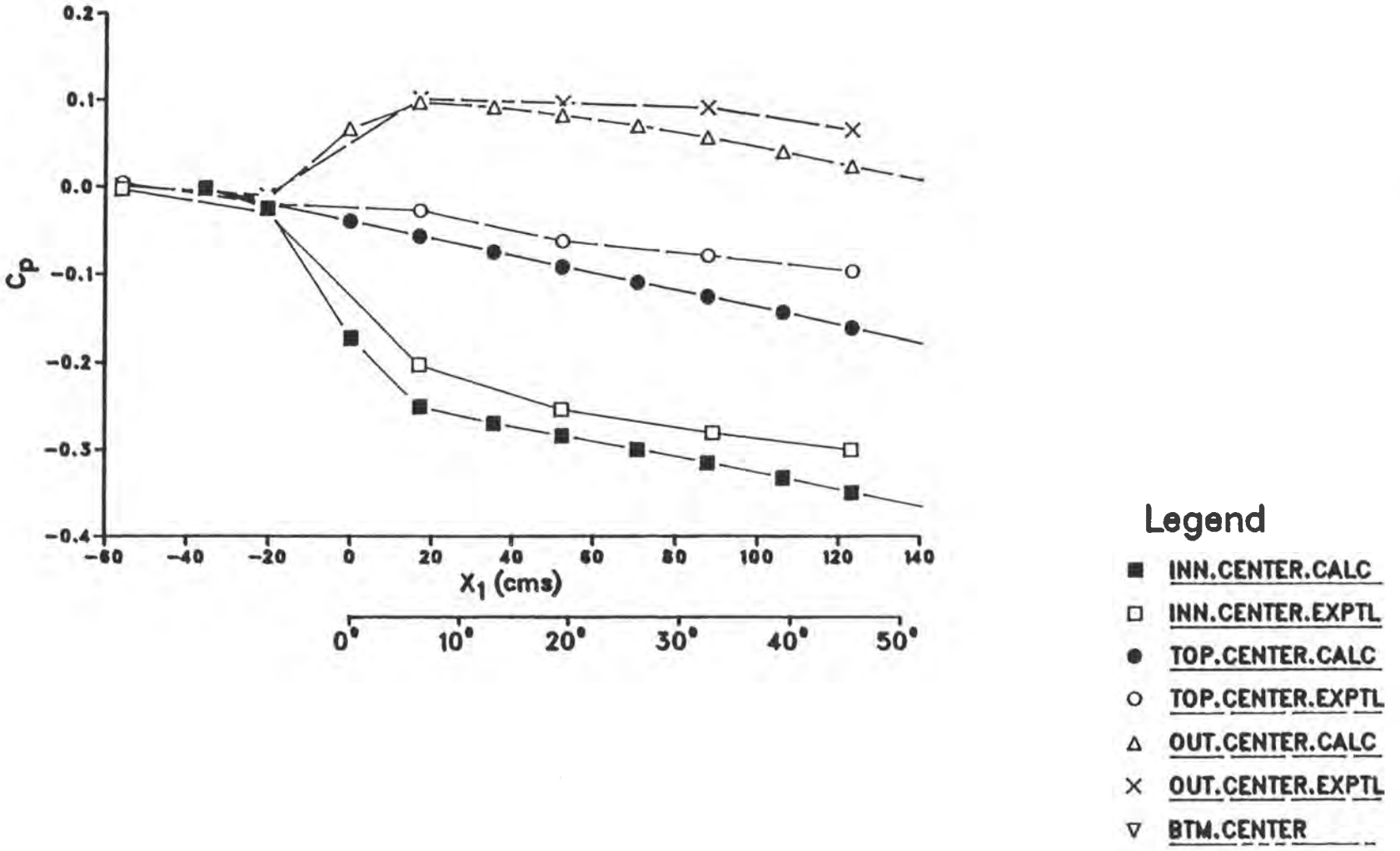

Figure 3.9. Calculated center line longitudinal Cp in comparison with experimental results.

should be noted that the calculations were performed for the top wall of the duct but, due to the symmetry about the horizontal centerplane, the results can be readily compared with the experimental data in the bottom half of the duct.

Figure 3.10 and 3.11 clearly show the evolution of the vortex in the convex corner. The vortex appears rather diffused at station D but is more pronounced at station F. At the latter position, its center is located almost symmetrically at a distance of about 0.16W from both walls. A comparison between the calculations of figure 3.10, 3.11 and the corresponding data shown in figures 2.33 and 2.34 indicates qualitative similarity but the experimental data, particularly at station F, show the vortex to an elongated structure rather than a well defined circular structure.

Examination of the calculation results near the outer wall indicates no peculiarities at station D but it appears that another vortex is forming at the center of the outer wall. Unfortunately, the present experiments did not extend to this region and therefore little can be said about this phenomenon.

The secondary flow in the corner region can be seen more clearly in the enlarged vector plots of figures 3.12 and 3.13. A comparison with the corner flow data show in figures 2.34 and 2.36 again shows qualitative resemblance.

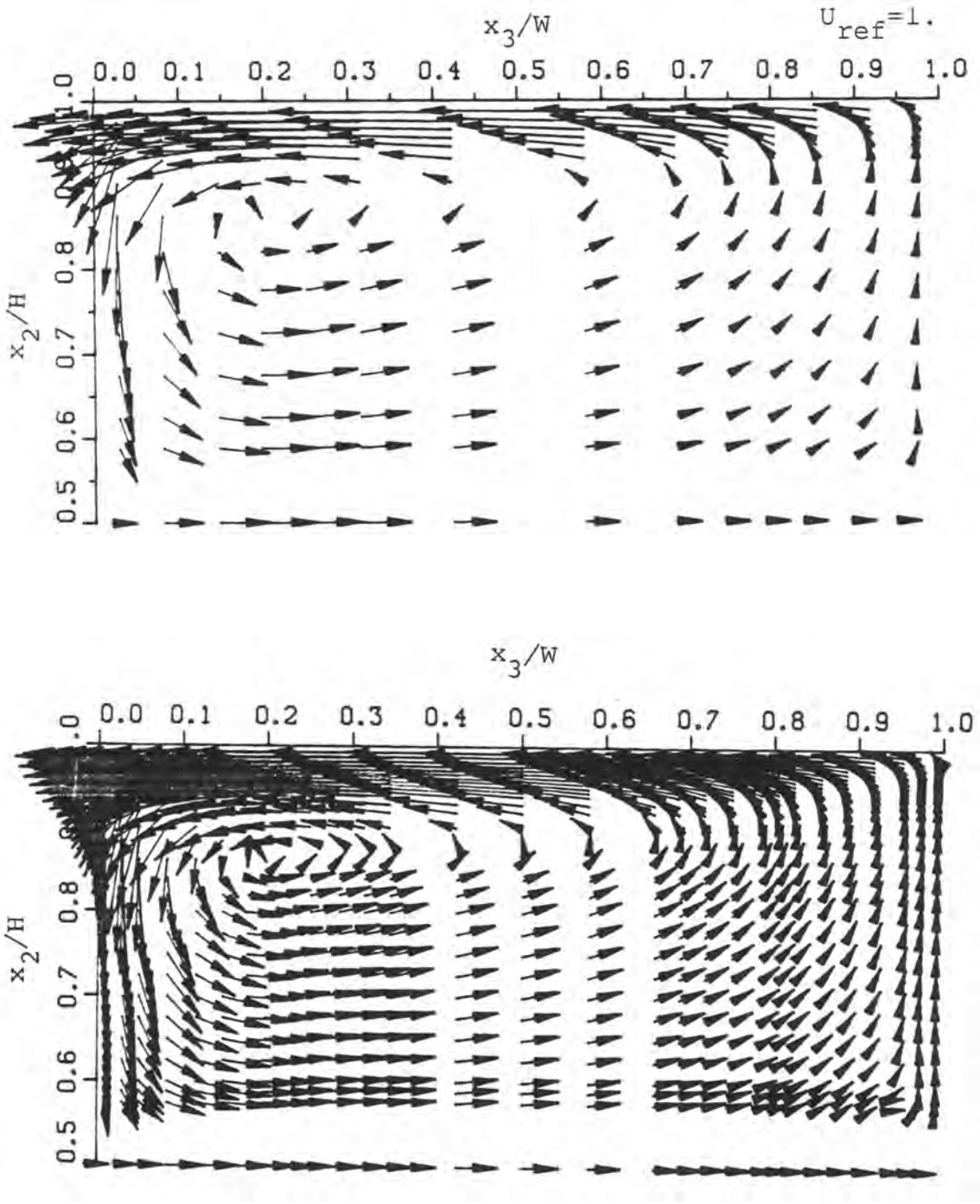

Figure 3.10. Vector plot of calculated secondary components at station D.

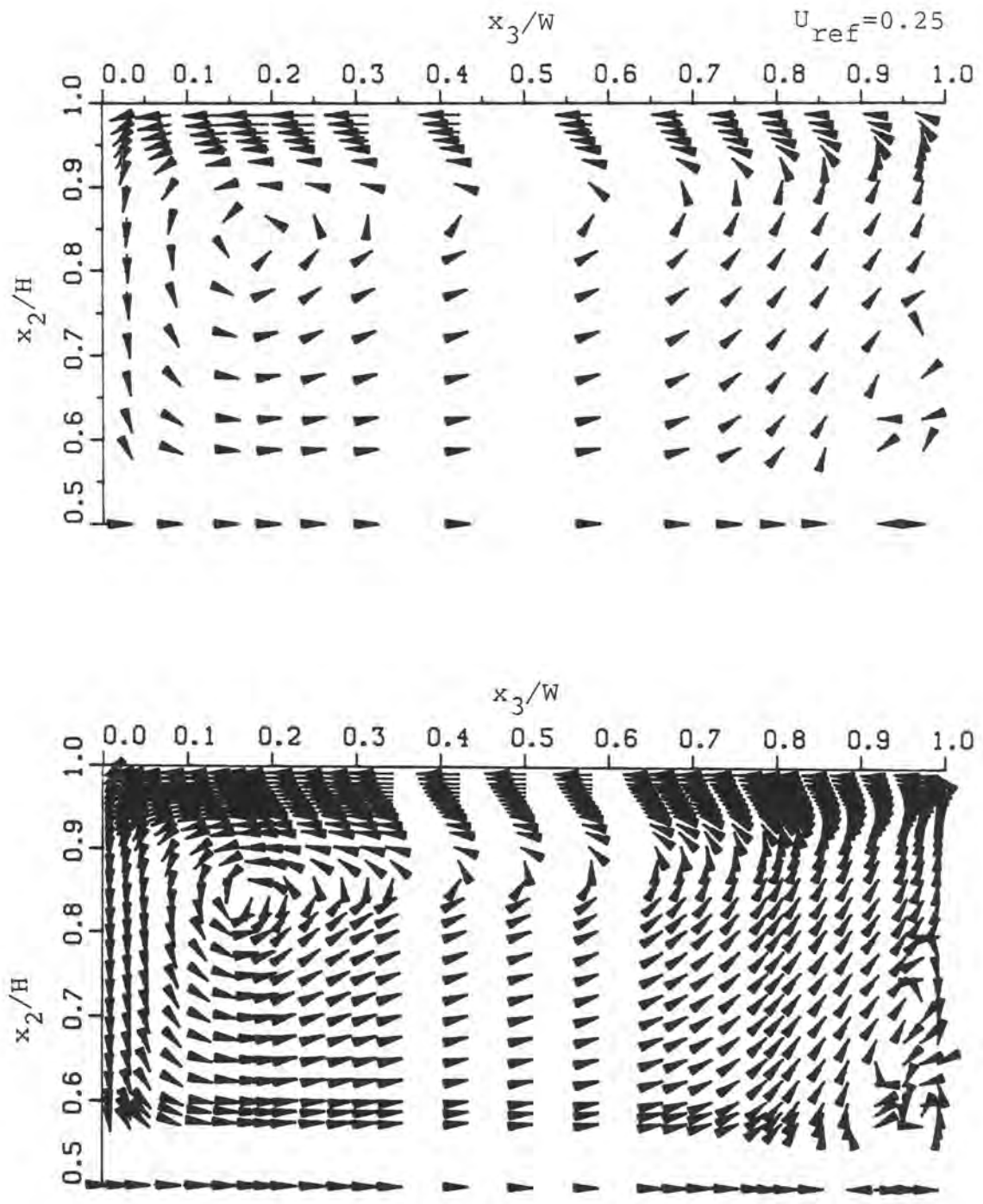

Figure 3.11. Vector plot of calculated secondary components at station F.

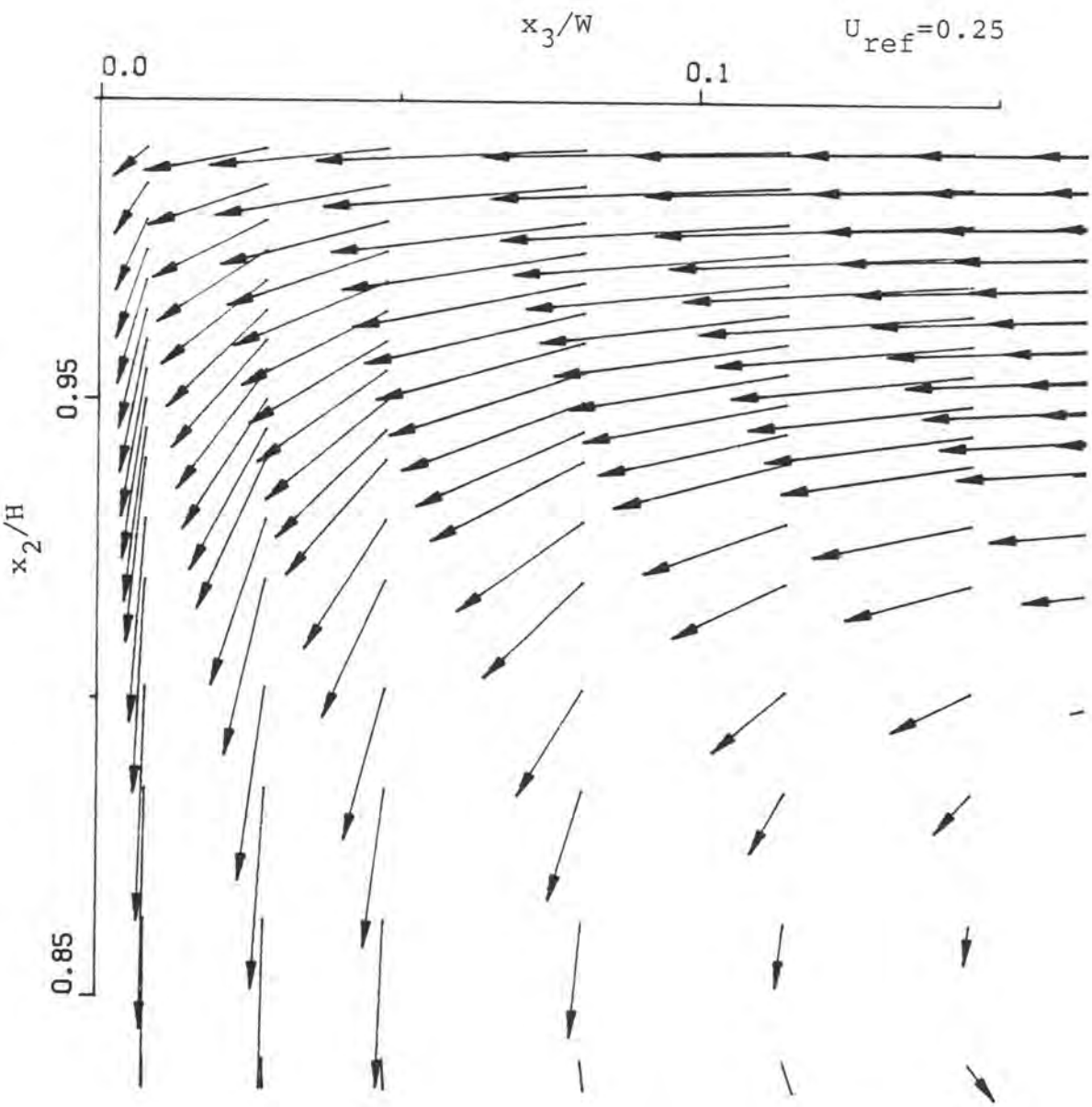

Figure 3.12. Vector plot of calculated corner secondary flow components at station D.

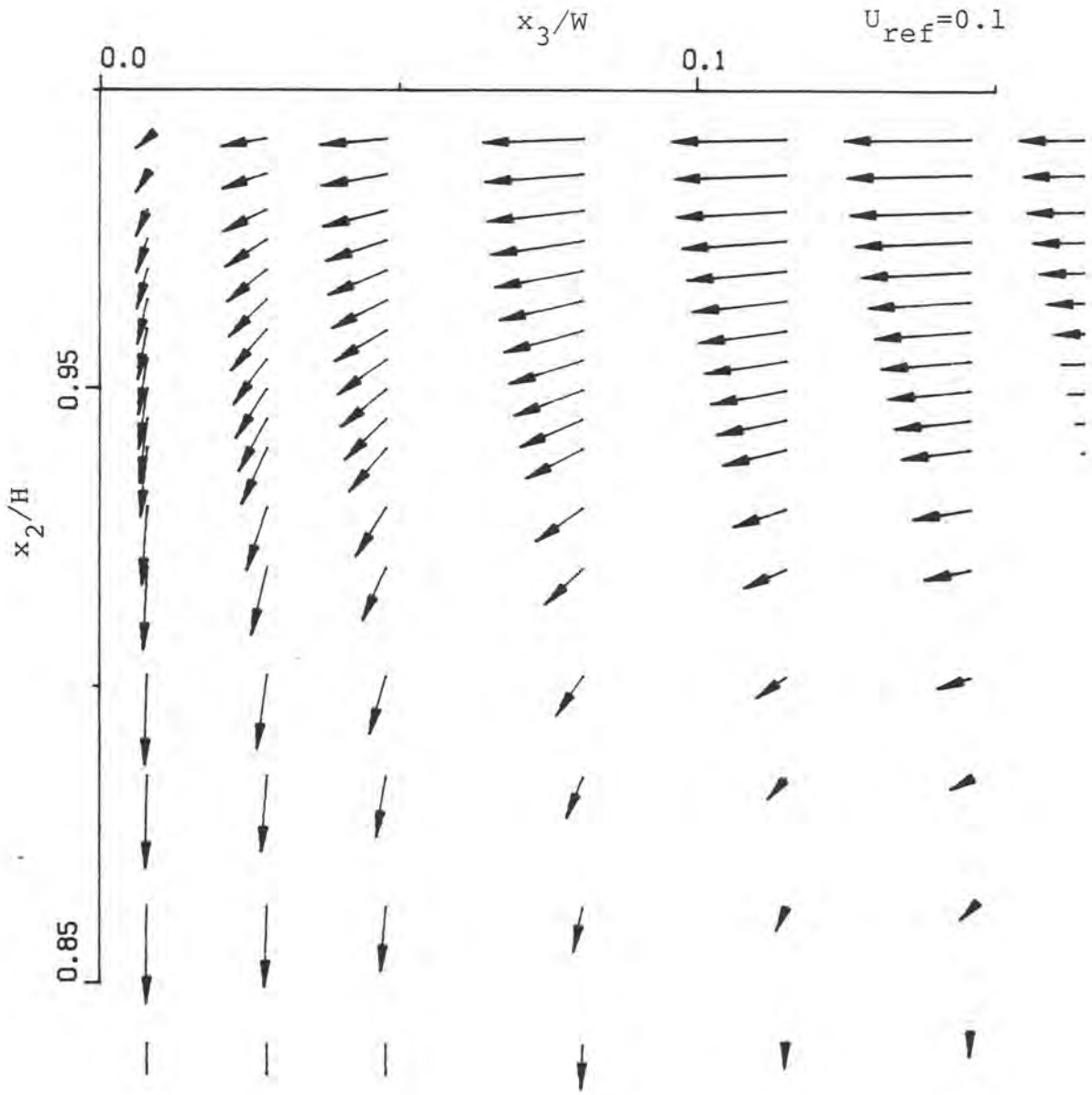

Figure 3.13. Vector plot of calculated corner secondary flow components at station F.

More quantitative comparisons between the measured and calculated velocity fields are made in figures 3.14 and 3.15 at stations D and F, respectively. Figure 3.14 shows the three velocity components at three locations (x_3/W = 0.5, 0.3, 0.115) from the inner wall of station D while figure 3.15 shows similar information at five such locations of station F (x_3/W = 0.775, 0.5, 0.238, 0.176, 0.115). In some cases the results for the calculations at a station nearest to the measurement station are shown. From these figures it is evident that the magnitudes and directions of the secondary velocity components U_2 and U_3 are predicted rather well at almost all stations at both sections but some discrepancies are seen in the U_3 component close to the convex wall at station F. The primary component of velocity, namely U_1, is overpredicted by about 9% at the centerline of section D but by station F the centerline velocities agree within 1%. However, in general, the velocity in the central invicid core is overpredicted and this is consistent with the lower calculated pressures noted in the previous section. The behavior of the longitudinal velocity distribution near the convex wall (see figure 3.14 c and figures 3.15 c, d, f) is particular noteworthy. With the exception of figure 3.15 (c) (at x_3/W = 0.283), the general trends are predicted rather well. The decrease in longitudinal velocity within the boundary layer over the

central part of the convex wall is obviously related to the vortex formation and is to be expected from the convergence of the secondary flow within the boundary layer. The disagreement in figure 3.15 (c) simply underscores the previous observation that the calculated secondary motion is not in complete agreement with that observed in the experiments.

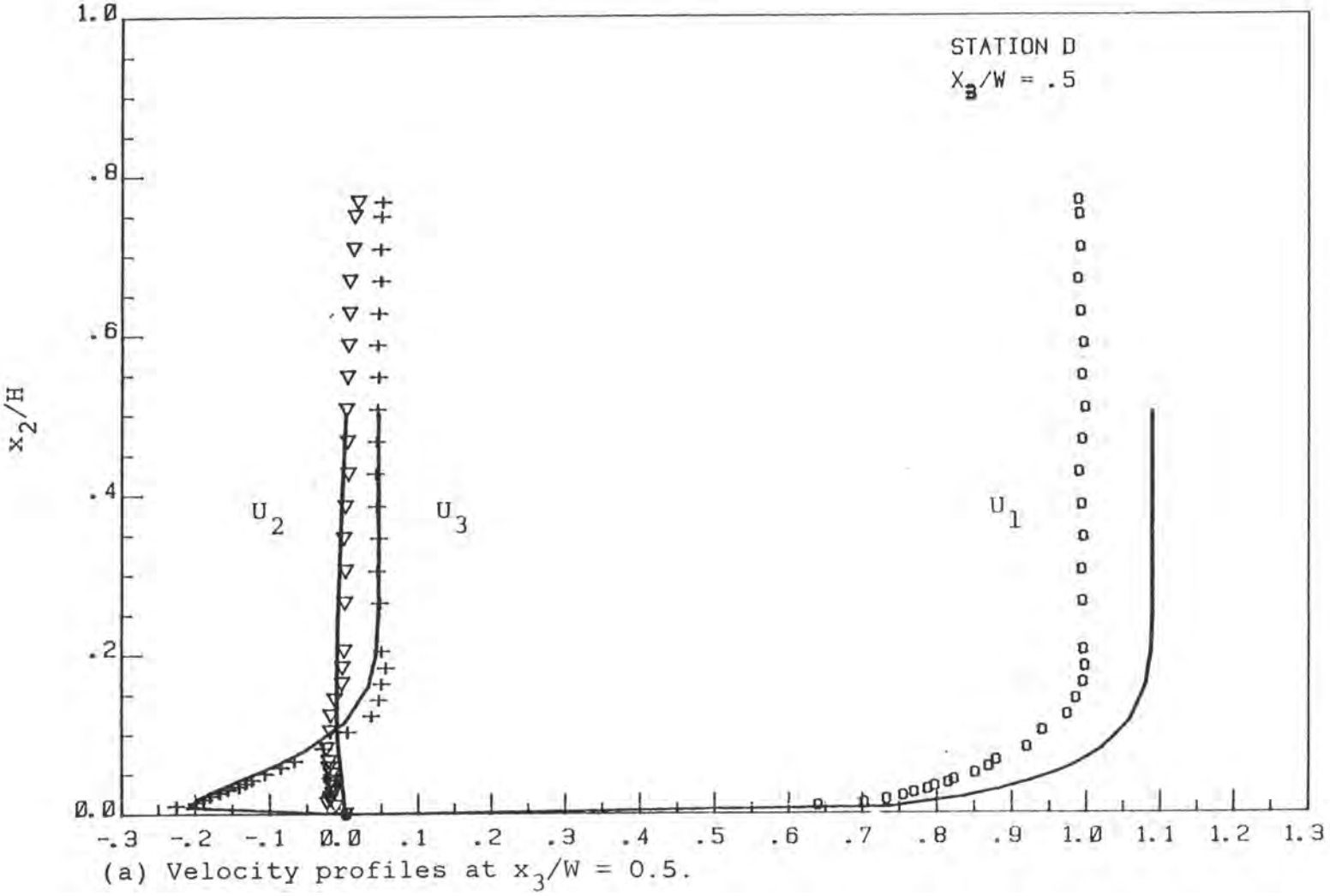

(a) Velocity profiles at $x_3/W = 0.5$.

Figure 3.14. Velocity profiles at station D.

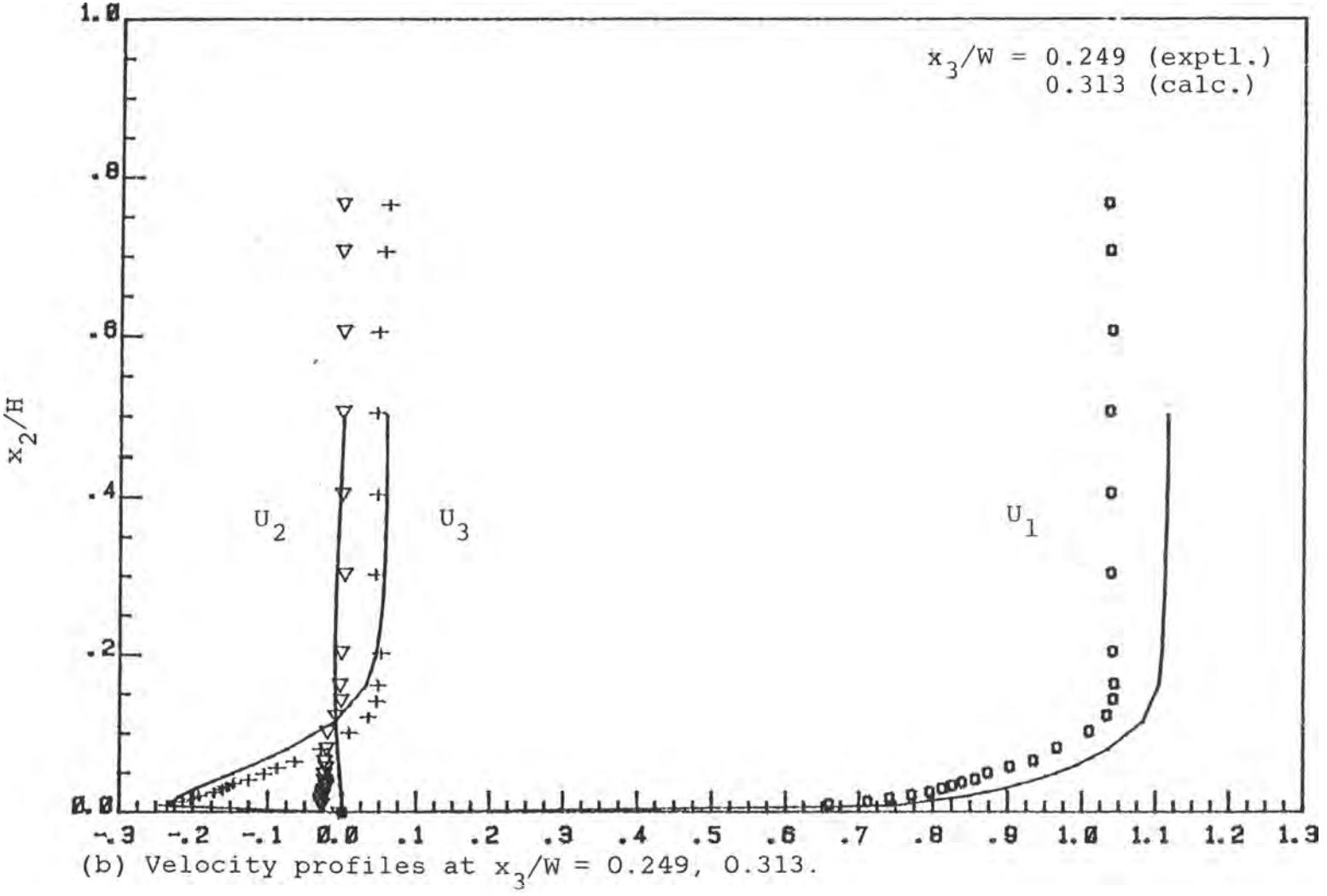

(b) Velocity profiles at x_3/W = 0.249, 0.313.

Figure 3.14. (continued)

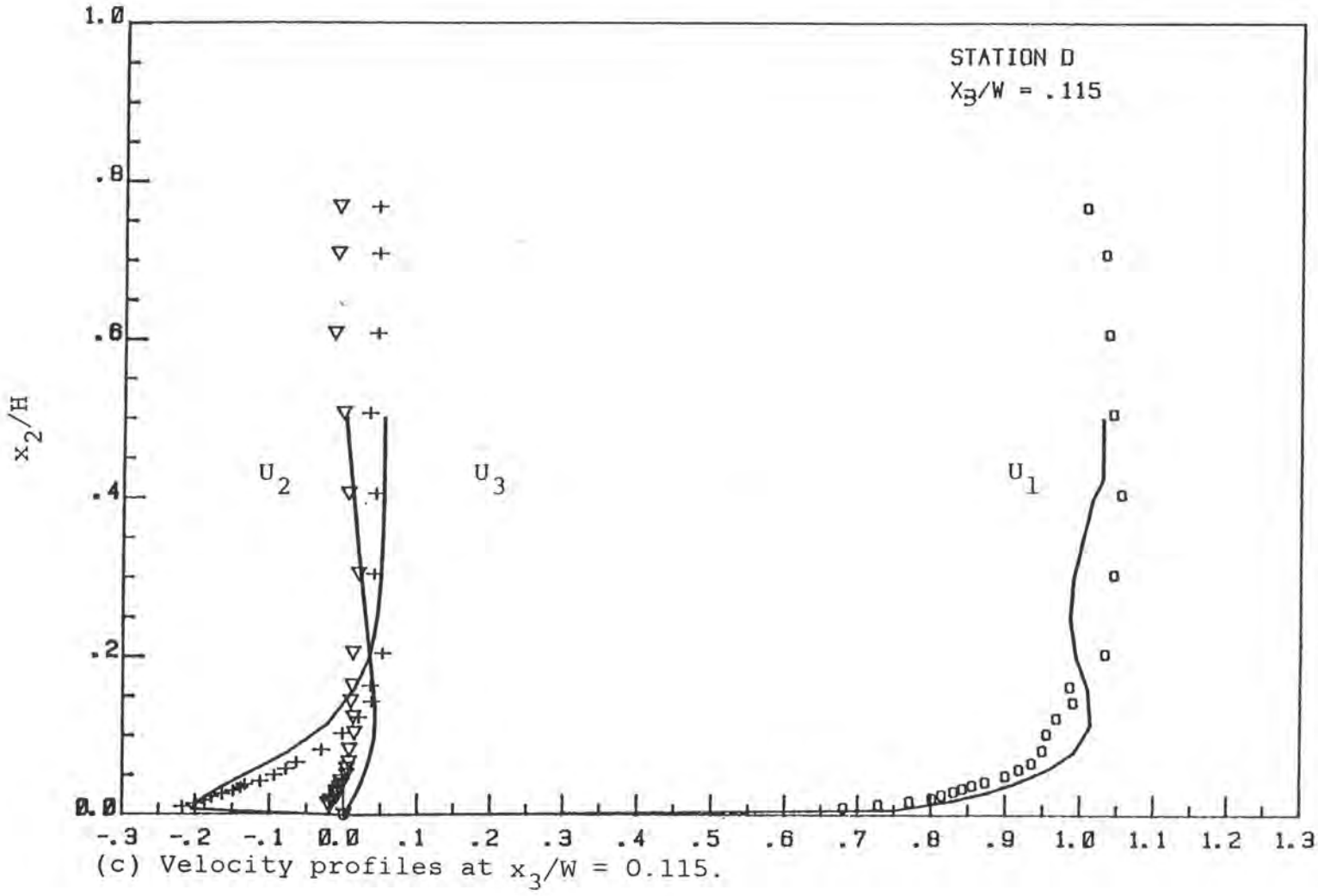

(c) Velocity profiles at $x_3/W = 0.115$.

Figure 3.14. (continued)

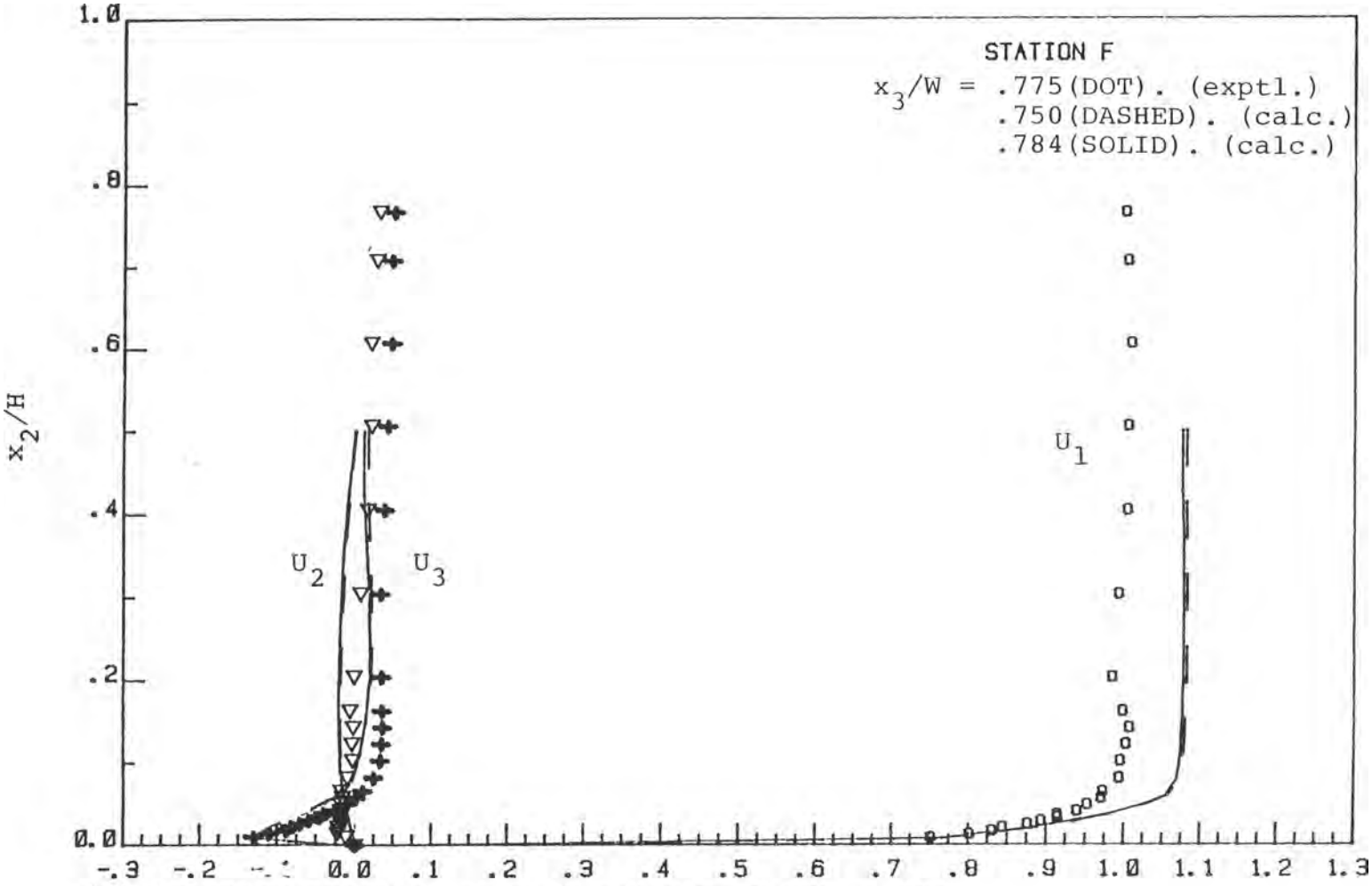

(a) Velocity profiles at x_3/W = 0.750, 0.775, 0.784.

Figure 3.15. Velocity profiles at station F.

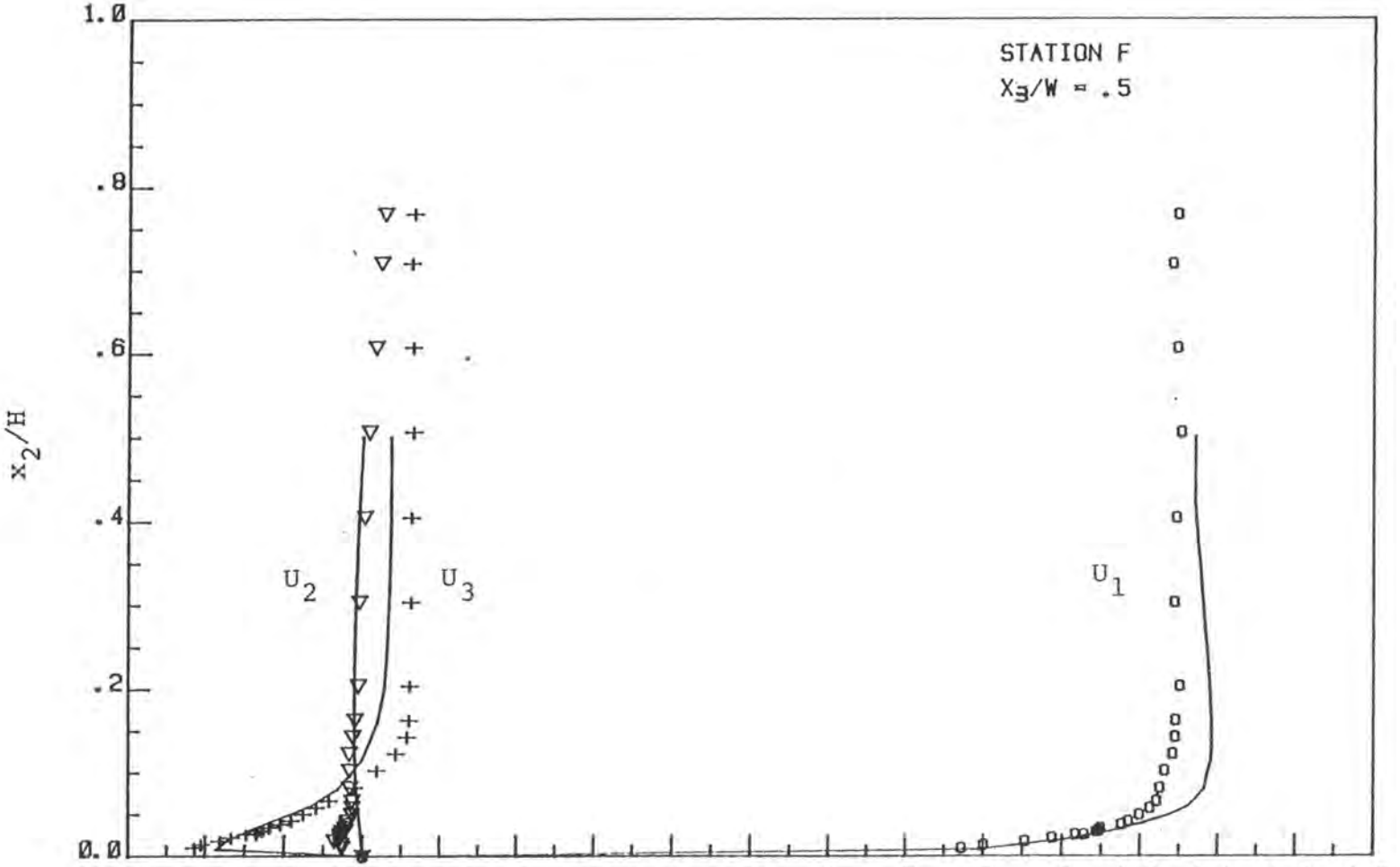

(b) Velocity profiles at $x_3/W = 0.5$.

Figure 3.15. (continued)

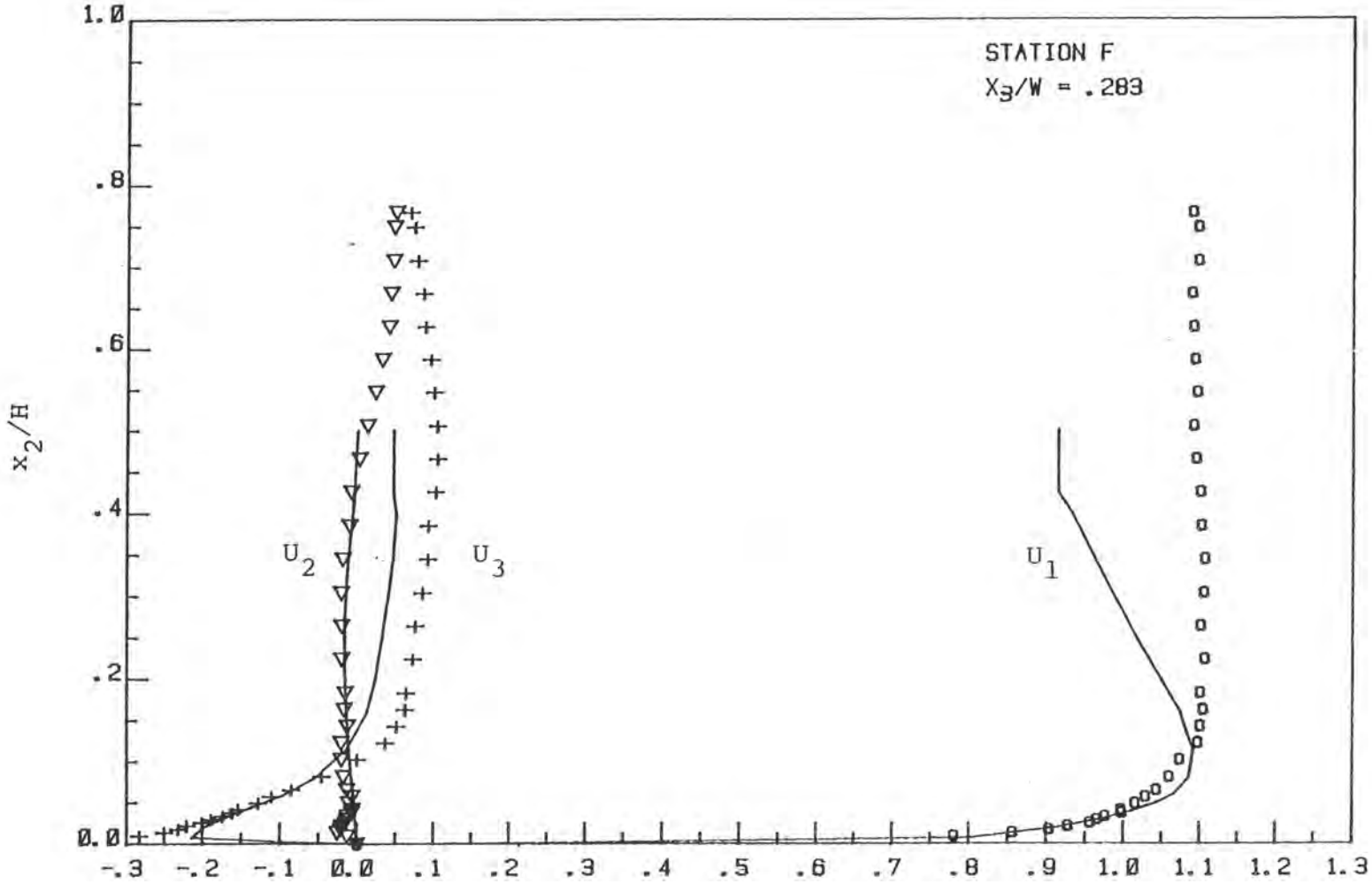

(c) Velocity profiles at $x_3/W = 0.283$.

Figure 3.15.(continued)

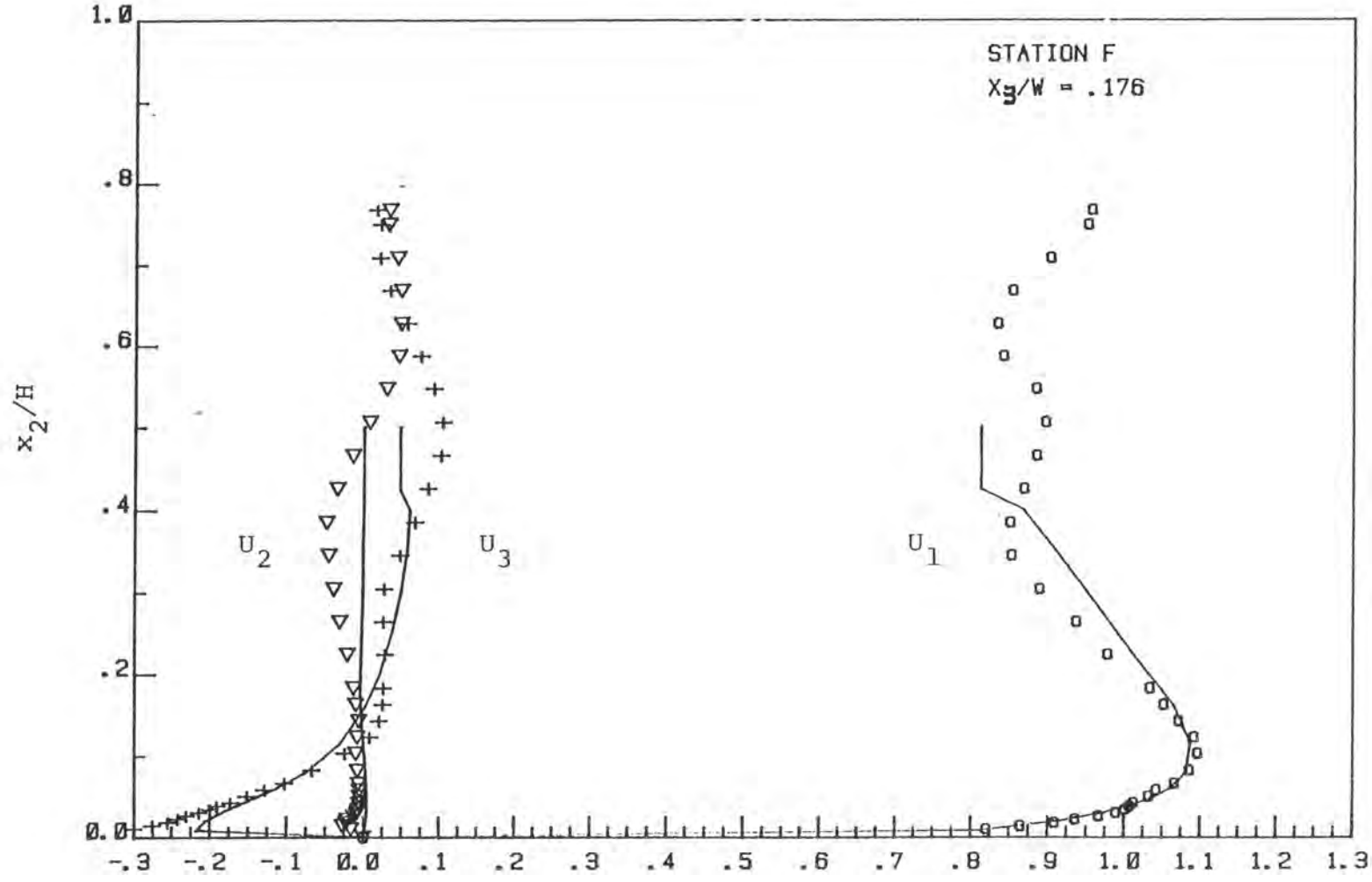

(d) Velocity profiles at $x_3/W = 0.176$.

Figure 3.15. (continued)

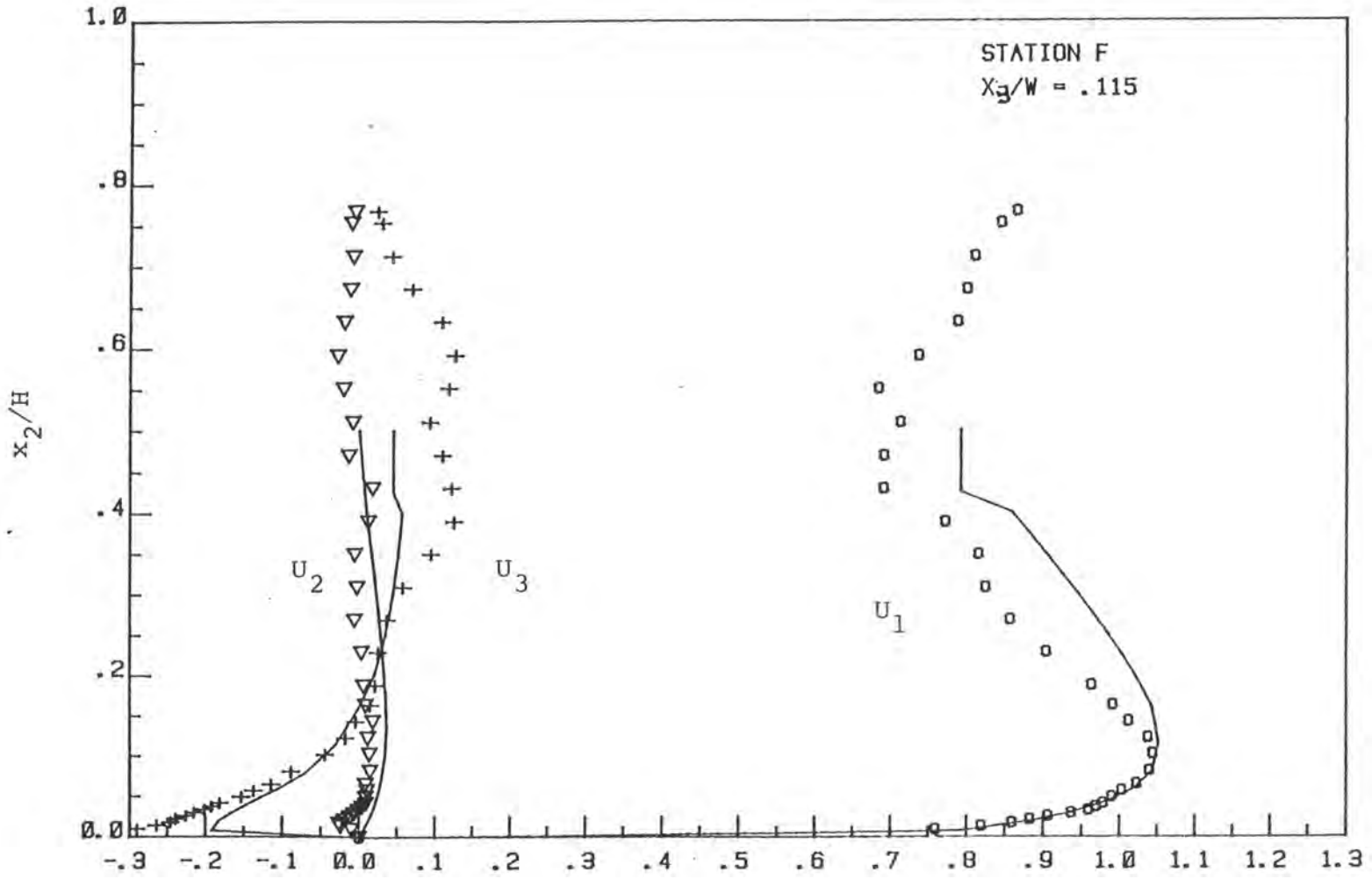

(e) Velocity profiles at $x_3/W = 0.115$.

Figure 3.15. (continued)

CHAPTER IV

CONCLUSIONS AND RECOMMENDATIONS

The developing turbulent flow along a curved streamwise corner in a 60-degree duct bend has been studied. Detailed measurements of the wall-static pressure and the three mean-velocity components have been made at three sections. A numerical method for the solution of the three-dimensional partially-parabolic equations for turbulent flow has been employed to explore the flow in the corner region in some detail. The study leads to the following major conclusions:

The experiments document the surface pressure distribution and the development of the vortex in the corner region, and provide data that can be used to validate calculation methods.

The calculation method of Singhal (1978) used here gives results which are in qualitative agreement with the data. This indicates that the flow in a curved duct can be predicted with the partially-parabolic equations. The experiments indicate a more gradual evolution of the pressure field and the secondary motion, and a more diffused vortex, than that predicted by the calculations. The method fails to converge with finer grids. Further calculations

are required to determine the source of the problem. Also, the boundary coditions employed at the exit from the duct and at the walls through the usual wall functions need to be examined in detail to ascertain their influence on the convergence of the solutions and the accuracy of the predicted pressure and velocity fields.

As noted in the Introduction, this was a preliminary investigation in which the principal objective was to establish a data base for the flow in the boundary layer in a corner and investigate the performance of a representative calculation method for such flows. These objectives have been realized in the present study. While it would be useful to conduct more refined measurements, using smaller probes and perhaps hot-wire anemometry for turbulence, in the present constant-area duct configuration, and to extend the measurement domain to the outer concave corner, a study designed to investigate the phenomena of corner-flow separation appears to be more worthwile. Thus, following some further evaluation of the calculation method, calculations should be performed to establish a duct geometry which would lead to separation. The tunnel can be readily modified to realize this geometry and refined instrumentation used to study the phenomena of flow separation in a corner.

REFERENCES

Berger, S.A., Talbot, L. and Yao, L.S. (1983) Flow in curved pipes. Annual Rev. Fluid Mech., vol. 15, p461-512.

Bruun, H.H. (1979) An experimental investigation of secondary flow losses in bends with rectangular cross-sections. Univ. of Cambridge, Dept. of Eng., Report CUED/A-Turbo/TR 95.

Caretto, L. S., Curr, R. M. and Spalding, D. B. (1973) Two numerical methods for three-dimensional boundary layers. J. Comp. Physics, vol. 14, p8. Also in Comp. Methods in Appl. Mech. and Engr., vol. 1, 1973, p39.

Chang, S. M. (1983) Measurement and calculation of developing turbulent flow in a U-bend and downstream tangent of square cross-section. Ph.D. Thesis, University of California,Berkely.

Christianson, T. and Bradshaw, P. (1981) Effect of turbulence on pressure probes. J. of Physics E, vol. 14, no. 8, p992.

Cramer, J. (1984) The IIHR scanivalve computer positioning circuit. IIHR Technical Report No 276. Iowa Institue of Hydraulic Research, The University of Iowa.

Demuren, A.O. and Rodi, W. (1982) Calculation of turbulence-driven secondary motion in non-circular ducts. SFB Report 80/7/220. UNIV. KARLSRUHE.

Dickinson, S. C. (1984) Flow vizualization and velocity measurements in the separated region of the appendage flat plate junction. Proc. 4th Symp. of Turbulent Shear Flow.

Gessner, F.B. (1973) The origin in turbulent flow along a corner. JFM, vol. 58, p1.

Hawthorne, W.R. (1951) Secondary circulation in fluid flow. Proc. R. Soc., vol. A206, p374.

Humpherey, J.A.C. (1977) Flow in ducts with curvature and roughness, Ph.D. thesis, Univ. of London, London.

Humphrey, J.A.C., Taylor, A.M.K. and Whitelaw, J.H. (1977) Laminar flow in a square duct of strong curvature, JFM, vol. 83, p509-27.

Humphrey, J.A.C., Whitelaw, J.H. and Yee, G. (1981) Turbulent flow in a square duct with strong curvature, JFM, vol. 103, p443-63.

Humphrey, J.A.C., Chang, S.M. and Modavi, A. (1982). Developing turbulent flow in a 180 bend and downstream tangent of square cross sections. Dept. of M.E., U. C. Berkley, CA. (LBL Report No.14844) Sep. 1982 for project titled Turbulent flow and heat transfer in passage around 180 bend - An experimental and numerical study.

Kline,S.J.,Cantwell,B and Lilly, G.M. Eds. Proc. 1980-81 AFOSR-HTTM Stanford Conference on Complex Turbulent Flows: Comparison of computation and experiment.

Kreskovsky, J. P., Briley, W. R. and McDonald, H. (1981) Pridiction of laminar and turbulent primary and secondary flows in strongly curved ducts. NASA Contractor Report 3388

Kubendran, L. R., McMahon, H. M. and Hubbartt, J. E. (1985). Turbulent flow around a wing-fuselage type juncture. AIAA 23rd Aerospace Sciences Meeting, Jan 14-17, Reno, Nevada.

Launder,B.E. and Ying,W.M. (1972) Secondary flows on ducts of square sross-section, JFM, vol. 54, p289-295.

Launder, B.E. and Ying, W.M. (1973) The prediction of flow and heat transfer in ducts of square cross section. Proc. Inst. Mech. Eng., vol. 187, p37.

Launder,B.E. and Spalding,D.B. (1974) The numerical calculation of turbulent flows. Computational Methods in Applied Mech. Engg., 3, 269-289.

McMahon, H., Hubbartt, J. and Kubendran, L. R. (1983) Mean velocities and Reynolds stresses upstream of a simulated wing-fuselage junction. NASA Contactor Report 3695.

McMillan, O. J. (1982) Mean fLow measurements of the flow field diffusing bend. NASA Contractor Report 3634.

Mojola,O.O. and Young, A.D. (1972) An experimental investigation of the turbulent boundary layer along a streamwise corner. AGARD CP-93.

Naot,D. and Rodi,W. (1982) Calculation of secondary currents in channel flow. J. Hydraulic Div.,ASCE, J. Hydraulic Div.,ASCE, vol. 108, p948-968.

Nikuradse, J.(1926). Untersuchungen uber die Geschwindigkeitsverteilung in turbulenten Stromungen. VDI Forschungsheft 281.

Patankar,S.V. and Spalding,D.B. (1972) A calculation procedure for heat, mass, and momentum transfer in three-dimensional parabolic flows, Intl. J. HMT, vol. 5, p1787-1806.

Patankar, S. V., Rafiinejad, D., and Spalding, D. B. (1975). Calculations of the three-dimensional boundary layer with solutions of all three momentum equations. Comp. Methods Appl. Mech. Eng., vol. 6, p283.

Prandtl, L. (1952) Essentials of Fluid Dynamics, Blackie, London.

Pratap, V. S. and Spalding, D. B. (1975) Numerical computation of the flow in curved ducts. Aeronaut. Q., vol. 26, p219.

Reece,G.J. (1977) Generalized Reynolds stress model of turbulence. Ph.D. thesis, Univ. of London, London.

Rojas, Whitelaw and Yianneskis (1983) flow in sigmoid diffusers of the moderate curvature. Fourth Symposium on the Turbulent Shear Flows. September 12-14, 1983. Karlsruhe, F.R. Germany.

Shabaka,I.M.M.A.(1979) Turbulence flow in a simulated wing-body junction. Ph.D. thesis,Aeronautics Dept. Imperial College, London.

Singhal, A. K. (1978) The FLAIR code: user's manual. CHAM Report TR/41.

Tatchell, D. G.(1975) Convection processes in confined three-dimensional boundary layers. Ph.D. Thesis, University of London, London.

Taylor, A.M.K.P., Whitelaw, J.H. and Yianneskis,M. (1982) Curved ducts with strong secondary motion: velocity measurements of developing laminar and turbulent flow, Transaction of the ASME, vol. 104, p350.

Wang, Tsun-Chung,(1982), Measurement of mean flow and Reynolds' stresses in a curved rectangular duct with crossed X-hot wire. CUED/A-Turbo/TR 108.

Ward-Smith, A. J. (1971) Pressure Losses in Ducted Flows. Butterworths, London.